STAR-SHAPED POLYMERS IN THE LOW MOLECULAR WEIGHT REGIME AND THEIR APPLICATION AS LOW ROUGHNESS PHOTORESISTS

A Dissertation

Presented to the Faculty of the Graduate School

of Cornell University

in Partial Fulfillment of the Requirements for the Degree of

Doctor of Philosophy

by

Drew C. Forman

January 2011

STAR-SHAPED POLYMERS IN THE LOW MOLECULAR WEIGHT REGIME AND THEIR APPLICATION AS LOW ROUGHNESS PHOTORESISTS

Drew C. Forman, Ph.D.

Cornell University 2011

Polymers synthesized with a star-shaped architecture can exhibit properties that differ from linear polymers. This has led several industries to use star polymers in their products. The utility of star polymers is currently restricted to high molecular weight applications because it is difficult to reproducibly isolate well controlled, low molecular weight star polymers. Consequently, little is known about the properties or behavior of star polymers in the low molecular weight regime. In this work, low molecular star polymers are reproducibly prepared using atom transfer radical polymerization. From simple homopolymers to more complex terpolymer compositions, stars with different cores, numbers of arms and arm lengths are studied. The potential of star polymers as photoresists is investigated to demonstrate the ability of stars in an application that requires extremely low (sub-10 kg/mol) molecular weights. Lithographic performance is comprehensively examined over a range of processing conditions using combinatorial techniques. This study reveals that the conformation of star polymers can result in smoother lithographic features, addressing a key challenge facing the photoresist community.

BIOGRAPHICAL SKETCH

Drew C. Forman received a Bachelor of Science in Ceramic and Materials Engineering with a concentration in nanomaterials from Rutgers University in 2005. He graduated with highest honors and was recognized as a James J. Slade Scholar for his research in the field of ceramic processing. As an undergraduate he worked in the Rutgers Fiber Optic Draw Tower laboratory where he prototyped new fiber optic materials for academic and industrial collaborators. He also interned at the Army Research Labs as a guest scientist working on the Ceramic Armored Vehicles project. As a graduate student at Cornell University's Department of Materials Science and Engineering, he received the Ubiquitous Electronics Motorola Fellowship and the Semiconductor Research Corporation Graduate Fellowship. In 2007 he was awarded a Global Research Collaboration/Applied Materials Fellowship. While researching *Star-shaped polymers in the low molecular weight regime and their application as low roughness photoresists*, he traveled to Germany five times. There, he spent nearly three months at the University of Bayreuth collaborating with the Departments of Macromolecular Chemistry I and Macromolecular Chemistry II. Following the completion of his dissertation in 2010, Dr. Forman began employment with Intel Corporation.

This work is dedicated to Ashley and the rest of my family for their support and understanding during my long nights in the laboratory.

ACKNOWLEDGEMENTS

Financial support from the Semiconductor Research Corporation (GRC-1677.001 and GRC-1675.002) is greatly appreciated. Research was performed in part at the Cornell NanoScale Facility, a member of the Nation Nanotechnology Infrastructure Network and the Cornell Center for Materials Research, which are supported by the National Science Foundation (ECS-0335765 and DMR-0520404). Macromolecular Chemistry I and Macromolecular Chemistry II at the University of Bayreuth are thanked for the generous use of their polymer synthesis and characterization facilities. D.C.F. was supported by a Global Research Collaboration/Applied Materials fellowship, a Semiconductor Research Corporation Fellowship and a Ubiquitous Electronics Motorola Fellowship. This work was made possible through collaborations with the talented members of Professor Müller's and Professor Schmidt's groups at the University of Bayreuth and Professor Ober's group at Cornell University.

TABLE OF CONTENTS

LIST OF TABLES

LIST OF FIGURES

CHAPTER 1. INTRODUCTION TO STAR-SHAPTED POLYMERS, ATOM TRANSFER RADICAL POLYMERIZATION, PHOTOLITHOGRAPHY, AND SIDEWALL ROUGHNESS

Drew C. Forman

Department of Materials Science and Engineering

Cornell University, Ithaca, NY 14853

The work that follows describes the synthesis of low molecular weight star-shaped polymers and their evaluation in one potential application: low roughness photoresists for semiconductor manufacturing. In this chapter, four areas of importance will be reviewed: (1.1) The star-shaped polymer architecture is introduced with a discussion of the theories, simulations and experiments that have benefited several industries. Additionally, the motivation for examining low molecular weight stars is explained. (1.2) The fundamentals of the polymerization technique *atom transfer radical polymerization*, which will be used throughout this work to synthesize low molecular star polymers, are reviewed. (1.3) An overview is given of photolithography and photoresists with emphasis placed on some of the reasons why star-shaped photoresists may exhibit superior performance. (1.4) Finally, an introduction is given to the characterization of roughness, a critical photoresist performance metric that is one of the unsolved problems facing high resolution photoresists.

1.1 The Star-Shaped Polymer Architecture

The word polymer originates from the Greek words 'poly' meaning many and 'mer' meaning unit.[1] Polymers are large, typically carbon-based molecules built from relatively simple, smaller molecules known as monomers. Plastics, such as Styrofoam, Teflon, Nylon, Kevlar and PVC, rubber, epoxy and even DNA are examples of polymers. In light of the United States producing 30 million tons of plastic a year,[2] it's safe to say that polymers are ubiquitous in modern life.

1.1.1 Linear Polymers

The most basic polymer consists of only a single monomer unit that is repeated over and over again from one end to the other. Such polymers are called homopolymers, because they are only comprised of a single monomer.

Architecturally, this material is a linear homopolymer because the monomer units are linked in series, one after the other. Linear polymers can also be synthesized from multiple types of monomers. These are known as copolymers. The monomer units might be arranged as a statistical copolymer, an alternating copolymer or a block copolymer.[3] (Figure 1-1)

Combining different monomers in a statistical copolymer allows one to tailor properties, such as crystallinity, flexibility, crystalline melting temperature and glass transition temperature.[4] A particular arrangement might be necessitated by the type of polymerization used, for example the condensation polymerization of nylon-6,6 always produces an alternating copolymer.[5] Block copolymers can phase separate creating unique morphologies not found with other arrangements.[6]

1.1.2 Polymer Architecture

So far, the discussion of polymer properties has been limited to changing the monomer species that comprise a polymer or their arrangement. Another way to alter a polymer's behavior is through the polymer's architecture. Not all polymers consist of monomers arranged in linear chains. Many architectures can be formed by introducing branching points into a polymer chain. This can be accomplished by adding species that can link three or more monomers, creating a branching point in a propagating chain. For example, low density polyethylene consists of a statistical arrangement of short and long branches.[7] Crosslinking can be used to create polymer networks. Alternatively, a polymer can contain monomers or end groups that are inert to the polymerization but can be utilized in subsequent reactions to form a wide array of architectures including H-branched, combs, ladders.[8] (Figure 1-2)

AABBABBBBABBBBAB

Random Copolymer

ABABABABABABABAB

Alternating Copolymer

AAAAAAABBBBBBB

Block Copolymer

Figure 1-1. Three possible monomer arrangements of a copolymer composed of two monomers ‘A’ and ‘B,’ adapted from reference.[3]

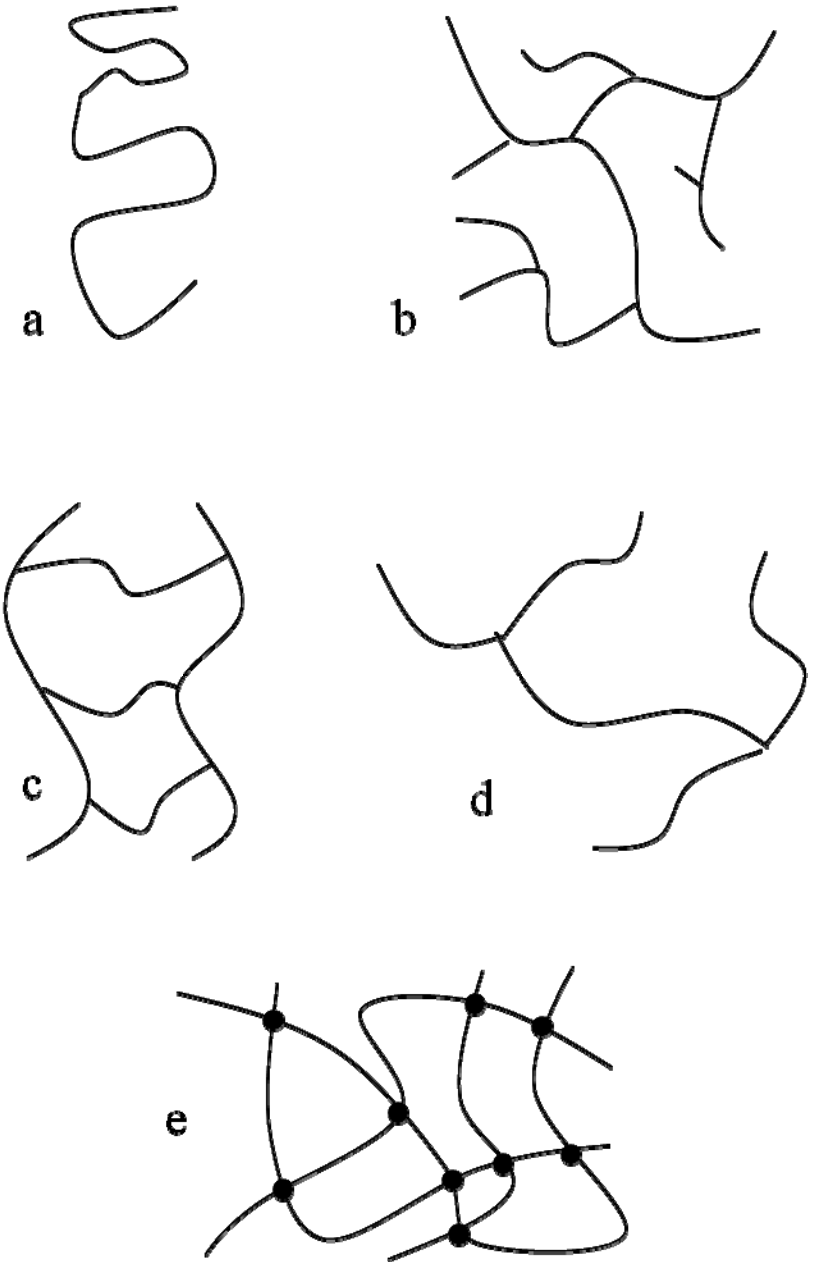

Figure 1-2. Select polymer architectures, adapted from reference:[7, 8] (a) linear; (b) statistical branching; (c) ladder; (d) H-branched; (e) crosslinked network.

1.1.3 Star-Shaped Polymers

A subcategory of branched polymers, known as star-shaped polymers or simply *star polymers*, only branch at a central core. Star polymers can be synthesized *arm first* by initially growing linear polymers. The linear polymers are then joined at the end through the use of a difunctional monomer that propagates and cross-links the linear chains[9] or through attachment to a multifunctional molecule that serves as the core.[10] Using difunctional monomers has the disadvantage of creating stars with a broad number of arms. Terminating to a multifunctional core requires additional purification steps to remove unreacted linear chains.

Star polymers can also be synthesized by means of a *core first* approach. First, a multifunctional initiator is prepared that will eventually serve as the core. Then, a polymerization reaction is carried out, causing polymer chains to propagate directly from the multifunctional initiator.[11, 12] This method yields star polymers without the broad arm dispersity or linear impurity disadvantages of the two arm-first approaches. However, care must be taken to ensure that the multifunctional initiator is soluble in the polymerization solvent.[13]

1.1.4 Star Polymer Conformations

A key reason why star polymers are of interest is because they are capable of diverse conformations. Star polymers with very few, long arms are conformationally similar to linear polymers. However, as a given number of monomers are divided into an ever increasing number of arms, a star polymer will approach the behavior of a hard sphere. Between these two extremes, star polymers can observe a broad array of behaviors and have been referred to as *ultrasoft colloids*. The properties of a star are therefore affected by both the *degree of polymerization*, *DP* (the number of monomer

units that compose the star) and the *functionality*, *f* (the number of arms in the star).[14-18] (Figure 1-3)

1.1.4.1 Daoud-Cotton Model

The center of a star can be a dense environment, with many arms in close proximity to each other. As one moves away from the center of the star, the space between adjacent chain segments increases. A spherical blob can be drawn around the chain segment, such that within that blob the chain behaves as a free chain, i.e. a chain not impacted by external influences. Since the space between chains increases as distance from the core increases, the spherical blobs size is dependent upon the distance from the core. At the center of the star, these blobs might only be the size of a single monomer, while at the outermost region of the star, such constructs can be quite large. This is the Daoud-Cotton model for a star polymer, which describes a star as a series of concentric shells of spherical blobs such that the blob size, $\xi(r)$, scales proportional to $rf^{-1/2}$, where *f* is the star's functionality and *r* is the radial distance from the center. One can define a swelling ratio $\alpha(r) = \xi(r)/\xi_0(r)$, where $\xi_0(r)$ is the ideal blob size (the size of a blob when the ideal chain conditions are met). From this swelling ratio, three regions can be defined based on the radial position *r*, between $r=0$ (the center) and $r=R_c$ (the furthest extent, or corona, of the star).[19] (Figure 1-4)

The Swollen Region: The outermost region is defined as $r_1<r< R_c$, and is known as the swollen region because the blob size is larger than the size of an ideal blob, $\alpha(r)>1$.

The Unswollen Region: Inside the swollen region exists an unswollen region for $r_2<r<r_1$. Within the unswollen region the blob size is equal to the ideal blob size, $\alpha(r)=1$.

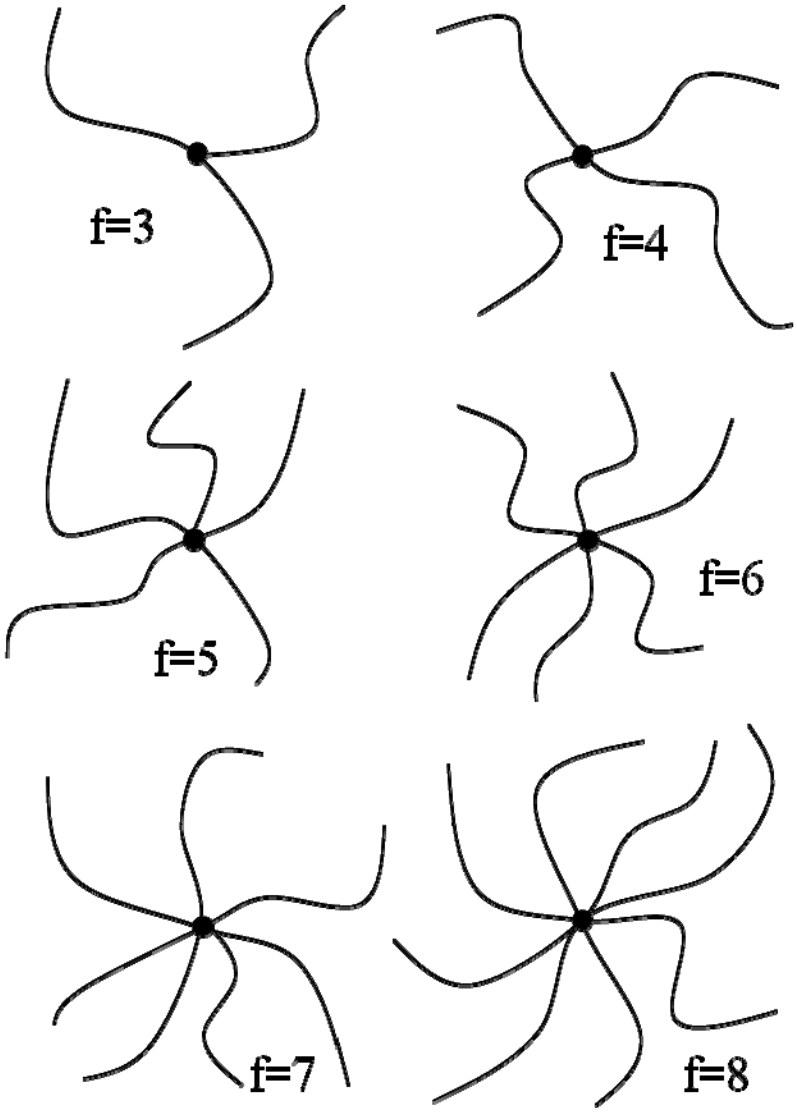

Figure 1-3. Star polymers with different functionality.

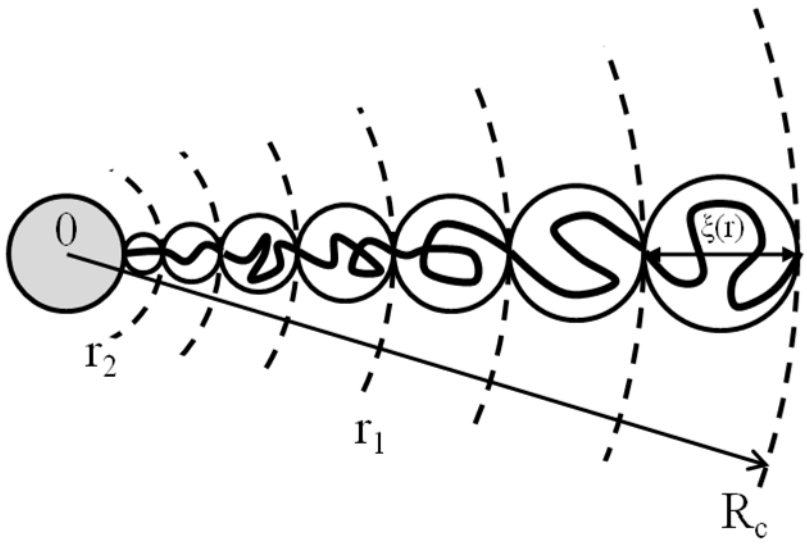

Figure 1-4. Daoud-Cotton[19] blob model of a star-shaped polymer, single arm depicted.

The Core: The innermost region, $0<r<r_2$, is known as the core. In the core, the blob size is equal to the monomer size, indicating that the chains are extended.

When the number of monomer units in a single arm, *N*, is much greater than $f^{1/2}\bar{v}^{-2}$, where $\bar{v}$ is the dimensionless excluded volume parameter, the majority of the star exists in the swollen region. Studies that consider stars with long arms in good solvents satisfy this condition and therefore consider the swollen region and core negligible. Generally, theoretical studies consider only this case, and therefore use only the scaling laws of the swollen region to describe the entire star.[15]

However, another two regimes exist for smaller stars. The number of monomers in an arm that occupy the core region in this model scales as $f^{1/2}$. Therefore, stars with arms much shorter than $f^{1/2}$ are dominated by the core region. The arms are extended as the blob size is equal to the monomer size. In other cases, where *N* is less than $f^{1/2}\bar{v}^{-2}$ but much larger than $f^{1/2}$, the unswollen region dominates and the star behaves as if it were in a θ-solvent, and therefore follows ideal chain scaling.

Even though the arm of a star is larger than an equivalent linear polymer, the star as a whole is smaller than a linear polymer with the same degree of polymerization as the star. The size of a linear chain scales as $DP^{1/2}$ in a θ-solvent and $DP^{3/5}$ in a good solvent. Large stars scale with similar exponentials to linear chains. However, the degree of polymerization is replaced by the number of monomer units in an arm which equals *DP/f*. Smaller stars that are dominated by the unswollen region scale by $(DP/f)^{1/2}$ whether they are in a θ-solvent or a good solvent. [15]

1.1.4.2 Simulations

The scaling behavior of star polymers has been confirmed by Monte Carlo and molecular dynamics simulations that track well with experimental findings.[15, 20-33] In addition, simulations have been useful in exploring the interaction between

neighboring stars[20, 28, 29, 34] and other materials.[35-37] Such studies have demonstrated, the hard sphere behavior as *f* approaches infinity, the linear behavior as *f* approaches two arms and the ultrasoft colloidal behavior that bridges the two extremes.[15] Simulations have also been used to examine the statistical thermodynamic partition functions of stars.[38] As a result of the arms being covalently attached to the core, the possible configurations of a star is restricted from that of a linear polymer with the same degree of polymerization. As such, it is not surprising that stars have been found to exhibit very different properties than linear polymers (that can be tuned by the functionality), including rheology,[39, 40] θ-temperature,[41] relaxation time,[30] and diffusivity.[42, 43]

1.1.5 Star Polyelectrolytes

Polyelectrolytes are charged polymers. Since electrical charges repel like charges, polymer conformation is altered by the presence of charge. Specifically, the repulsion forces a polymer into an extended conformation. In the case of star polyelectrolytes, extension is limited due to the arms being covalently bound to the core. Consequently, a star polyelectrolyte cannot expand to the same extent as a linear molecule with the same degree of polymerization. A contraction factor can be defined by the ratio of the star's radius of gyration and the radius of gyration of an equivalent linear polyelectrolyte. As functionality increases, the contraction factor decreases.[44] Simulations and experimental studies have further investigated the nature of counterion distributions on the conformation of star polyelectrolytes and star-like molecules, including micelles and brushes grafted to small particles. [45-49]

In addition to contraction, star polyelectrolytes differ significantly from their linear counterparts in the manner that they accommodate charge. Polyelectrolyte stars confine charges to a far greater degree than their linear counterparts, indicating that

the arms must be severely extended.[45, 47, 48, 50] In the presence of multivalent counterions, the arms of a star will collapse as the counterions interact with several charged positions along the arms. In the presence of a trivalent counterion that decomposes into a monovalent and divalent counterion when exposed to UV light, stars polyelectrolytes have been shown to expand. This demonstrates that the counterion contraction effect is significantly more pronounced with trivalent counterions than diavalent counterions.[51] It further suggests that the extension of star polyelectrolytes can be controlled with the correct ratio of counterions, a feature with no counterpart in linear polyelectrolytes.

1.1.6 Star Polymer Applications

The unique conformations and properties of star-shaped polymers have led to several industrial applications. Star polymers are used as viscosity index modifiers by the oil industry.[52] Contact lens manufacturers use star polymers to enhance the oxygen permeability and hardness of contact lenses.[53] Star polymers are also used as additives in coatings, binder in toner and as an encapsulation material for pharmaceuticals.[30, 54] Studies continue to examine star polymers for future drug delivery applications.[55] However, star polymers may be too large to deliver drugs through specific membranes.[56] The size of most star polymers may prove prohibitive to other applications, including nanoparticle dispersion stabilizers,[57] cosmetic dyes,[58] *in vivo* sensors for cancer and other diseases.[59]. It is a problem that the majority of star polymer studies focus exclusively on large stars. Clearly, additional knowledge of the low molecular weight star polymer regimes is required to enable these size sensitive fields to take advantage of star polymers. Such knowledge must, by necessity, begin with the capability to synthesize well-defined, low molecular weight stars. The goal of this work is to demonstrate the reproducible synthesis of low

molecular weight star polymers, or *star oligomers*, and to explore the potential benefits of stars in a field with severe molecular size requirements: photoresists for semiconductor manufacturing.[60, 61]

1.1.7 Summary

The properties of a polymer are dependent on both the monomer units that comprise the polymer and also the polymer architecture. Star-shaped polymers consist of a single core to which multiple polymer arms are attached. This attachment to a central core results in conformations that are highly dependent on the star functionality. As the number of arms approaches the linear limit of f=1,2 a star polymer will become conformationally similar to a linear chain. In contrast, as the number of arms approaches infinity, the star behaves as a hard sphere. Between these two limits, stars exhibit unique sets of properties that can be tuned by functionality. These behaviors have been confirmed by theory, simulation and experiment, leading to several industrial applications. Star polymers have the potential to be beneficial in multiple low molecular weight fields. However, at the time of this writing, low molecular weight star oligomers have been largely ignored. This work seeks to demonstrate the reproducible synthesis of star oligomers and the potential benefits of stars as photoresists, an application where size can adversely impact performance.

1.2 Atom Transfer Radical Polymerization

Up until this point, the discussion of polymers has ignored a critical issue: *polydispersity*. Aside from select biopolymers, polymers synthesized in a single batch do not have the same degree of polymerization. Size exclusion chromatography techniques, such as gel permeation chromatography (GPC), can be used to measure the molecular weight distribution of polymers. The ratio of weight average molecular

weight (Mw) and number average molecular weight (Mn) are used to quantitatively describe the dispersity (Mw/Mn). Due to chain transfer and termination, polymers synthesized by conventional polymerization techniques have dispersity values higher than 1, the value of a monodisperse polymer. For example, Mw/Mn=2 is a typical value for condensation polymerizations. Atom transfer radical polymerization (ATRP) is one of several polymerization techniques known as *living polymerization*, which are capable of achieving significantly lower dispersity values. In the case of ATRP, Mw/Mn=1.1 is not uncommon.

1.2.1 Atom Transfer Radical Polymerization Overview

ATRP was simultaneously discovered in 1995 by two groups; one working out of Kyoto University in Japan[62] and the other working from Carnegie-Mellon University in Pennsylvania.[63] In ATRP the polymer chain (P_m) is capped by a halogen atom (X) such as chlorine or bromine. The halogen atom cap prevents chain ends from coupling and undergoing disproportionation but it also prevents propagation of the chain. A transition-metal (M_t^n) abstracts the halogen atom, forming an oxidized transition metal ($M_t^{n+1}X$) and a radical at the chain end ($P_m\bullet$). This is a reversible redox process. The oxidation of the metal and generation of the radical end is known as the activation process (kinetic: k_{act}), while the reduction process, which returns the halogen atom to the end of the chain is known as the deactivation process (kinetic: k_{deact}). While a chain end is in the activated state monomer can be added to the chain through radical polymer propagation (kinetic: k_p). Termination (kinetic: k_t) can also occur while a chain end is in the activated state. However, termination by coupling and disproportionation, which require the reaction of two radicals, become statistically rare because most chain ends are in the deactivated state.[64] (Figure 1-5)

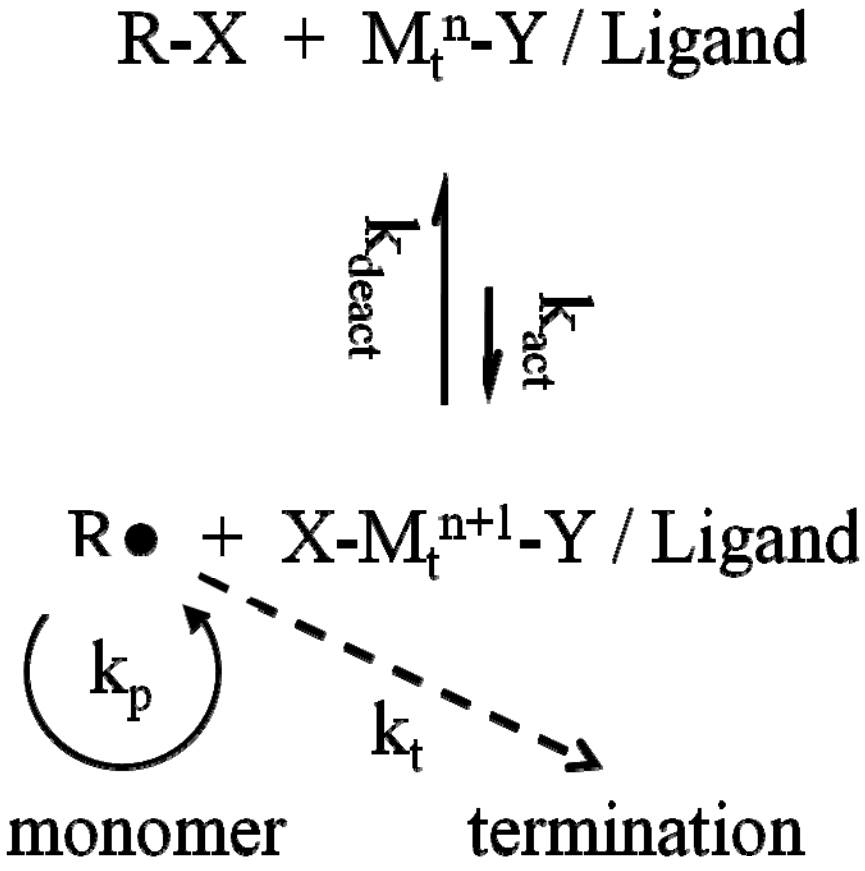

Figure 1-5. Generic ATRP scheme, adapted from reference.[65]

Achieving a narrow dispersity requires that both the reversible deactivation process and initiation occur rapidly compared to the rate of propagation. If initiation is too slow, some chain ends will propagate multiple times before all chains are initiated. If the reversible deactivation process occurs with insufficient speed, multiple additions can occur in a single activation cycle. Among other factors, the specific kinetics of a system depend on the compatibility of the metal-ligand complex, initiator, and monomer.[66, 67]

1.2.2 Metal-Ligand Complexes

ATRP is an extension of atom transfer radical addition,[68-70] transition metal catalyzed telomerization[71] and the transition metal initiated redox process.[72, 73] A major advance in ATRP is the catalyst that consists of the transition metal compound and ligand, which enables the efficient and reversible redox process. Numerous transition metal complexes have been investigated based on molybdenum,[74] chromium,[75] rhenium,[76, 77] ruthenium,[62, 78, 79] iron,[80-82] rhodium,[83, 84] nickel,[85-87] palladium,[88] and copper.[63, 66, 89-91] Copper catalysts have been very successful due to their low cost and good performance with a variety of different monomers.[65] The ligand N,N,N′,N″,N″-pentamethyldiethylenetriamine (PMDETA) and copper chloride were selected for the work that follows. (Figure 1-6)

1.2.3 Kinetics

The conversion of monomer into polymer can be expressed as a percentage or as the logarithmic conversion index: $\ln([M]_0/[M]_t)$. Plots of the conversion index versus time will result in a linear trend, indicating that ATRP polymerization progresses with first-order reaction kinetics.[65, 92-97] The slope is dependent on the propagation kinetics (k_p), the ratio of activation and deactivation kinetics ($K_{ATRP}=k_{act}/k_{deact}$), the

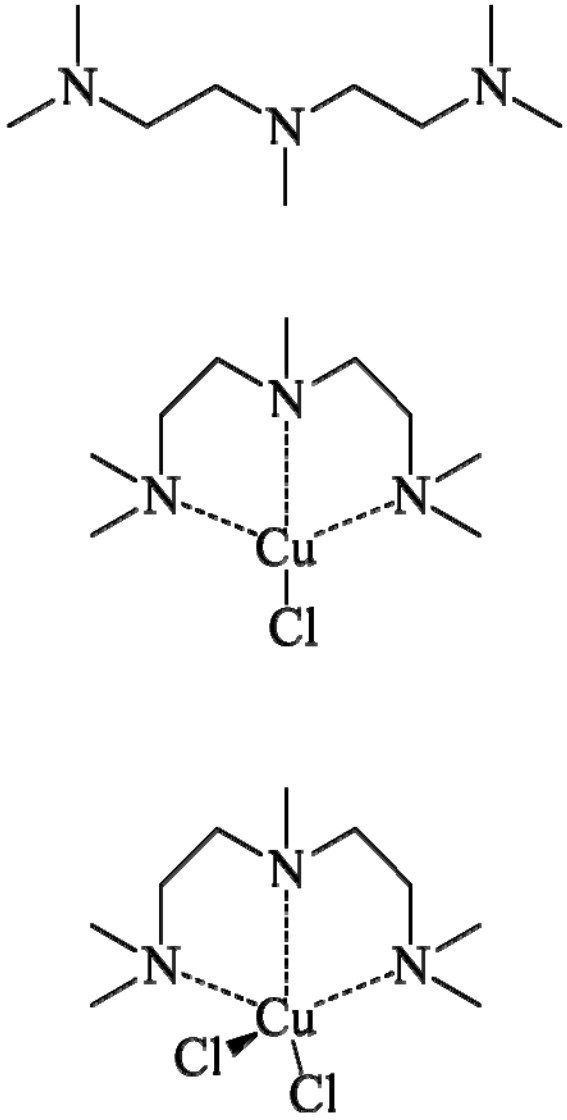

Figure 1-6. (a) N,N,N′,N″,N″-Pentamethyldiethylenetriamine (PMDETA) ligand. (b) PMDETA ligand complexed with Cu(I)Cl transition metal. (c) PMDETA ligand complexed with Cu(II)Cl_2 transition metal. Adapted from reference.[65]

concentration of chain ends [P_mX], and the concentration of reduced ([M_t^n]) and oxidized transition metal ([[M_t^{n+1}]). [See Equation 1-1]

$$\ln\left(\frac{[M]_0}{[M]_t}\right) = \frac{k_p K_{ATRP}[P_mX][M_t^n]}{[M_t^{n+1}]} t \qquad \text{Equation 1-1}$$

Studies have also examined the factors governing polydispersity in an ATRP reaction.[65, 92, 93, 98] The dispersity has three terms. The first term is a constant (1) and represents the minimum possible dispersity. The second term is the Poisson term, which describes how the statistics of monomer additions impact the dispersity. As the degree of polymerization becomes large, the Poisson term goes to zero. The final term is dependent on kinetics, concentration of oxidized transition metal, percent conversion (p), and the concentration of terminated chains ($[P_mX]_0$-[P_mX]). Values on the order of 0.1 are not uncommon. [See Equation 1-2]

$$\frac{Mw}{Mn} = 1 + (\overline{DP}_n)^{-1} + \left(\frac{k_p([P_mX]_0-[P_mX])}{k_{deact}[M_t^{n+1}]}\right)\left(\frac{2}{p}-1\right) \qquad \text{Equation 1-2}$$

1.2.4 ATRP Stars

Star-shaped polymers have previously been synthesized via ATRP using both the arm first and core first approaches.[65] Previous studies using the arm first approach have propagated a short divinyl block to the end of the synthesized arms, which were subsequently linked together to form stars.[99, 100] This approach resulted in a broad number of arms per star. Furthermore, the arms produced in these studies were far larger than the lengths necessary for synthesizing star-shaped oligomers. There is no evidence that it is possible to produce arms with a length on the order of a few monomer units with this method. For this reason, the core first approach was selected for the work that follows.

1.2.4.1 Core First Star Polymers via ATRP

The first star polymer synthesized by ATRP followed the core first approach, utilizing a hexakis(bromomethyl)benzene multifunctional initiator.[12] This material had low polydispersity (M_w/M_n = 1.23) and a molecular weight of 62.4 kg/mol, roughly an order of magnitude larger than a star oligomer. Over the next few years, many researchers reported the use of diverse cores to produce star polyacrylates,[13, 101-103] polymethacrylates,[13, 103-113] and polystyrene.[12, 13, 106, 113-116] In these studies, the existence of star oligomers is occasionally demonstrated with the initial data point of a kinetics plot. However, the isolation of star oligomers as a reproducible product is never reported.

1.2.4.2 The Path to Star-Shaped Oligomers

Haddleton et al. have previously reported the synthesis of linear methyl methacrylate oligomers from the initiator ethyl 2-bromoisobutyrate via ATRP,[112] although this was not the stated purpose of the study. In their work, 400:1 and 200:1 ratios of monomer to initiator were utilized. An aliquot polymerized for 1 hour at the 400:1 monomer ratio had a Mn = 1.0 kg/mol, DP_n = 10. In an aliquot polymerized for 2 hours at the 200:1 monomer ratio, the measured Mn = 2.5 kg/mol, DP_n = 25. Both polymerizations followed pseudo-first-order reaction kinetics. They exhibited an offset time of 50 minutes. In addition, molecular weight, conversion plots were not perfectly linear. Aliquots around 20% conversion were a higher molecular weight than predicted and later aliquots exhibited lower molecular weight than predicted.

Following their work with the 2-bromoisobutyrate initiator, Haddleton et al. demonstrated the synthesis of a multifunctional initiator from the similar initiator 2-bromo-2-methylpropanoyl bromide and glucose.[113] This versatile technique allows for the synthesis of multifunctional ATRP initiators from virtually any molecule with

multiple hydroxyl groups. It has since been used to synthesize saccharose and cyclodextrin based multifunctional ATRP initiators.[117-120] The star polymer synthesis technique found in the following work uses Haddleton's studies as a starting point. Whereas Haddleton's star polymerizations targeted higher molecular weights, the following work targets reproducible molecular weights on the order of Haddleton's initial oligomer aliquots from the linear study. At first, this was accomplished using a 400:1 monomer to multifunctional initiator ratio, rather than a 400:1 monomer to initiating site ratio. However, this greatly increased the rate of the reaction, which was slowed via dilution. Later synthesis increased the technique's complexity by further adjusting the ratio of monomer-initiator and transition metal catalyst as well as introducing new initiators and statistical copolymers. Reproducibility was enhanced by refinement of the polymerization initiation and termination procedures and by measuring conversion during propagation.

1.2.4.3 Complications in Star Polymerization

In addition, there are specific considerations that must be taken when synthesizing star polymers, which do not impact the synthesis of linear polymers by ATRP. Contaminants that simply reduce initiation efficiency in linear polymerizations will reduce the number of arms in a star. In addition, initiation sites can be blocked due to sterics, especially when bulkier monomers are polymerized.[109] As the polymerization continues, high molecular weight shoulders can appear in GPC traces, in some cases as early as 20% conversion. This is caused by the recombination of chain ends linking two stars together.[114] In linear polymers, this results in the termination of that molecule. However, stars have multiple chain ends and can continue to grow when one of them terminates, leading to a high molecular weight, dumbbell-shaped polymer side product.

The characterization of stars can also be a challenge. The molecular weight of linear polymers is typically characterized by GPC based on a polystyrene standard. A star's radius of gyration is smaller than an equivalent linear polymer and dependent on the star's functionality. These factors make GPC an imprecise characterization method for determining a star's molecular weight. However, GPC with light scattering and/or viscometry detectors have been used to correctly characterize the molecular weight of stars.[13] Other studies have characterized the molecular weight of stars by cleaving the arms from the star and characterizing them as linear polymers.[105] However, this method is impractical for star oligomers because it requires the purification of the arms, which are on the order of a few monomer units and are therefore difficult to handle. ^{1}H-NMR has also been used to characterize molecular weight; however this method is dependent on a system with monomer and core peaks that do not overlap.[107] All three of these methods show good agreement with theoretical values based on monomer conversion.

1.2.5 Summary

ATRP is an ideal polymerization technique for demonstrating the reproducible synthesis of star-shaped oligomers with well-defined architectures. Established procedures can produce varied multifunctional initiators that are compatible with copper catalyst. Synthesizing star oligomers with the core first approach requires a reduction in the polymerization rate. Fortunately, the kinetics of ATRP is well understood and there are several parameters that can be adjusted to slow the conversion of monomer.

1.3 Photoresists

The semiconductor industry's ability to continuously improve both the cost and speed of transistors, leading to more powerful processors year after year, is due to miniaturization. As size decreases, a greater number of transistors can fit into the same unit area, driving down cost per transistor. At the same time, decreasing the critical dimension (CD) of a transistor gate leads to faster switching speeds and shorter computation times. By developing the technology necessary for further miniaturization, the semiconductor industry has managed to keep pace with Moore's Law, which states that circuit densities double at regular intervals.[121]

1.3.1 Photolithography Overview

A key challenge towards further miniaturization originates from a material known as a photoresist that is used during the fabrication of semiconductors, specifically in the process of photolithography. During photolithography, a film of photoresist is applied to a silicon substrate, baked to remove residual application solvents and exposed with high intensity light through a mask, which causes a chemical change within the photoresist film and enables the removal of photoresist through a development step. The mask is designed to block light in some areas and transmit light in others, creating a pattern of exposed and unexposed regions throughout the film. A positive tone photoresist is initially insoluble and exposure renders it soluble in developer, leading to the selective removal of the exposed regions. In a negative tone photoresist, the film is initially soluble with exposure decreasing solubility in developer and allowing the unexposed regions to be selectively removed. Following development, additional processing, such as etching, can be performed to transfer patterns into the underlying substrate. Remaining photoresist is then stripped and the process repeated many times to build a working computer chip. (Figure 1-7)

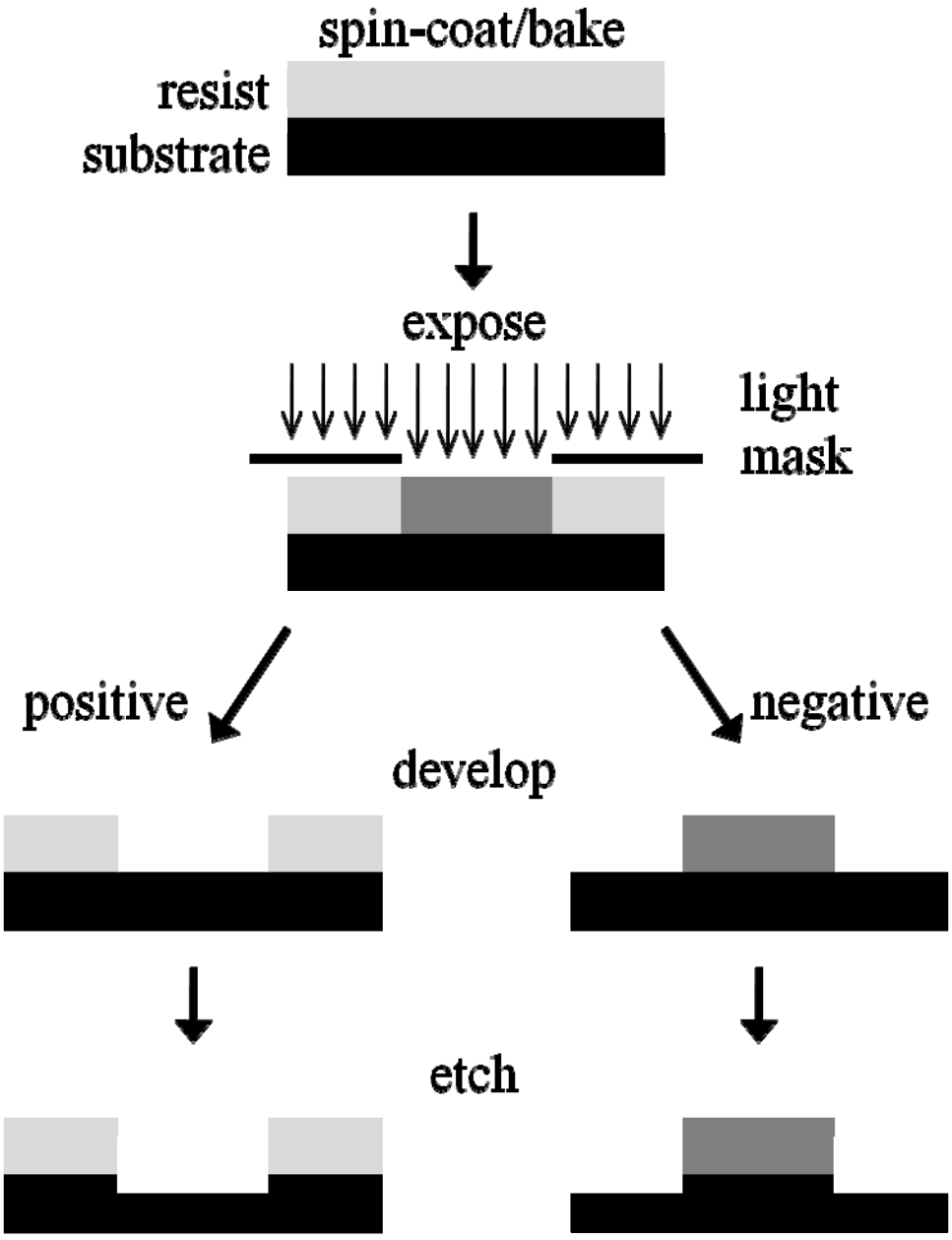

Figure 1-7. Conventional photolithographic process, adapted from reference.[60]

1.3.2 Brief History of Photoresists

Due to their cost, exposure tools tend to be the bottleneck during fabrication.[122] In order to increase throughput, more sensitive photoresists were designed that would require shorter exposure times. The diazonaphthoquinone (DNQ)/novolac resist contains two components: the novolac resin and a photoactive compound (PAC), DNQ.[123] By itself, the novolac resin is soluble in aqueous base developer. However, the DNQ molecule acts as a dissolution inhibitor, preventing the novolac from developing. When exposed to UV radiation the DNQ releases nitrogen and forms a carbene intermediate, which rearranges to a ketene and finally, in the presence of water, results in an indenecarboxylic acid.[124] (Figure 1-8) The indenecarboxylic acid is soluble in the base developer resulting in development contrast. The exposed region develops faster than the unexposed region and the system acts as a positive-tone resist. DNQ/novolac resists are able to achieve sub-0.5 μm features with i-line stepper tools.[60]

A tool's resolution, or the finest feature capable of being printed by that tool, is proportional to the wavelength of light divided by the tool's numerical aperture. For on-axis illumination the constant of proportionality is 0.5 while off-axis illumination gives a constant of 0.25.[122] The light from i-line tools has a wavelength of 365 nm. In order to achieve finer resolutions, short wavelengths are required. A krypton fluoride (KrF) light source can produce 248 nm light. However, the DNQ/novolac resist absorbs light in this region, resulting in less light reaching the DNQ at the bottom of the resist. Efforts to discover a replacement resin and dissolution inhibitor combination that was less absorbing at this wavelength met with only limited success.[60]

A breakthrough occurred in 1982 when chemical amplification was proposed by Ito, Willson and Fréchet.[125, 126] A photoacid generator (PAG) additive in the

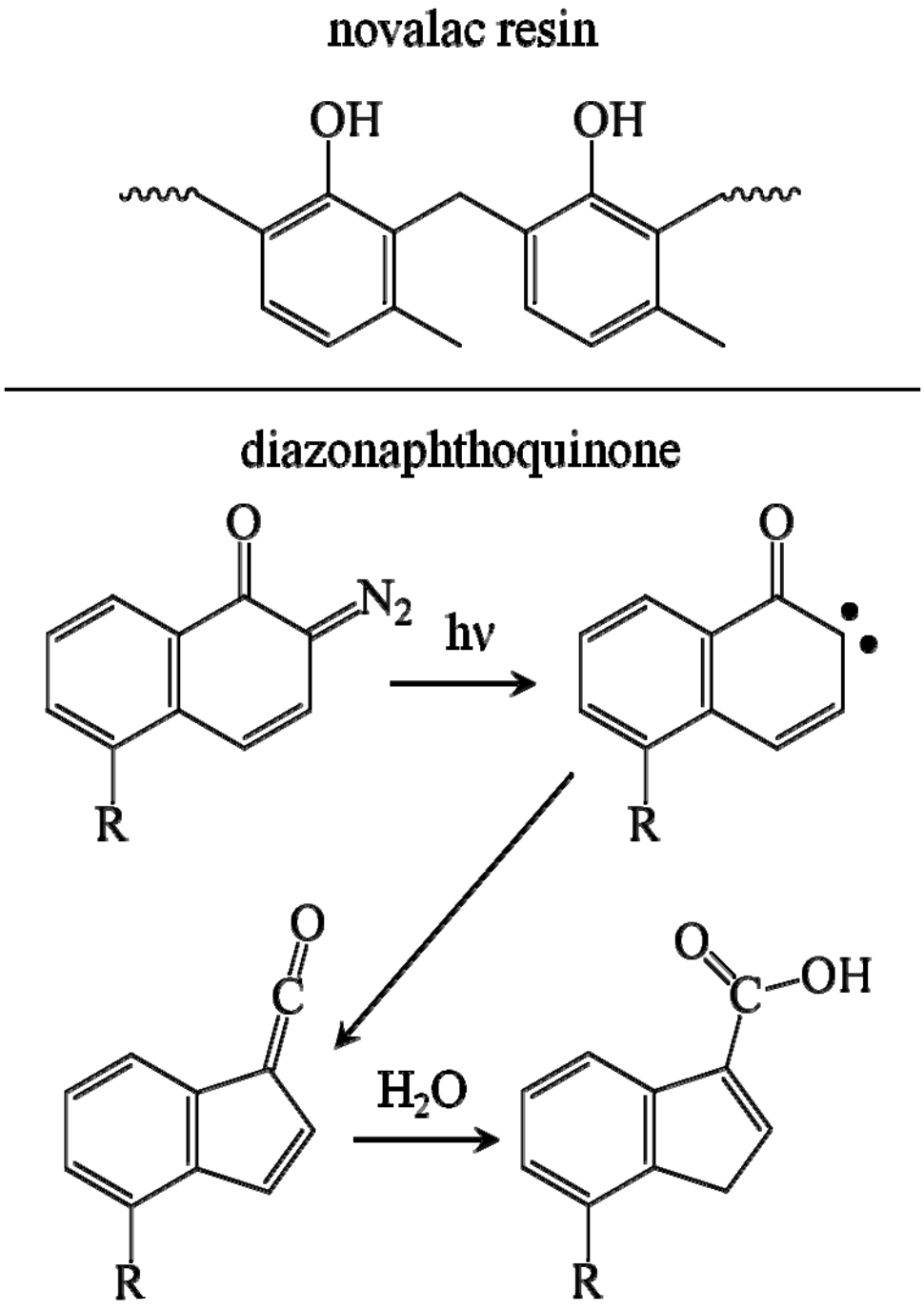

Figure 1-8. DNQ/Novalak resist, adapted from reference.[60]

photoresist film was used to generate acid upon exposure. Following exposure, the generated acid could catalyze multiple chemical reactions in the photoresist during a post-exposure bake (PEB) step. (Figure 1-9) Devices were miniaturized to the 130 nm node using chemically amplified resists with KrF exposure tools. Sub-130 nm devices have been manufactured using argon fluoride (ArF) light sources with chemically amplified resists transparent to 193 nm wavelength light. Fluorine (F_2) excimer lasers produce 157 nm light.[60] Rather than moving to the 157 nm wavelength, the numerical aperture of the tools was increased. Current devices (32 nm node) are manufactured using 193 nm wavelength light that is passed through an immersion fluid to increase the numerical aperture.

1.3.3 KrF (248nm) Resists

The earliest chemically amplified photoresists used in manufacturing consisted of a triphenylsulfonium hexafluoroantimonate PAG and poly(4-tert-butoxycarbonyloxystyrene) (PBOCST).[127] The aqueous base soluble phenolic functionality is protected by an acid-labile group. In the presence of acid and heat, deprotection of the *tert*-butoxycarbonyl (tBOC) acid-labile group occurs, generating carbon dioxide, isobutene and a new proton. (Figure 1-10) In this manner, a single photoacid can deprotect approximately 1000 acid-labile groups, vastly increasing the quantum yield over conventional photoresists.[128] The resulting poly(4-hydroxystyrene) PHOST resin is soluble in aqueous base developer. Polar organic solvents can also be used to obtain a positive-tone image, while negative-tone images can be obtained using non-polar organic solvents.[60] It is worth noting that the polymer end group can impact the chemical amplification reaction.[129]

It is difficult to find a single monomer unit that contains all of the properties necessary to make a good photoresist. Consequently, modern photoresists are

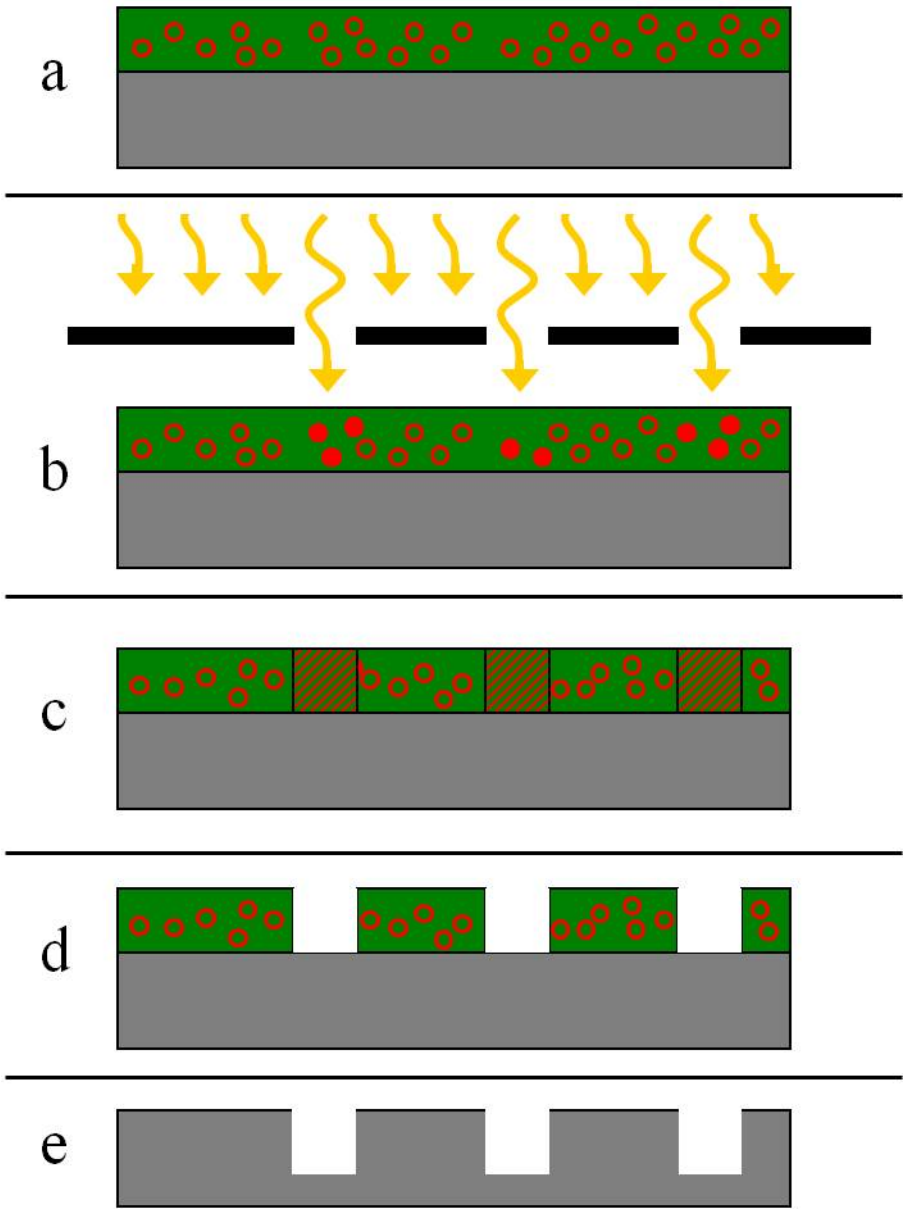

Figure 1-9. The photolithographic process for a positive tone, chemically amplified photoresist, viewed sideways. (a) Spin-coat & post apply bake. (b) Exposure. (c) Post-exposure bake. (d) Development. (e) Etching and stripping.

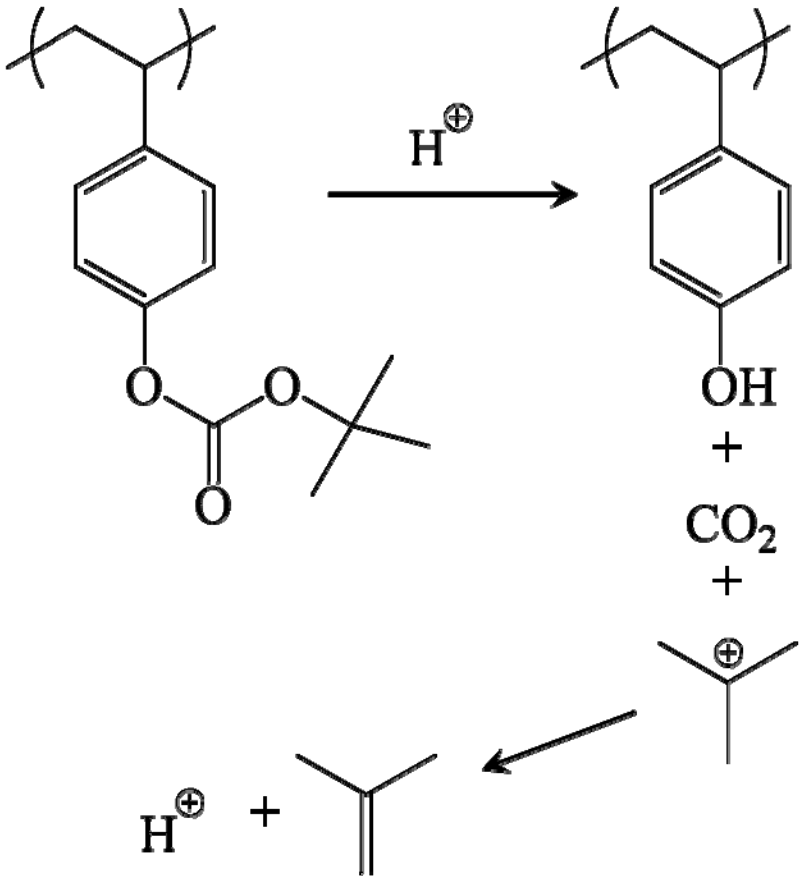

Figure 1-10. Chemical amplification scheme for poly(4-tert-butoxycarbonyloxystyrene), adapted from reference.[60]

copolymers. Early copolymer resists consisted of PBOCST copolymerized with maleimide derivatives. [130, 131] However, it wasn't until styrene based monomers were copolymerized with methacrylate based monomers that the importance of copolymerization was demonstrated. Such copolymer resists required fewer deprotection reactions to generate a chemical switch, thereby increasing both contrast and sensitivity.[132] The inclusion of methacrylates, which generally exhibit poor dry etch resistance, did not significantly degrade the etch resistance of the copolymer. This is due to an energy quenching "sponge effect" exhibited by aromatic groups on the surrounding material, over a length scale equal to several monomer units.[133, 134]

Copolymers of PHOST and PBOCST can be prepared several ways,[135, 136] although the predominant method is the partial protection of PHOST.[137] 20-30% tBOC protection is a typical value.[60] The presence of unprotected PHOST can reduce the thermal deprotection temperature to 130 °C, restricting PAB and PEB temperatures.[138] Free volume in the film allowed airborne bases, such as N-methylpyrrolidone, to diffuse into the surface of the film where they neutralized acid, preventing deprotection and rendering the surface insoluble (T-topping).[139] The environmentally stable chemical amplification photoresist (ESCAP) is a statistical copolymer of 4-hydroxystyrene and tert-butyl acrylate.[140] It does not thermally deprotect until 180 °C. ESCAP can therefore undergo PAB at a sufficient temperature to reduce the free volume in the film, preventing airborne contaminants from entering the resist.[141, 142] ESCAP type resists form the bulk of commercial KrF photoresists.

1.3.4 ArF (193nm) Resists

Aromatic groups absorb 193 nm light. This required the chemically amplified photoresist to be redesigned without PHOST to continue miniaturization. Polymethacrylates are transparent at the 193 nm wavelength but do not exhibit

sufficient etch resistance. Early resists included a terpolymer of tert-butyl methacrylate (tBMA), methyl methacrylate (MMA), and methacrylic acid (MAA).[143]

Incorporating alicyclic structures into polymethacrylate as a pendent group was found to improve dry etch resistance without the absorption of aromatics.[144-146] Adamantyl methacrylate has a dry etch resistance similar to novolac.[60] However, the adamantyl group is extremely non-polar, which can result in poor adhesion and crack formation.[144, 146, 147] This can be alleviated by incorporating a hydroxyl group onto the adamantyl structure.[148, 149] Lactone rings, which undergo hydrolysis in aqueous base, can be incorporated onto a methacrylate to further enhance polarity.[150] Finally, a methyl adamantyl group can serve as the acid labile group in a chemically amplified resist and also improve etch performance.[151, 152]

1.3.5 Next Generation Resists

For now, 193 immersion technology continues to be the workhorse of the semiconductor industry. Double patterning, which extends the resolution limit by working with 1:3 line:space features instead of dense features, may extend 193 immersion further. However, double patterning is time intensive. It requires twice as many processing steps and is also sensitive to overlay errors.[153] Double exposure techniques are currently being researched that could alleviate these problems.[154]

The next exposure source being investigated for future technology nodes is extreme ultraviolet (EUV), 13.4 nm wavelength light. EUV photons are high energy by virtue of their short wavelength. This will reduce the number of photons and exacerbate shot noise due to Poisson statistics.[155] Despite this, EUV tools are currently being developed, however the resists are not ready.[156]

Photoresists that operate under a different mechanism than chemical amplification are also being researched. Directed self-assembly using block copolymers has

attracted considerable interest. However, the ability to create arbitrary features does not yet exist. Ongoing research into directing patterns using sparse features is underway.[157, 158]

1.3.6 Polyelectrolyte Behavior of Photoresists

While rarely referred to as such, exposed positive-tone chemically amplified photoresists are weak polyelectrolytes. Specifically, they are weak polyelectrolytes with a polymer backbone that is insoluble in the developer. As the chemically amplified, deprotection reaction progresses more sites along the photoresist become available for charging in aqueous base developer. The repulsion of charges can be so strong that it can force the poorly soluble polymer chain to uncoil. Charges build along the polymer in locations that minimizes the charge density. This leads to charged and uncharged regions. The polymer backbone in the charged regions extends, while the uncharged regions remain coiled resulting in a "pearl necklace" conformation.[159-162] Synthetic beaded chains, comprised of small stars linked by linear regions have recently been synthesized to study this transition.[163]

The repulsion of like charges is a potent thermodynamic term compared to the chemical term that causes a poorly soluble polymer to remain coiled in solvent. The difference in terms is sufficient that with n charges a photoresist might remain coiled (and undeveloped) but at n+1 charges a photoresist might completely extend (undergoing dissolution and developing). The intermediate pearl necklace conformations may be skipped if the chain length is sufficiently short. This is one of the reasons why chemically amplified photoresists can exhibit high contrast; a single charge can make the difference between a photoresist developing or remaining in the sidewall. However, the large expansion between the coiled photoresist (size scales as $\sqrt{DP}$) and uncoiled photoresist (size scales as DP) and the rapid speed of the

transformation suggests a strong force at the sidewall. This may damage the sidewall and increase roughness. [164] In this regard, star resists are an interesting alternative. As discussed in section 1.1.5, star polyelectrolytes expand less than equivalent linear polyelectrolytes because a star's expansion is restricted by arm length. This expansion might be further reduced with multivalent developer additives, a subject currently being investigated.[165]

1.3.7 Summary

Since its invention in 1982, chemically amplified photoresists have been the material of choice for fabricating high-resolution features using photolithography. Historically, the design of photoresists has been dependent on the light source. For several technology nodes the light source has remained 193 nm. However, as lithographers discover new methods to push technology to finer resolutions, a new problem is arising that will require a revolution in photoresist design: roughness.

1.4 Roughness

The International Technology Roadmap for Semiconductors (ITRS) identifies photoresist roughness as a key, unresolved challenge facing the continued miniaturization of transistors.[166] Roughness in the photoresist is transferred during the etch processes and leads to roughness in the final device.[167] In moving towards the long term goal of inventing new photoresists with improved roughness, it is important to understand how roughness can be characterized.

1.4.1 Line Edge Roughness and Line Width Roughness

A measurement for side-wall roughness can be calculated from a top-down SEM image of lines and spaces. There are many metrics for roughness and the two most

common are line edge roughness (LER) and line width roughness (LWR). Both are descriptions of statistical deviation along the length of a line, generally expressed as a three sigma value. LER measures the positional deviation perpendicular to a line's edge from the line's average position. LWR measures the deviation of a line's width from its average width. Both of these measurements examine average position or width rather than the intended position or width. As lines of shorter length are examined, the average values begin to deviate strongly from the intended values, artificially reducing the measured values of LER and LWR.[168]

This can be illustrated through an example involving an artificial line edge generated by the sum of three sin waves with different periods and magnitudes. (Figure 1-11) When the entire length of the line is examined, the average position occurs at 0.07 arbitrary units (a.u.) in the x-direction and there is a standard deviation of 1.61 a.u. from the average. However, if the same line is divided into four equal sections, each section will have its own average position and standard deviation. The average positions, from top to bottom, become 1.51, -1.42, 1.27 and -1.09 a.u. with standard deviations of 0.66, 0.79, 0.96 and 1.11 a.u., respectively. The change in average position effectively reduces the deviation experienced along the line. A clear example of this occurs at the point of greatest deviation in the positive-x direction. The deviation at this point is 3.1 a.u. from the line's average position but only 1.9 a.u. from the section's average position. This demonstrates a serious shortcoming of both LER and LWR, their value changes with the length of the measurement.

1.4.2 Sigma Versus Length and Length Independent Roughness Metrics

An important function known as sigma versus length or SVL can be obtained when one examines how LER and LWR change with the measured line edge length of a real test pattern. (Figure 1-12) When the data is plotted on a log scale for both the

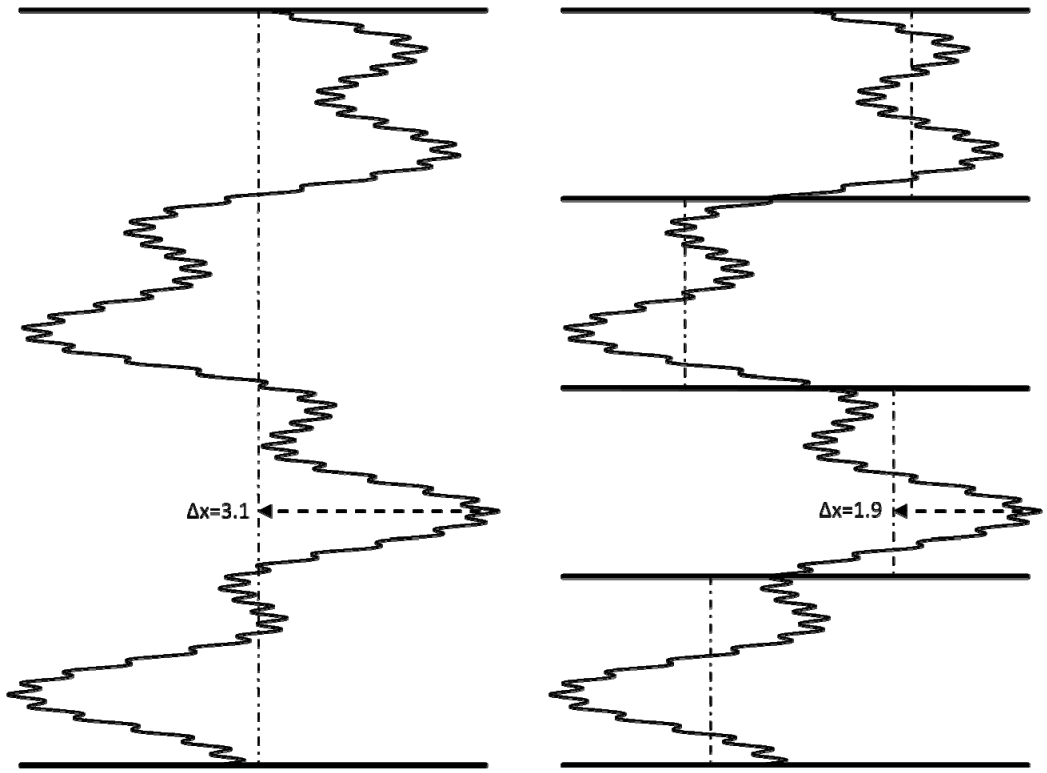

Figure 1-11. A simulated rough line edge generated from the sum of three sin waves. Deviation from the average (dash dot) decreases when shorter fragments of the line are examined rather than the full line length.

Figure 1-12. Processed SEM image for a linear photoresist comprised of 50% GBLMA, 30% MAMA and 20% HAMA with a number average degree of polymerization of 19.2. The resist was spincoated on a primed silicon to a thickness of 50 nm. The resulting film was baked at 130 °C for 5 minutes. 96 nm half-pitch lines and spaces were exposed with a 100kV electron beam with a FWHM beam diameter of approximately 4.3 nm, and a scan pitch of 6 nm at a current of 500 pA and a shot time that yielded a dose of 283 μC/cm2. A proximity correction to account for electron scattering was applied using the program Layout Beamer with data from a Monte Carlo simulation using the program Sceleton. Following exposure the film was baked for 30s at 116 °C and developed for 60 seconds using a double puddle technique in an industrial developer containing 0.26N TMAH and surfactants to obtain a positive tone image. The film was sputtered with gold/palladium and a 3072 x 2304 pixel resolution image was recorded in a SEM operated at 1.5 kV with a 2.5mm working distance and a magnification of 40 000x. This image was processed using SuMMIT software from EUVL technologies to locate the line edges and to export a black and white image where the lines appear white and the trenches or spaces between lines appear black.

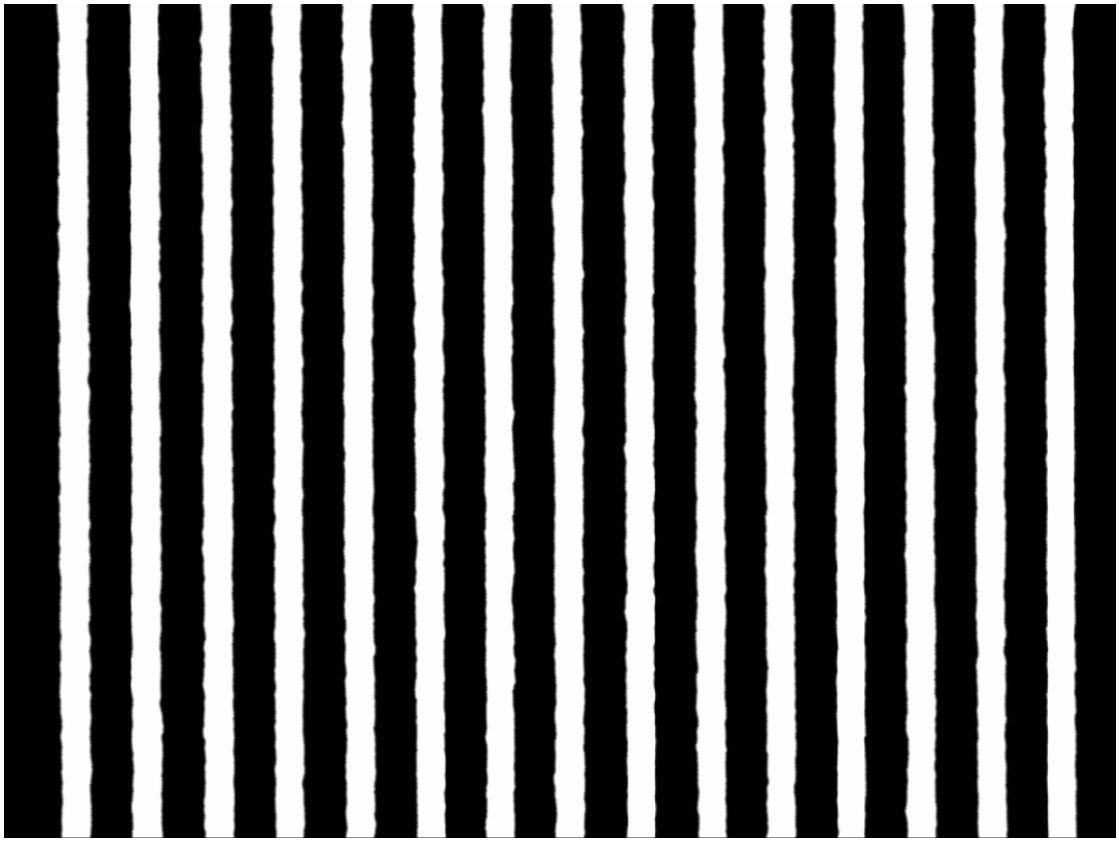

vertical LWR axis and the horizontal line length axis a linear trend can be observed at small line lengths, in this case below 17.6 nm. This length is called the correlation length (ξ or L_c). The slope of the linear region below L_c is known as the roughness exponent (α) and it is 0.5 in this example. For line lengths greater than the correlation length, the measured roughness begins to saturate, approaching a maximum at a length that is typically between 6-10 times L_c.[169-171] (Figure 1-13) For this reason, the ITRS recommends measuring line lengths of at least 2 microns to determine LER and LWR.[166]

Another metric exists for measuring roughness that is independent of measured line length. As the measured line length increases CD variation, the statistical deviation in average line width of the line, decreases. There exists a quadratic relationship between LWR and CD variation. The sum of their squares results in a constant value that is independent of the measured line length. The square root of this constant is known as the infinite LWR (iLWR, LWR_{inf}, LWR_{∞}). A similar metric exists for infinite LER (iLER, LER_{inf}, LER_{∞}). In addition to producing a useful metric, this relationship explains the importance of roughness for semiconductor manufacturing. (Figure 1-14) The shrinking of transistor width is similar to reducing the length of the measured line edge. This artificially reduces roughness by increasing CD variation thereby resulting in greater deviation of transistor gate length. In addition, as the gate length shrinks, this deviation becomes a greater percentage of the total gate length, increasing its contribution to the transistor performance. Therefore, roughness must be reduced to shrink either the transistor width or gate length without adversely impacting device performance.[171-173]

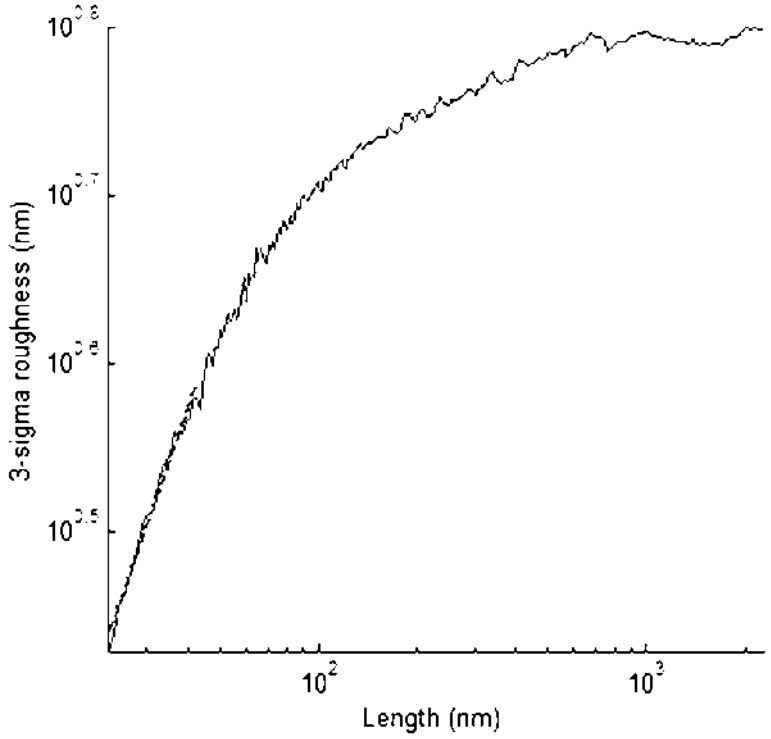

Figure 1-13. Sigma Versus Length (SVL) plot of LWR corresponding to the sample reported in Figure 1-12.

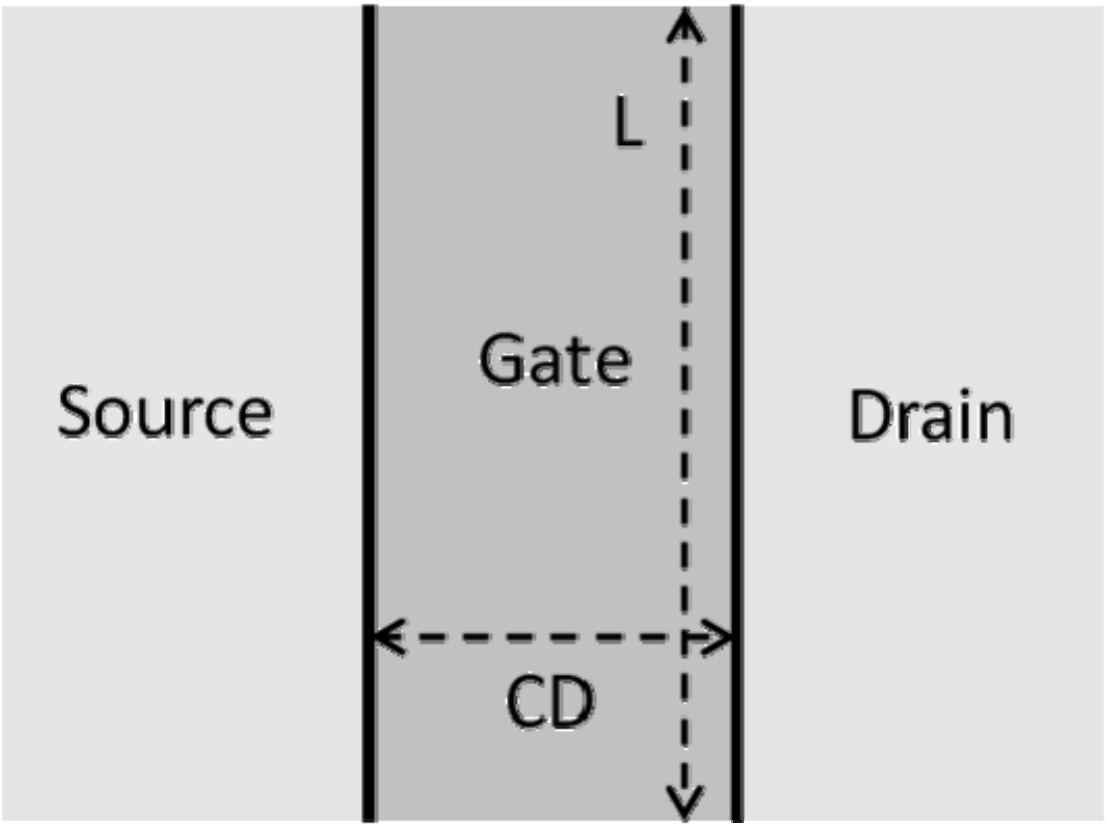

Figure 1-14. Simple transistor diagram depicting the relationship between measured line length (L) to transistor width and the critical dimension (CD) and CD variation to gate length for real semiconductor devices. Adapted from reference.[172]

1.4.3 Height-Height Correlation Function and Fractal Dimension

The SVL plot is a convenient model for discussing the relationship between transistor shrinking, roughness and CD variation. However, there exists a function known as a Height-Height Correlation Function (G(r) or HHCF) that can provide a more rigorous mathematical model of the line edge. [See Equation 1-3] The HHCF describes the perpendicular displacement between a pair of points that are offset by a distance r. Periodic patterns of displacement can be observed by measuring all displacements for all pairs of points. (Figure 1-15) The HHCF reaches a maximum at a value equal to $\sigma\sqrt{2}$ where σ is the statistical one sigma deviation in LWR (or LER for a HHCF of line edges). Similar to SVL, the HHCF exhibits a characteristic correlation length and roughness exponent. A rigorous mathematical definition for the correlation length exists at $G(L_c) = \sigma\sqrt{2(1-1/e)}$, in this case, occurring at 22.35 nm. Using this mathematically defined correlation length, a precise measurement for alpha can be determined, in this example 0.61. It is worth noting that for small offset values the HHCF gives a very accurate value due to the large number of pairs that can be sampled for each offset. At higher offset values, there are few pairs of points offset by that amount, resulting in the observed fluctuations in Figure 1-15. Therefore, high accuracy measurements in the large offset region can only be achieved by measuring many lines.[168, 169, 171, 174]

$$G(md)=\left[\frac{1}{N-m}\sum_{i=1}^{N-m}(\delta_{i+m}-\delta_i)^2\right]^{1/2} \qquad \text{Equation 1-3}$$

The HHCF plot for the edges and widths of lithographic lines and spaces is consistent with a self-affine fractal, which are characterized by their anisotropic scaling.[175] At short length scales (length scaled below the correlation length) the fractal dimension (d_f) is equal to $2-\alpha$ (and for two-dimensional surfaces $d_f=3-\alpha$).[172]

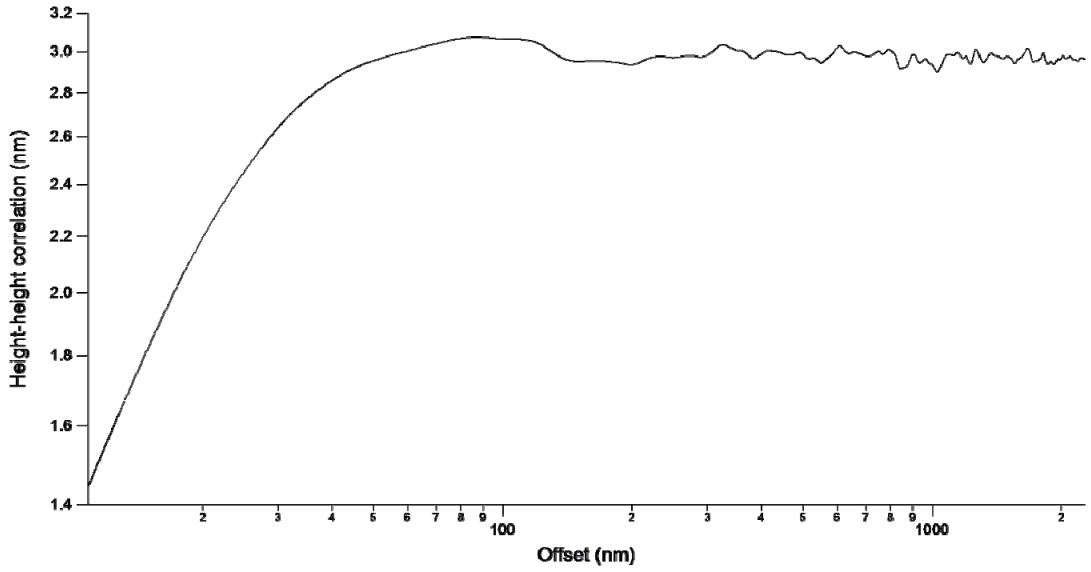

Figure 1-15. Height-Height Correlation Function (HHCF) plot corresponding to the sample reported in Figure 1-12.

At length scales much larger than the correlation length d_f=1. Therefore, an α approaching 1 is desirable, as this will lead to a fractal dimension that approaches 1 and a smoother line.[168]

1.4.4 Power Spectral Density

A final function that is used to describe roughness is the power spectral density (P(k) or PSD), which is a Fourier transformation that describes roughness as the sum of waves with frequency k and amplitude P. (Figure 1-16) This function provides the most direct spatial information. As such, it can be useful in interpreting the underlying cause of roughness differences between different resists or processing conditions. Similar to the log-log SVL and HHCF plots, there exists a linear region, which saturates to a maximum. However, as the x-axis is in frequency space the linear slope occurs in the high frequency region and begins to saturate below a value of 1/ξ. Furthermore, the linear slope is –(2α+1) not α. However, the L_c and α measured by PSD can sometimes differ significantly from the values determined by SVL and HHCF.[171] One reason for this is that PSD gives the noisiest plot. This is because there is less data to examine when measuring frequency rather than length or offset, especially in the low frequency regime.[171, 173, 176]

1.4.5 SEM Artifacts and Image Processing

Another important feature found in the PSD is a constant minimum that occurs at high frequencies. This minimum is a result of SEM noise. When measuring roughness this region should be filtered out.[177] SEM technique can have additional impact on the roughness measurements. In a study examining the impact of pixel size on roughness, pixel sizes between 0.5nm and 4nm were examined and found to have an impact on α but not on ξ. Large pixel sizes cause a decrease (roughening) in α due to

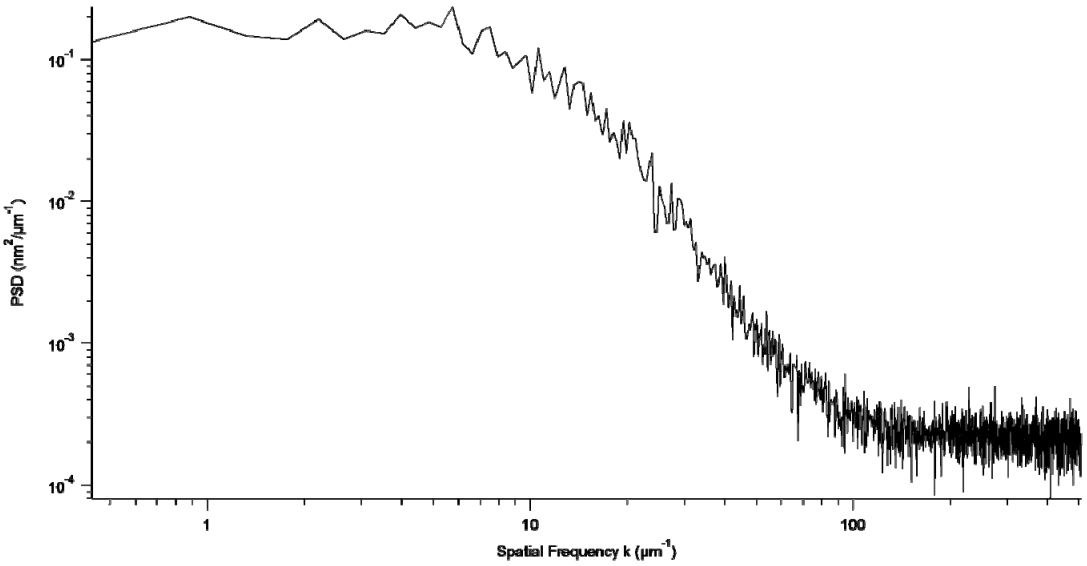

Figure 1-16. Power Spectral Density (PSD) plot corresponding to the sample reported in Figure 1-12.

the coarser image.[168] The ITRS calls for pixel sizes no larger than 4nm as it is clear that roughness cannot be observed at low magnifications. In addition to magnification, focus and stigmation variation have been shown to increase high frequency roughness as these settings are adjusted from their nominal values.[176]

Prior to processing, the image shown in Figure 1-12 appears very different. (Figure 1-17) Rather than black spaces and white lines a grey-scale image is obtained. The spaces still appear darker than the lines, however the brightest position tends towards the line edge, rather than the center of the line. Furthermore, if one examines the SEM image at a pixel level, the edge is found to be noisy. Line edge detection algorithms must be used to locate the edge. A standard algorithm will examine the grayscale number for each pixel (integers ranging from 0-255) and select a threshold value that represents the line edge.[169] Each horizontal line of pixels (perpendicular to the line edge) is smoothed using, for example, a Gaussian noise-smoothing filter with a specified width to eliminate the noise and correctly identify the line edge. The three roughness parameters (σ, ξ, α) can be impacted if the filter width or threshold is too low. They have been observed to be independent when the filter width is greater than 3 pixels and the threshold greater than 30% of the maximum intensity.[174] The image in Figure 1-17 was analyzed with a 6 pixel wide Gaussian noise-smoothing filter and a 50% edge detection threshold. No smoothing is performed in the direction parallel to the line edge.

1.4.6 Photoresists and Roughness

The discussion thus far has been limited to the case of measuring the roughness for a set of lines and spaces. However, measuring the roughness of a material is a much more challenging problem as roughness is not only dependent on the material

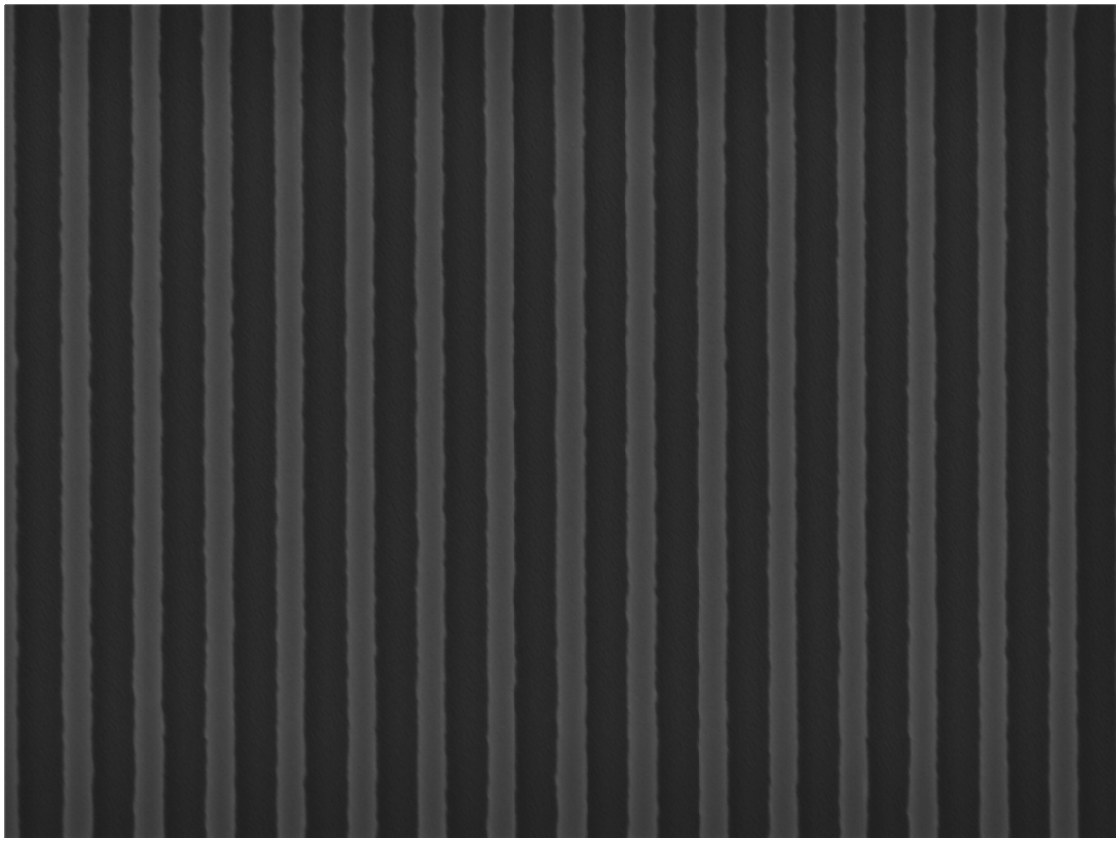

Figure 1-17. SEM image of 1-4-2 prior to image processing to identify line edges.

composition but also on how that material is processed. The lithographic PEB step is of particular importance in chemically amplified resists. In the PEB step, acid generated during the exposure both diffuses through the resist film and catalyzes the chemical deprotections that result in a solubility switch.[60] An optimal PEB will enable the acid to diffuse over a length scale that smoothes statistical deviations in acid concentration. However, if the acid is allowed to diffuse too far, the diffusion-deprotection front can progress at different rates along a line edge leading to an increase in low frequency roughness.[122] Only the roughness exponent has been observed as highly invariant with regards to most processing parameters and is regarded as characteristic of the material composition at the sidewall. As such, for a given resist the roughness exponent only changes when the developer or development time changes, revealing in a sidewall composition with a different degree of deprotection.[170]

As roughness is highly dependent on processing, comparing the roughness of different materials is not a trivial task. Monte Carlo simulations have been used to demonstrate that lower molecular weights and higher branching can lead to lower roughness.[178, 179] However, such results are difficult to prove experimentally. Similar experimental studies tend to report a single number for the roughness of a resist and often do not disclose what method, if any, was used to determine that the reported roughness is, in fact, the best roughness achievable for that material.[170, 180]

Processing conditions can impact more than simply the roughness of the resist. For example, the CD of a developed feature is not necessarily the same as the width of the exposed area. The difference between the exposure and final CD is known as pattern blur or simply blur. Small amounts of blur are not detrimental to a photoresist, as the

exposure dimensions can be shrunk by a similar amount to achieve the target CD. However, large blur distances are problematic because they can be resolution limiting. Under many conditions, roughness can be observed to decrease as blur increases. (Figure 1-18) For this reason, it is important to compare the roughness of photoresists that have blurred a similar distance.

When measuring the roughness of a resist, many sets of processing conditions must be measured. For example, when the PEB temperature is increased, the exposure dose of the processing window decreases. Less acid must be generated to achieve the same deprotection at the higher PEB temperature. Generally, large distances of blur are observed near the processing window's high dose limit for a given PEB, while short distances of blur are observed near the low dose limit. The roughness for a given blurring distance is different for each PEB temperature. An optimal PEB temperature can be defined as the temperature at which the smoothest lines are observed at the shortest blur distances. As the PEB temperature is either decreased or increased from the optimal temperature, greater blurring is required to maintain the same roughness. This can be visually demonstrated with an iso-roughness contour plot of PEB temperature and blur. (Figure 1-19)

The roughness performance of multiple resists can therefore be contrasted by first identifying the optimal PEB temperature for each resist. Once this is accomplished, the roughness of patterns processed at the optimal PEB temperature can be directly contrasted with other patterns blurred the same distance. Without identifying the optimal PEB temperature it is not possible to compare the roughness of different resists. Similarly, contrasting patterns that are blurred different amounts can lead to inaccurate comparisons.

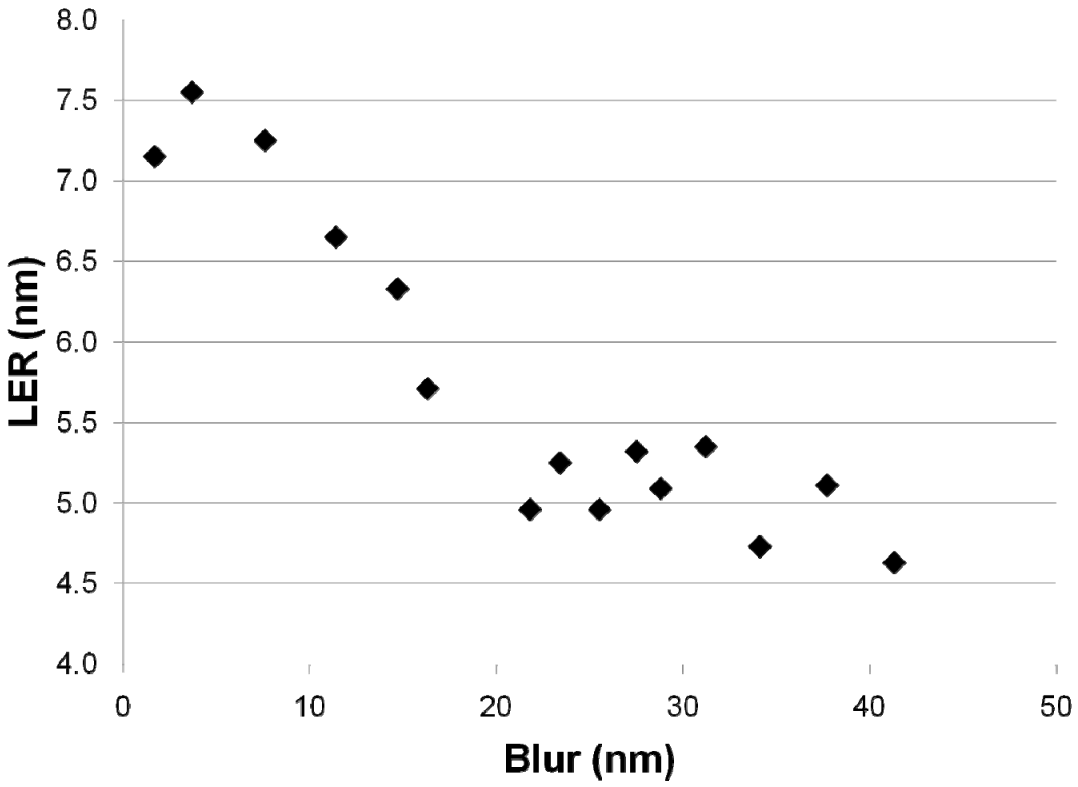

Figure 1-18. Sample plot of LER and blur for a resist with dose varied but other processing conditions held constant.

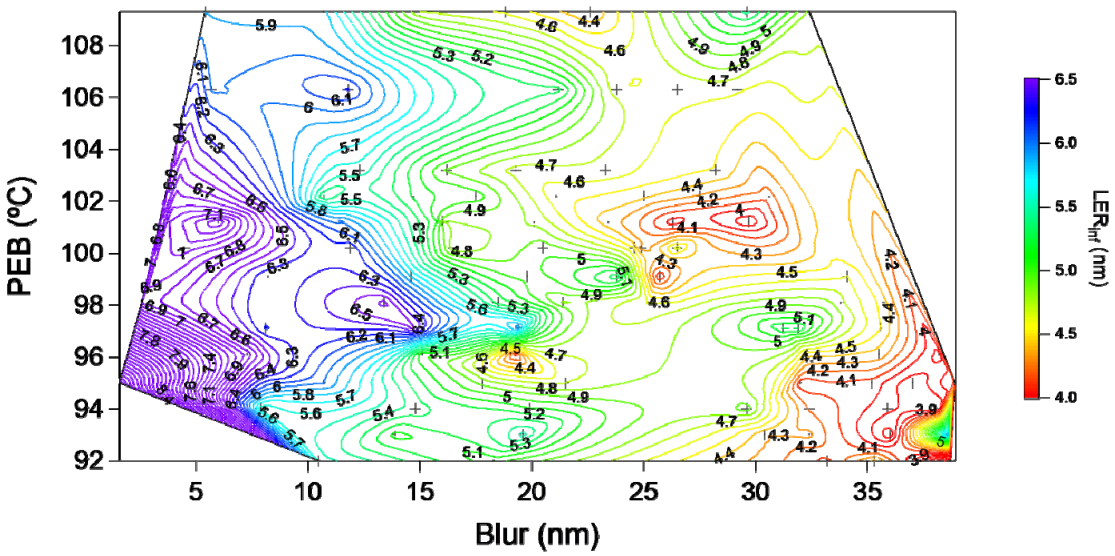

Figure 1-19. Iso-roughness contour plot of LER_{inf} demonstrating an optimum PEB at 101 °C. Real data points are labeled with a + marker. A triangulation algorithm is used to calculate the roughness between data points. Data boundaries are indicated with a solid black line. Triangulation performed with IGOR Pro software.

1.4.7 Summary

The most common metrics for reporting roughness, LER and LWR, are dependent on measurement length and leave out important spatial information that can be of assistance in understanding roughness behavior. The two spatial roughness parameters, the correlation length and roughness exponent, stem from the self-affine fractal behavior of a photoresist's sidewall and can be observed in SVL, HHCF and PSD plots. The characterization of a material's roughness can present a substantial challenge as the roughness metrics are dependent on not just the material's composition but also its processing and the SEM technique and image analysis algorithm used to perform the roughness measurement.

REFERENCES

1. *Polymer*, in *Oxford English Dictionary*. 2000. Internet resource., Oxford University Press: Oxford, England.

2. Agency, U.S.E.P. *Wastes - Resource Conservation - Common Wastes & Materials - Plastics*. 2009; Available from: http://www.epa.gov/osw/conserve/materials/plastics.htm.

3. Cowie, J.M.G., *Polymers: Chemistry & Physics of Modern Materials*. 2nd edition ed. 1991, Boca Rotan, Florida: CRC Press.

4. Odian, G., *Principles of Polymerization, Fourth Edition*. 2004, Hoboken, New Jersey: John Wiley & Sons, Inc.

5. McCrum, N.G., C.P. Buckley, and C.B. Bucknall, *Principles of Polymer Engineering*. Second Edition ed. 2003, Oxford: Oxford University Press.

6. Bates, F.S. and G.H. Fredrickson, *Block Copolymers - Designer Soft Materials.* Physics Today, 1999. **52**(2): p. 32-38.

7. Strobl, G.R., *The Physics of Polymers: Concepts for Understanding Their Structures and Behavior*. 2nd Corrected Edition ed. 1997, Berlin: Springer.

8. Rubinstein, M. and R.H. Colby, *Polymer Physics*. 2003: Oxford University Press.

9. Morton, M., et al., *Preparation and properties of monodisperse branched polystyrene.* Journal of Polymer Science, 1962. **57**(165): p. 471-482.

10. Simms, J.A. and H.J. Spinelli, *Macromolecular design of polymeric materials*, ed. K. Hatada, T. Kitayama, and O. Vogl. 1997, New York: Marcel Dekker.

11. Rein, D., P. Rempp, and P.J. Lutz, *Recent developments in the field of star-shaped polymers.* Makromolekulare Chemie, Macromolecular Symposia, 1993. **67 (EPF Workshop on Anionic Polymerization and Related Processes, 1992)**: p. 237-249.

12. Wang, J.-S., D. Greszta, and K. Matyjaszewski, *Atom transfer radical polymerization (ATRP): A new approach towards well-defined (co)polymers.* Polymeric Materials Science and Engineering, 1995. **73**: p. 416-417.

13. Matyjaszewski, K., et al., *Synthesis and Characterization of Star Polymers with Varying Arm Number, Length and Composition from Organic and Hybrid Inorganic/Organic Multifunctional Initiators.* Macromolecules, 1999. **32**(20): p. 6526-6535.

14. Likos, C.N., et al., *Star Polymers Viewed as Ultrasoft Colloidal Particles.* Physical Review Letters, 1998. **80**(20): p. 4450-4453.

15. Likos, C.N., *Effective Interactions in Soft Condensed Matter Physics.* Physics Reports, 2001. **348**: p. 267-439.

16. Likos, C.N. and H.M. Harreis, *Star polymers: from conformations to interactions to phase diagrams.* Condensed Matter Physics, 2002. **29**: p. 173-200.

17. Likos, C.N., *Soft matter with soft particles.* Soft Matter, 2006. **2**: p. 478-498.

18. Vlassopoulos, D., *Colloidal star polymers: Models for studying dynamically arrested states in soft matter.* Journal of Polymer Science, Part B: Polymer Physics, 2004. **42**(16): p. 2931-2941.

19. Daoud, M. and J.P. Cotton, *Star-shaped polymers: a model for the conformation and its concentration dependence.* Journal of Physics, 1982. **43**(3): p. 531-538.

20. Jusufi, A., M. Watzlawek, and H. Löwen, *Effective Interaction between Star Polymers.* Macromolecules, 1999. **32**(13): p. 4470-4473.

21. Freire, J.J., et al., *Monte Carlo calculations for linear and star polymers with intramolecular interactions. 1. Dimensions.* Macromolecules, 1986. **19**(2): p. 452-457.

22. Freire, J.J., A. Rey, and J. Garcia de la Torre, *Monte Carlo calculations for linear and star polymers with intramolecular interactions. 2. Nonpreaveraged study of hydrodynamic properties at the θ state.* Macromolecules, 1986. **19**(2): p. 457-462.

23. Batoulis, J. and K. Kremer, *Thermodynamic properties of star polymers: good solvents.* Macromolecules, 1989. **22**(11): p. 4277-4285.

24. Zifferer, G., *Shape asymmetry of star-branched random walks with many arms.* Journal of Chemical Physics, 1995. **102**(9): p. 3720-3726.

25. Zifferer, G., *Shape asymmetry of star-branched random walks and nonreversal random walks.* Macromolecular Theory and Simulations, 1997. **6**(2): p. 381-392.

26. Zifferer, G., *Shape distribution and correlation between size and shape of star-branched tetrahedral lattice chains in athermal and theta systems.* Journal of Chemical Physics, 1999. **110**(9): p. 4668-4677.

27. Sikorski, A. and P. Romiszowski, *Shape of star-branched polymers at various solvent conditions. A computer simulation study.* Journal of Chemical Physics, 1998. **109**(14): p. 6169-6174.

28. Grest, G.S., K. Kremer, and T.A. Witten, *Structure of many arm star polymers: a molecular dynamics simulation.* Macromolecules, 1987. **20**(6): p. 1376-1383.

29. Grest, G.S., *Structure of Many-Arm Star Polymers in Solvents of Varying Quality: A Molecular Dynamics Study.* Macromolecules, 1994. **27**(13): p. 3493-3500.

30. Grest, G., L.J. Fetters, and J.S. Huang, *Star polymers: experiment, theory, and simulation.* Advances in Chemical Physics, 1996. **94**((Polymeric Systems)): p. 67-163.

31. Shida, K., et al., *Dimensional and Hydrodynamic Factors for Flexible Star Polymers in the Good Solvent Limit.* Macromolecules, 1998. **31**(7): p. 2343-2348.

32. Forni, A., F. Ganazzoli, and M. Vacatello, *Local Conformation of Regular Star Polymers in a Good Solvent: A Monte Carlo Study.* Macromolecules, 1996. **29**(8): p. 2994-2999.

33. Rubio, A.M. and J.J. Freire, *Monte Carlo Calculation of Second Virial Coefficients for Linear and Star Chains in a Good Solvent.* Macromolecules, 1996. **29**(21): p. 6946-6951.

34. Jusufi, A. and C.N. Likos, *Colloquium: Star-branched polyelectrolytes: The physics of their conformations and interactions.* Reviews of Modern Physics, 2009. **81**(4): p. 1753-1772.

35. Dzubiella, J. and A. Jusufi, *Star-polymer-colloid mixtures.* Condensed Matter Physics, 2002. **30**: p. 285-305.

36. Romiszowski, P., *Temperature dependence of some properties of star-branched polymers in confined space. A Monte Carlo study.* Condensed Matter Physics, 2002. **29**: p. 5-14.

37. Romiszowski, P. and A. Sikorski, *Properties of star-branched and linear chains in confined space. A Monte-Carlo study.* Journal of Molecular Modeling, 2005. **11**(4-5): p. 335-340.

38. Hsu, H.-P., W. Nadler, and P. Grassberger, *Scaling of Star Polymers with 1-80 Arms.* Macromolecules, 2004. **37**(12): p. 4658-4663.

39. Erwin, B.M., et al., *Dynamics and rheology of colloidal star polymers.* Soft Matter, 2010. **6**: p. 2825-2833.

40. Padding, J.T., et al., *Computer simulation of the rheology of concentrated star polymer suspensions.* Rheologica Acta, 2010. **49**: p. 473-484.

41. Ganazzoli, F., *Conformations and dynamics of stars and dendrimers: the Gaussian Self-Consistent approach.* Condensed Matter Physics, 2002. **5**(1): p. 37-71.

42. Vlassopoulos, D., et al., *Multiarm star polymers dynamics.* Journal of Physics Condensed Matter, 2001. **13**: p. R855-R876.

43. von Ferber, C. and Y. Holovatch, *Field-theoretical renormalization group analysis for the scaling exponents of star polymers.* Condensed Matter Physics, 2002. **29**: p. 117-136.

44. Bohrisch, J., et al., *New Polyelectrolyte Architectures.* Advances in Polymer Science, 2004. **165**: p. 1-41.

45. Borisov, O.V. and E.B. Zhulina, *Effects of ionic strength and charge annealing in star-branched polyelectrolytes.* European Physical Journal B: Condensed Matter Physics, 1998. **4**(2): p. 205-217.

46. Guenoun, P., et al., *Rodlike Behavior of Polyelectrolyte Brushes.* Physical Review Letters, 1998. **81**(18): p. 3872-3875.

47. Pincus, P., *Colloid stabilization with grafted polyelectrolytes.* Macromolecules, 1991. **24**(10): p. 2912-2919.

48. Jusufi, A., C.N. Likos, and H. Löwen, *Conformations and Interactions of Star-Branched Polyelectrolytes.* Physical Review Letters, 2002. **88**(1): p. 018301/1-018301/4.

49. Jusufi, A., C.N. Likos, and M. Ballauff, *Counterion distributions and effective interactions of spherical polyelectrolyte brushes.* Colloid and Polymer Science, 2004. **282**(8): p. 910-917.

50. Jusufi, A., C.N. Likos, and H. Löwen, *Counterion-induced entropic interactions in solutions of strongly stretched, osmotic polyelectrolyte stars.* Journal of Chemical Physics, 2002. **116**(24): p. 11011-11027.

51. Plamper, F.A., et al., *Nanoblossoms: Light-Induced Conformational Changes of Cationic Polyelectrolyte Stars in the Presence of Multivalent Counterions.* Nano Letters, 2007. **7**(1): p. 167-171.

52. Sutherland, R.J. and R.B. Rhodes, *Dispersant viscosity index improvers*, U.S. Patent, Editor. 1994, Shell Oil Company: United States. p. 1-7.

53. Spinelli, H.J., *Silicone containing acrylic star polymers*. 1991, E. I. du Pont de Nemours and Company. p. 1-9.

54. Hunter, R.J., *Foundations of Colloid Science, Vol. 1*. 1986, New York: Oxford University Press.

55. Wiltshire, J.T. and G.G. Qiao, *Recent advances in star polymer design: degradability and the potential for drug delivery.* Australian Journal of Chemistry, 2007. **60**: p. 699-705.

56. Liechty, W.B., et al., *Polymers for drug delivery systems.* Annual Review of Chemical and Biomolecular Engineering, 2010. **1**: p. 149-173.

57. Adair, J.H., et al., *Recent developments in the preparation and properties of nanometer-size spherical and platelet-shaped particles and composite particles.* Materials Science & Engineering: R: Reports, 1998. **23**(4-5): p. 139-242.

58. Matz, G.F., et al., *Low molecular weight water soluble polymer composition and method of use*, in *PCT Int. Appl.*, W.I.P. Organization, Editor. 2001, Calgon Corporation, USA.

59. De Leon-Rodriguez, L.M., et al., *MRI Detection of VEGFR2 in Vivo Using a Low Molecular Weight Peptoid-$(Gd)_8$-Dendron for Targeting.* Journal of the American Chemical Society, 2010. **132**(37): p. 12829-12831.

60. Ito, H., *Chemical Amplification Resists for Microlithography.* Advances in Polymer Science, 2005. **172**: p. 37-245.

61. De Silva, A., et al., *A fundamental study on dissolution behavior of high-resolution molecular glass photoresists.* Chemistry of Materials, 2008. **20**(23): p. 7292-7300.

62. Kato, M., et al., *Polymerization of Methyl Methacrylate with the Carbon Tetrachloride/Dichlorotris-(triphenylphosphine)ruthenium(II)/Methylaluminum Bis(2,6-di-tert-butylphenoxide) Initiating System: Possibility of Living Radical Polymerization.* Macromolecules, 1995. **28**(5): p. 1721-1723.

63. Wang, J.-S. and K. Matyjaszewski, *Controlled/"Living" Radical Polymerization. Atom Transfer Radical Polymerization in the Presence of Transition-Metal Complexes.* Journal of the American Chemical Society, 1995. **117**(20): p. 5614-5615.

64. Fischer, H., *The persistent radical effect in controlled radical polymerizations* Journal of Polymer Science, Part A: Polymer Chemistry, 1999. **37**(13): p. 1885-1901.

65. Matyjaszewski, K. and J. Xia, *Atom Transfer Radical Polymerization.* Chemical Reviews, 2001. **101**(9): p. 2921-2990.

66. Wang, J.-S. and K. Matyjaszewski, *Controlled/"Living" Radical Polymerization. Halogen Atom Transfer Radical Polymerization Promoted by a Cu(I)/Cu(II) Redox Process* Macromolecules, 1995. **28**(23): p. 7901-7910.

67. Percec, V. and B. Barboiu, *"Living" Radical Polymerization of Styrene Initiated by Arenesulfonyl Chlorides and CuI(bpy)nCl.* Macromolecules, 1995. **28**(23): p. 2970-2972.

68. Curran, D.P., *The design and application of free radical chain reactions in organic synthesis. Part 2* Synthesis, 1988. **1988**(7): p. 489-513.

69. Kharasch, M.S., E.V. Jensen, and W.H. Urry, *Addition of carbon tetrachloride and chloroform to olefins* Science, 1945. **102**(2640): p. 128.

70. Minisci, F., *Free-radical additions to olefins in the presence of redox systems* Accounts of Chemical Research, 1975. **8**(5): p. 165-171.

71. Boutevin, B., *From telomerization to living radical polymerization* Journal of Polymer Science, Part A: Polymer Chemistry, 2000. **38**(18): p. 3235-3243.

72. Bengough, W.I. and W.H. Fairservice, *Effects of salts of metals on vinyl polymerization. 6. Polymerization of methyl methacrylate in the presence of cupric bromide.* Transactions of the Faraday Society, 1971. **67**(Pt. 2): p. 414-419.

73. Qiu, J. and K. Matyjaszewski, *Metal complexes in controlled radical polymerization* Acta Polymerica, 1997. **48**(5-6): p. 169-180.

74. Brandts, J.A.M., et al., *Controlled radical polymerization of styrene in the presence of lithium molybdate(v) complexes and benzylic halides* Journal of Organometallic Chemistry, 1999. **584**(2): p. 246-253.

75. Stump, M.A., et al., *Polymerization of methyl methacrylate using a novel chromium compound* Polymer Preprints (American Chemical Society, Division of Polymer Chemistry), 1997. **38**(1): p. 508-509.

76. Kotani, Y., M. Kamigaito, and M. Sawamoto, *Re(V)-Mediated Living Radical Polymerization of Styrene:1 ReO2I(PPh3)2/R-I Initiating Systems.* Macromolecules, 1999. **32**(8): p. 2420-2424.

77. Matyjaszewski, K., S. Gaynor, and J.-S. Wang, *Controlled Radical Polymerizations: The Use of Alkyl Iodides in Degenerative Transfer.* Macromolecules, 1995. **28**(6): p. 2093-2095.

78. Ando, T., et al., *Living Radical Polymerization of Methyl Methacrylate with Ruthenium Complex: Formation of Polymers with Controlled Molecular Weights and Very Narrow Distributions.* Macromolecules, 1996. **29**(3): p. 1070-1072.

79. Nishikawa, T., et al., *Evidence for Living Radical Polymerization of Methyl Methacrylate with Ruthenium Complex: Effects of Protic and Radical Compounds and Reinitiation from the Recovered Polymers.* Macromolecules, 1997. **30**(8): p. 2244-2248.

80. Ando, T., M. Kamigaito, and M. Sawamoto, *Iron(II) Chloride Complex for Living Radical Polymerization of Methyl Methacrylate.* Macromolecules, 1997. **30**(16): p. 1407-1510.

81. Matyjaszewski, K., et al., *Controlled/"Living" Radical Polymerization of Styrene and Methyl Methacrylate Catalyzed by Iron Complexes.* Macromolecules, 1997. **30**(26): p. 8161-8164.

82. Moineau, G., et al., *Alternative Atom Transfer Radical Polymerization for MMA Using FeCl3 and AIBN in the Presence of Triphenylphosphine: An Easy Way to Well-Controlled PMMA* Macromolecules, 1998. **31**(2): p. 545-547.

83. Percec, V., et al., *Metal-Catalyzed "Living" Radical Polymerization of Styrene Initiated with Arenesulfonyl Chlorides. From Heterogeneous to Homogeneous Catalysis.* Macromolecules, 1996. **29**(10): p. 3665-3668.

84. Moineau, G., et al., *Controlled Radical Polymerization of Methyl Methacrylate Initiated by an Alkyl Halide in the Presence of the Wilkinson Catalyst.* Macromolecules, 1998. **31**(2): p. 542-544.

85. Granel, C., et al., *Controlled Radical Polymerization of Methacrylic Monomers in the Presence of a Bis(ortho-chelated) Arylnickel(II) Complex and Different Activated Alkyl Halides* Macromolecules, 1996. **29**(27): p. 8576-8582.

86. Uegaki, H., et al., *Nickel-Mediated Living Radical Polymerization of Methyl Methacrylate.* Macromolecules, 1997. **30**(8): p. 2249-2253.

87. Uegaki, H., et al., *NiBr2(Pn-Bu3)2-Mediated Living Radical Polymerization of Methacrylates and Acrylates and Their Block or Random Copolymerizations.* Macromolecules, 1998. **31**(20): p. 6756-6761.

88. Lecomte, P., et al., *Controlled Radical Polymerization of Methyl Methacrylate in the Presence of Palladium Acetate, Triphenylphosphine, and Carbon Tetrachloride.* Macromolecules, 1997. **30**(24): p. 7631-7633.

89. Patten, T.E. and K. Matyjaszewski, *Atom-transfer radical polymerization and the synthesis of polymeric materials.* Advanced Materials, 1998. **10**(12): p. 901-915.

90. Matyjaszewski, K., *Transition metal catalysis in controlled radical polymerization: atom transfer radical polymerization.* Chemistry - A European Journal, 1999. **5**(11): p. 3095-3102.

91. Patten, T.E. and K. Matyjaszewski, *Copper(I)-catalyzed atom transfer radical polymerization.* Accounts of Chemical Research, 1999. **32**(10): p. 895-903.

92. Tang, W. and K. Matyjaszewski, *Kinetic Modeling of Normal ATRP, Normal ATRP with $[Cu^{II}]_0$, Reverse ATRP and SR&NI ATRP.* Macromolecular Theory and Simulations, 2008. **17**: p. 359-375.

93. Goto, A. and T. Fukuda, *Kinetics of living radical polymerization.* Progress in Polymer Science, 2004. **29**: p. 329-385.

94. Matyjaszewski, K., T.E. Patten, and J. Xia, *Controlled/"Living" Radical Polymerization. Kinetics of the Homogeneous Atom Transfer Radical Polymerization of Styrene.* Journal of the American Chemical Society, 1997. **119**(4): p. 674-680.

95. Percec, V., B. Barboiu, and H.-J. Kim, *Arenesulfonyl Halides: A Universal Class of Functional Initiators for Metal-Catalyzed "Living" Radical Polymerization of Styrene(s), Methacrylates, and Acrylates.* Journal of the American Chemical Society, 1998. **120**(2): p. 305-316.

96. Davis, K.A., H.-j. Paik, and K. Matyjaszewski, *Kinetic Investigation of the Atom Transfer Radical Polymerization of Methyl Acrylate.* Macromolecules, 1999. **32**(6): p. 1767-1776.

97. Wang, J.-L., T. Grimaud, and K. Matyjaszewski, *Kinetic Study of the Homogeneous Atom Transfer Radical Polymerization of Methyl Methacrylate.* Macromolecules, 1997. **30**(21): p. 6507-6512.

98. Matyjaszewski, K., *The importance of exchange reactions in controlled/living radical polymerization in the presence of alkoxyamines and transition metals.* Macromolecular Symposia, 1996. **111**: p. 47-61.

99. Xia, J., X. Zhang, and K. Matyjaszewski, *Synthesis of Star-Shaped Polystyrene by Atom Transfer Radical Polymerization Using an "Arm First" Approach.* Macromolecules, 1999. **32**(13): p. 4482-4484.

100. Zhang, X., J. Xia, and K. Matyjaszewski, *End-Functional Poly(tert-butyl acrylate) Star Polymers by Controlled Radical Polymerization.* Macromolecules, 2000. **33**(7): p. 2340-2345.

101. Kasko, A.M., A.M. Heintz, and C. Pugh, *The Effect of Molecular Architecture on the Thermotropic Behavior of Poly[11-(4'-cyanophenyl-4"-phenoxy)undecyl acrylate] and Its Relation to Polydispersity.* Macromolecules, 1998. **31**(2): p. 256-271.

102. Matyjaszewski, K., et al., *Synthesis of Block, Graft and Star Polymers from Inorganic Macroinitiators.* Applied Organometallic Chemistry, 1998. **12**: p. 667-673.

103. Heise, A., et al., *Starlike Block Copolymers with Amphiphilic Arms as Models for Unimolecular Micelles.* Journal of the American Chemical Society, 1999. **121**(37): p. 8647-8648.

104. Ueda, J., et al., *Multifunctional Initiators for the Ruthenium-Mediated Living Radical Polymerization of Methyl Methacrylate: Di- and Trifunctional Dichloroacetates for Synthesis of Multiarmed Polymers.* Macromolecules, 1998. **31**(3): p. 557-562.

105. Ueda, J., M. Kamigaito, and M. Sawamoto, *Calixarene-Core Multifunctional Initiators for the Ruthenium-Mediated Living Radical Polymerization of Methacrylates.* Macromolecules, 1998. **31**(20): p. 6762-6768.

106. Percec, V., et al., *Designing functional aromatic multisulfonyl chloride initiators for complex organic synthesis by living radical polymerization.* Journal of Polymer Science, Part A: Polymer Chemistry, 2000. **38**(S1): p. 4776-4791.

107. Heise, A., et al., *Novel Starlike Poly(methyl methacrylate)s by Controlled Dendritic Free Radical Initiation.* Macromolecules, 1999. **32**(1): p. 231-234.

108. Heise, A., et al., *Starlike Polymeric Architectures by Atom Transfer Radical Polymerization: Templates for the Production of Low Dielectric Constant Thin Films* Macromolecules, 2000. **33**(7): p. 2346-2354.

109. Heise, A., et al., *Investigation of the Initiation Behavior of a Dendritic 12-Arm Initiator in Atom Transfer Radical Polymerization.* Macromolecules, 2001. **34**(11): p. 3798-3801.

110. Hedrick, J.L., et al., *Dendrimer-like Star Block and Amphiphilic Copolymers by Combination of Ring Opening and Atom Transfer Radical Polymerization.* Macromolecules, 1998. **31**(25): p. 8691-8705.

111. Miller, R.D., et al., *Tandem polymerizations combining controlled radical and ring opening techniques with transition metal mediated arylene condensation* Polymeric Materials Science and Engineering, 1999. **80**: p. 24-25.

112. Haddleton, D.M., et al., *Atom Transfer Radical Polymerization of Methyl Methacrylate Initiated by Alkyl Bromide and 2-Pyridinecarbaldehyde Imine Copper(I) Complexes.* Macromolecules, 1997. **30**(7): p. 2190-2193.

113. Haddleton, D.M., et al., *Glucose derived star polymers by atom transfer polymerization.* Polymeric Materials Science and Engineering, 1999. **80**: p. 145-146.

114. Angot, S.K., et al., *Atom Transfer Radical Polymerization of Styrene Using a Novel Octafunctional Initiator: Synthesis of Well-Defined Polystyrene Stars.* Macromolecules, 1998. **31**(21): p. 7218-7225.

115. Collins, J.E. and C.L. Fraser, *Transition Metals as Templates for Multifunctional Initiators: Bulk Atom Transfer Radical Polymerization of Styrene Using Di-, Tetra- and Hexafunctional Ruthenium Tris(bipyridine) Reagents* Macromolecules, 1998. **31**(19): p. 6715-6717.

116. Fraser, C.L. and A.P. Smith, *Metal complexes with polymeric ligands: chelation and metalloinitiation approaches to metal tris(bipyridine)-containing materials* Journal of Polymer Science, Part A: Polymer Chemistry, 2000. **38**(S1): p. 4704-4716.
117. Ohno, K., et al., *Synthesis of well-defined cyclodextrin-core star polymers by atom transfer polymerization.* Polymer Preprints (American Chemical Society, Division of Polymer Chemistry), 2000. **41**(1): p. 478-479.

118. Plamper, F.A., et al., *Synthesis, Characterization and Behavior in Aqueous Solution of Star-Shaped Poly(acrylic acid).* Macromolecular Chemistry and Physics, 2005. **206**: p. 1813-1825.

119. Stenzel-Rosenbaum, M.H., et al., *Synthesis of Poly(styrene) Star Polymers Grown from Sucrose, Glucose, and Cyclodextrin Cores via Living Radical Polymerization Mediated by a Half-Metallocene Iron Carbonyl Complex.* Macromolecules, 2001. **34**(16): p. 5433-5438.

120. Edmonds, R., S.A.F. Bon, and D.M. Haddleton, *Carbohydrate-based initiators for transition-metal mediated atom transfer polymerization.* Polymer Preprints (American Chemical Society, Division of Polymer Chemistry), 2000. **41**(1): p. 444-445.

121. Schaller, R.R., *Moore's law: past, present, and future.* IEEE Spectrum, 1997. **34**(6): p. 52-59.

122. Mack, C., *Fundamental Principles of Optical Lithography: The Science of Microfabrication*. 2007: John Wiley & Sons, Ltd.

123. Süss, O., *Nature of the irradiation products of diazo compounds; conversion of aromatic six-membered into five-membered rings.* Annalen der Chemie, Justus Liebigs, 1944. **556**: p. 65-84.

124. Pacansky, J. and J.R. Lyerla, *Photochemical decomposition mechanisms for AZ-type photoresists.* IBM Journal of Research and Development, 1979. **23**(1): p. 42-55.

125. Ito, H., G.C. Willson, and J.H.J. Frechet. *New UV Resists with Negative or Positive Tone*. in *Symposium on VLSI Technology*. 1982. Tokyo, Japan.

126. Ito, H. and G.C. Willson, *Chemical Amplification in the Design of Dry Developing Resist Materials.* Polymer Engineering and Science, 1983. **23**(18): p. 1012-1018.

127. Maltabes, J.G., et al., *1X deep-UV lithography with chemical amplification for 1-micron DRAM production.* Proceedings of SPIE, 1990. **1262**(Advances in Resist Technology and Processing VII): p. 2-7.

128. McKean, D.R., U. Schaedeli, and S.A. MacDonald, *Acid photogeneration from sulfonium salts in solid polymer matrices.* Journal of Polymer Science, Part A: Polymer Chemistry, 1989. **27**(12): p. 3927-3935.

129. Ito, H., W.P. England, and S.B. Lundmark, *Effects of polymer end groups on chemical amplification.* Proceedings of SPIE, 1992. **1672**(Advances in Resist Technology and Processing IX): p. 2-14.

130. Turner, S.R., et al., *High-Tg base-soluble copolymers as novolac replacements for positive photoresists.* Polymer Engineering & Science, 1986. **26**(16): p. 1096-1100.

131. Ahn, K.-D., D.-I. Koo, and S.-J. Kim, *t-BOC maleimide copolymers for thermally stable deep UV resists by chemical amplification.* Journal of Photopolymer Science and Technology, 1991. **4**(3): p. 433-443.

132. Kikuchi, H., N. Kurata, and K. Hayashi, *Positive chemical amplification resist for deep UV lithography.* Journal of Photopolymer Science and Technology, 1991. **4**(3): p. 357-360.

133. Koike, M. and A. Danno, *Radiation Effects on Dimethyl-diphenyl Siloxane Copolymer. I. Protective Effect of Phenyl Radical on the Cross-linking.* Journal of the Physical Society of Japan, 1960. **15**: p. 1501-1508.

134. Tsuda, M., S. Oikawa, and K. Kimura, *Potential-Energy Surfaces in the Lower Excited States of Benzene, Dewar-Benzene Isomerization Process.* International Journal of Quantum Chemistry, 1980. **18**(1): p. 157-164.

135. Choi, S.-J., et al., *Design and properties of new deep-UV positive photoresist.* Proceedings of SPIE, 1996. **2724**(Advances in Resist Technology and Processing XIII): p. 323-331.

136. Ito, H., et al., *Silyl-protected hydroxystyrenes: Living anionic polymerization at room temperature and selective desilylation.* Journal of Polymer Science, Part A: Polymer Chemistry, 2000. **38**(13): p. 2415-2427.

137. Houlihan, F., et al., *Phase transfer catalysis in the tert-butyloxycarbonylation of alcohols, phenols, enols, and thiols with di-tert-butyl dicarbonate.* Canadian Journal of Chemistry, 1985. **63**(1): p. 153-162.

138. Ito, H., *Solid-state thermolysis of poly(p-t-butoxycarbonyloxystyrene) catalyzed by polymeric phenol: Effect of phase separation.* Journal of Polymer Science, Part A: Polymer Chemistry, 1986. **24**(11): p. 2971-2980.

139. Ito, H., et al., *Molecular design for stabilization of chemical amplification resist toward airborne contamination.* Proceedings of SPIE, 1993. **1925**(Advances in Resist Technology and Processing X): p. 65-75.

140. Ito, H., et al., *Environmentally stable chemical amplification positive resist: principle, chemistry, contamination resistance, and lithogrpahic feasibility.* Journal of Photopolymer Science and Technology, 1994. **7**(3): p. 433-447.

141. Breyta, G., et al., *The lithographic performance and contamination resistance of a new family of chemically amplified DUV photoresists.* Journal of Photopolymer Science and Technology, 1994. **7**(3): p. 449-460.

142. Conley, W., et al., *The lithographic performance of an environmentally stable chemically amplified photoresists (ESCAP).* Proceedings of SPIE, 1996. **2724**(Advances in Resist Technology and Processing XIII): p. 34-60.

143. Kunz, R.R., et al., *Acid-catalyzed single-layer resists for ArF lithography.* Proceedings of SPIE, 1993. **1925**(Advances in Resist Technology and Processing X): p. 167-175.

144. Kaimoto, Y., et al., *Alicyclic polymer for ArF and KrF excimer resist based on chemical amplification.* Proceedings of SPIE, 1992. **1672**(Advances in Resist Technology and Processing IX): p. 66-73.

145. Imoto, M., et al., *Vinyl polymerization. LXXIII. Polymerization and copolymerization of bornyl or isobornyl methacrylate.* Journal of Polymer Science, Part A: Polymer Chemistry, 1964. **2**(3): p. 1407-1419.

146. Allen, R.D., et al., *Single Layer Resists with Enhanced Etch Resistance for 193 nm Lithography.* Journal of Photopolymer Science and Technology, 1994. **7**(3): p. 507-516.

147. Allen, R.D., et al., *Resolution and etch resistance of a family of 193nm positive resists.* Journal of Photopolymer Science and Technology, 1995. **8**(4): p. 623-626.

148. Ishii, Y., et al., *Hydroxylation of polycyclic alkanes with molecular oxygen catalyzed by N-hydroxyphthalimide (NHPI) combined with transition metal salts.* Tetrahedron Letters, 1996. **37**(28): p. 4993-4996.

149. Sakaguchi, S., M. Eikawa, and Y. Ishii, *N-hydroxyphthalimide (NHPI)-catalyzed reaction of adamantane under nitric oxide atmosphere.* Tetrahedron Letters, 1997. **38**(40): p. 7075-7078.

150. Nozaki, J. and E. Yano, *Evaluation of Alicyclic Methacrylate Resist with a γ-Butyrolactone Protective Group for 193-nm Lithography.* Journal of Photopolymer Science and Technology, 1998. **11**(3): p. 493-498.

151. Takahashi, M., et al., *Evaluation of chemically amplified resist based on adamantyl methacrylate.* Proceedings of SPIE, 1995. **2438**(Advances in Resist Technology and Processing XII): p. 422-432.

152. Takechi, S., et al., *Impact of 2-methyl-2-adamantyl group used for 193-nm single-layer resist.* Journal of Photopolymer Science and Technology, 1996. **9**(3): p. 475-488.

153. Wiaux, V., et al., *The potential of double patterning immersion lithography for the 32nm half pitch node.* Euroasia Semiconductor, 2007. **2007**(August): p. 19-22.

154. Maenhoudt, M., et al., *Alternative process schemes for double patterning that eliminate the intermediate etch step.* Proceedings of SPIE, 1998. **6924**(Optical Microlithography XXI): p. 69240P/1-69240P/12.

155. Okoroanyananwu, U. and J.H. Lammers, *Resist Road to the 22 nm Technology Node.* Future Fab International, 2004(17).

156. Koh, C., et al., *Characterization of promising resist platforms for sub-30-nm HP manufacturability and EUV CAR extendibility study.* Proceedings of SPIE, 2010. **7636**(Extreme Ultraviolet (EUV) Lithography): p. 763604/1-763604/16.

157. Poelma, J.E. and C.J. Hawker, *Block copolymers: With a little help form above.* Nature Nanotechnology, 2010. **5**: p. 243-244.

158. Ross, C.A., et al., *Templated self-assembly of Si-containing block copolymers for nanoscale device fabrication.* Proceedings of SPIE, 2010. **7637**(Alternative Lithographic Technologies II): p. 76370H/1-76370H/7.

159. Kantor, Y. and M. Kardar, *Instabilities of charged polyampholytes.* Physical Review E: Statistical Physics, Plasmas, Fluids, and Related Interdisciplinary Topics, 1995. **51**(2): p. 1299-1312.

160. Dobrynin, A.V., M. Rubinstein, and S.P. Obukhov, *Cascade of Transitions of Polyelectrolytes in Poor Solvents.* Macromolecules, 1996. **29**(8): p. 2974-2979.

161. Aseyev, V.O., S.I. Klenin, and H. Tenhu, *Conformational changes of a polyelectrolyte in mixtures of water and acetone.* Journal of Polymer Science, Part B: Polymer Physics, 1998. **36**(7): p. 1107-1114.

162. Aseyev, V.O., et al., *Neutron Scattering Studies of the Structure of a Polyelectrolyte Globule in a Water-Acetone Mixture.* Macromolecules, 2001. **34**(11): p. 3706-3709.

163. Plamper, F.A., et al., *Pearl Necklace Architecture: New Threaded Star-Shaped Copolymers.* Macromolecules, 2010. **43**(5): p. 2190-2203.

164. Ballauff, M., *Personal Communication*. 2008.

165. Schmidt, H.-W., *Personal Communication*. 2010.

166. Akira, M., et al., *International Technology Roadmap for Semiconductors - Lithography*. 2009.

167. Constantoudis, V., et al., *Modeling of line edge roughness transfer during plasma etching.* Microelectronic Engineering, 2009. **86**(4-6): p. 968-970.

168. Constantoudis, V., et al., *Quantification of line-edge roughness of photoresists. II. Scaling and fractal analysis and the best roughness descriptors.* Journal of Vacuum Science & Technology, B: Microelectronics and Nanometer Structures--Processing, Measurement, and Phenomena, 2003. **21**(3): p. 1019-1026.

169. Constantoudis, V., G.P. Patsis, and E. Gogolides, *Photoresist line-edge roughness analysis using scaling concepts.* Proceedings of SPIE, 2003. **5038**: p. 901-909.

170. He, D. and F. Cerrina, *Process dependence of roughness in a positive-tone chemically amplified resist.* Journal of Vacuum Science & Technology, B: Microelectronics and Nanometer Structures, 1998. **16**(6): p. 3748-3751.

171. Constantoudis, V., et al., *Line edge roughness and critical dimension variation: Fractal characterization and comparison using model functions.* Journal of Vacuum Science & Technology B, 2004. **22**(4): p. 1974-1981.

172. Gogolides, E., et al., *A review of line edge roughness and surface nanotexture resulting from patterning processes.* Microelectronic Engineering, 2006. **83**(4-9): p. 1067-1072.

173. Yamaguchi, A., et al., *Characterization of line-edge roughness in resist patterns and estimation of its effect on device performance.* Proceedings of SPIE, 2003. **5038**: p. 689-698.

174. Patsis, G.P., et al., *Roughness analysis of lithographically produced nanostructures: off-line measurement and scaling analysis.* Microelectronic Engineering, 2003. **67-68**: p. 319-325.

175. Barabasi, A.-L. and H.E. Stanley, *Fractal Concepts in Surface Growth*. 1st ed. ed. 1995, Cambridge, England: Cambridge University Press.

176. Bunday, B.D., et al., *CD-SEM measurement line-edge roughness test patterns for 193-nm lithography.* Proceedings of SPIE, 2003. **5038**: p. 674-688.

177. Naulleau, P.P. and J.P. Cain, *Experimental and model-based study of the robustness of line-edge roughness metric extraction in the presence of noise.* Journal of Vacuum Science & Technology, B: Microelectronics and Nanometer Structures--Processing, Measurement, and Phenomena, 2007. **25**(5): p. 1647-1657.

178. Patsis, G.P., E. Gogolides, and K. Van Werden, *Effects of photoresist polymer molecular weight and acid-diffusion on line-edge roughness.* Japanese Journal of Applied Physics, Part 1: Regular Papers, Brief Communications & Review Papers, 2005. **44**(8): p. 6341-6348.

179. Patsis, G.P. and E. Gogolides, *Effects of model polymer chain architectures of photoresists on line-edge-roughness. Monte Carlo simulations.* Journal of Physics: Conference Series, 2005. **10**: p. 389-392.

180. Chochos, C.L., et al., *Hyberbranched Polymers for Photolithographic Applications - Towards Understanding the Relationship between Chemical Structure of Polymer Resin and Lithographic Performance.* Advanced Materials, 2009. **21**: p. 1121-1125.

CHAPTER 2: SYNTHESIS, CHARACTERIZATION AND PROPERTIES OF STAR-SHAPED POLY(TERT-BUTYL METHACRYLATE) OLIGOMERS

Drew C. Forman, Xavier Andre, Joan K. Bosworth, Priscilla Taylor, Marvin Paik,
Jin Kyun Lee, and Christopher K. Ober
Department of Materials Science and Engineering
Cornell University, Ithaca, NY 14853

Florian Wieberger and Hans-Werner Schmidt
Macromolecular Chemistry I
University of Bayreuth, Bayreuth, Germany 95440

Andreas Walther, Marietta Böhm, and Axel H. E. Müller
Macromolecular Chemistry II
University of Bayreuth, Bayreuth, Germany 95540

2.0 Abstract

A series of star oligomers consisting of poly(tert-butyl methacrylate) (tBMA) arms was synthesized via core-first atom transfer radical polymerization (ATRP) from 2,3,4,6,1',3',4',6'-octa-O-(2-bromoisobutyryl)-saccharose (SAC-Br_8). In order to achieve the reproducible synthesis of star oligomers, the rate of polymerization was reduced by decreasing the initial ratio of Cu(I):Cu(II) and diluting the reaction. Dilutions resulting in initial initiator concentrations as low as 1.4 mmol/L were studied, enabling the synthesis of star oligomers with arms as short as dimers at low conversions and allowing glass transition temperature (T_g) dependence on molecular weight to be determined. Reproducibility was verified at larger quantities and an initial examination was conducted into the impact of molecular size and polarity on dissolution behavior.

2.1 Introduction

The star-shaped polymer architecture, consisting of multiple linear polymer arms attached to a central core, has garnered attention as a result of properties that are dependent on the number of arms.[1, 2] As its functionality, or number of arms, increases a star polymer's behavior will continuously deviate from that of a linear polymer chain and more closely resemble a colloidal sphere.[3] This hybridization of behaviors results in unique material properties and has led to commercial applications for star polymers as viscosity index modifiers for oil,[4] oxygen permeability and hardness enhancers in contact lenses,[5] and as coating additives, toner binder and pharmaceutical encapsulations.[6, 7] Theoretical studies have successfully modeled thermodynamic partition functions that link functionality to scaling law behavior for molecular size, osmotic pressure, rheology and colloidal behavior.[8-10] Current experimental work, backed by simulations, continues to explore star phenomena such

as the contraction of star polyelectrolytes compared to equivalent linear polyelectrolytes.[11-13]

Similar to the scaling derivations based on the Daoud-Cotton blob model for star-shaped polymers, current theoretical and experimental work is limited to the case of high molecular weight stars.[1, 2] However, there exists significant applications for low molecular weight materials, including conjugates for drug delivery,[14] nanoparticle dispersion stabilizers,[15] cosmetic dyes,[16] photoresists for semiconductor manufacturing[17, 18] and *in vivo* sensors.[19] If the capability to reproducibly synthesize star-shaped oligomers could be developed, there exists the potential to introduce the architectural advantages of star-polymers to low molecular weight applications. Furthermore, new phenomena might be observed in the star-shaped oligomer regime.

Since its inception,[20, 21] the architectural complexity of polymers synthesized by ATRP has advanced from simple linear acrylates and methacrylates[22-24] to cylindrical brushes[25, 26], hyperbranched[27, 28] and star polymers[29-35] and highly specialized architectures such as pearl necklaces[36]. However, excluding initial aliquots taken at the start of molecular weight-conversion plots for larger star polymers there are no reports of star-shaped oligomers.[32] There exists a fundamental challenge to reproducibly synthesize star oligomers as the target molecular weight of the polymer arms must decrease with increasing functionality in order to maintain an overall low molecular weight.

In this chapter we report on a successful approach for the reproducible preparation of star poly(tBMA) oligomers by "core-first"[37, 38] ATRP. Two factors known to reduce the reaction rate,[39, 40] dilution and the inclusion of Cu(II), are combined with low conversions to isolate star-shaped oligomers with average arm lengths as low as dimers. (Figure 2-1) The full, Fox-Flory T_g dependence on molecular weight is determined for this system. While a separate study will further elaborate on the

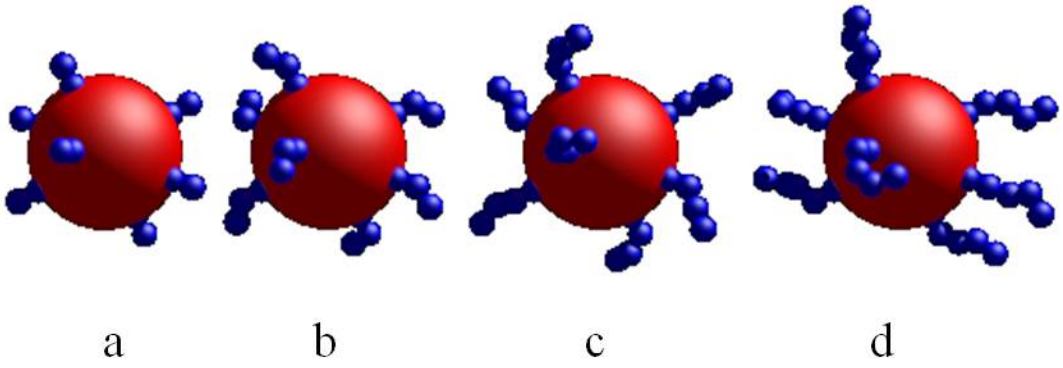

Figure 2-1. Graphical depiction of star-shaped p(tBMA) oligomers comprised of 7 arms with (a) 2, (b) 3, (c) 4 and (d) 5 monomer units per arm, corresponding to the samples (a) $\mathbf{(PtBMA_2)_7}$, (b) $\mathbf{(PtBMA_3)_7}$, (c) $\mathbf{(PtBMA_4)_7}$ and (d) $\mathbf{(PtBMA_5)_7}$ respectively. The core and monomer units are represented by spheres with volumes equal to the molecular weight of $\mathbf{SAC\text{-}Br_8}$ (excluding bromide) and tBMA.

solution properties of star-shaped oligomers,[41] herein we present initial findings by examining the dissolution of star-shaped oligomers in thin films .

2.2 Experimental

2.2.1 Materials

2-Bromo-2-methylpropanoyl bromide and 4-(dimethylamino)pyridine, anhydrous pyridine, CH_2Cl_2 CuCl, $CuCl_2$, pentamethyldiethylenetriamine (PMDETA), D(+)-Saccharose and N,N,N',N",N"- were purchased from Aldrich and prepared according to standard procedures. The tBMA monomer was purchased from Aldrich and passed through a basic alumina column to remove the inhibitor.

The poly(tBMA) polymers prepared in this chapter are named for their architecture: $(PtBMA_n)_f$ where n is the number average of monomer units per arm and f is the number average of arms per molecule.

2.2.2 Synthesis

2.2.2.1 Preparation of Multifunctional Initiators

The core-first[37] approach and ATRP were selected to synthesize star-shaped poly(tBMA) oligomers. 2,3,4,6,1',3',4',6'-octa-O-(2-bromoisobutyryl)-saccharose, which has eight initiating sites, was prepared from saccharose as previously published.[13]

2.2.2.2 Preparation of tert-Butyl Methacrylate Star Oligomer Homopolymers

A general procedure for ATRP of star poly(tert-butylacrylate)[42] was modified for star-shaped poly(tBMA) oligomers as follows: 480.7mg (0.31mmol) of **SAC-Br$_8$**,

17.50g (123.09mmol) tBMA, 426.6mg (2.46mmol) PMDETA, 170.6mg (1.72mmol) CuCl and 99.3mg (0.74mmol) $CuCl_2$ were stirred in 170 mL of acetone and 10 mL of Toluene under an inert atmosphere. The solution was heated in a 60 °C oil bath for 2 hours.

Additional $CuCl_2$ was added and the reaction quenched in cold water. The solution was concentrated under reduced pressure, taken up in dichloromethane and filtered through silica powder to remove the copper catalyst. The solution was then concentrated under reduced pressure a second time, taken up in 1,4-dioxane and placed in 1000 Dalton dialysis tubing. Dialysis in one liter of 1,4-dioxane was performed overnight, twice. The contents of the dialysis tubing were concentrated under reduced pressure and precipitated into water/methanol. The precipitate was collected and freeze-dried to obtain star poly(tBMA) **$(PtBMA_n)_7$**.

The conversion of monomer was carefully monitored by collecting aliquot samples at the start of polymerization, throughout polymerization and at the end of polymerization. Monomer content was measured by the ^{1}H-NMR integration of tert-butyl methacrylate monomer vinyl peaks calibrated to the $-CH_3$ peak of a toluene marker. Conversion is reported as a percentage of the initial monomer concentration and in the logarithmic conversion index form: $\ln([M]_0/[M]_t)$.

Similar procedures were followed with polymerization times modified to achieve samples with different conversions, resulting in samples with varied molecular weights. (Figure 2-2)

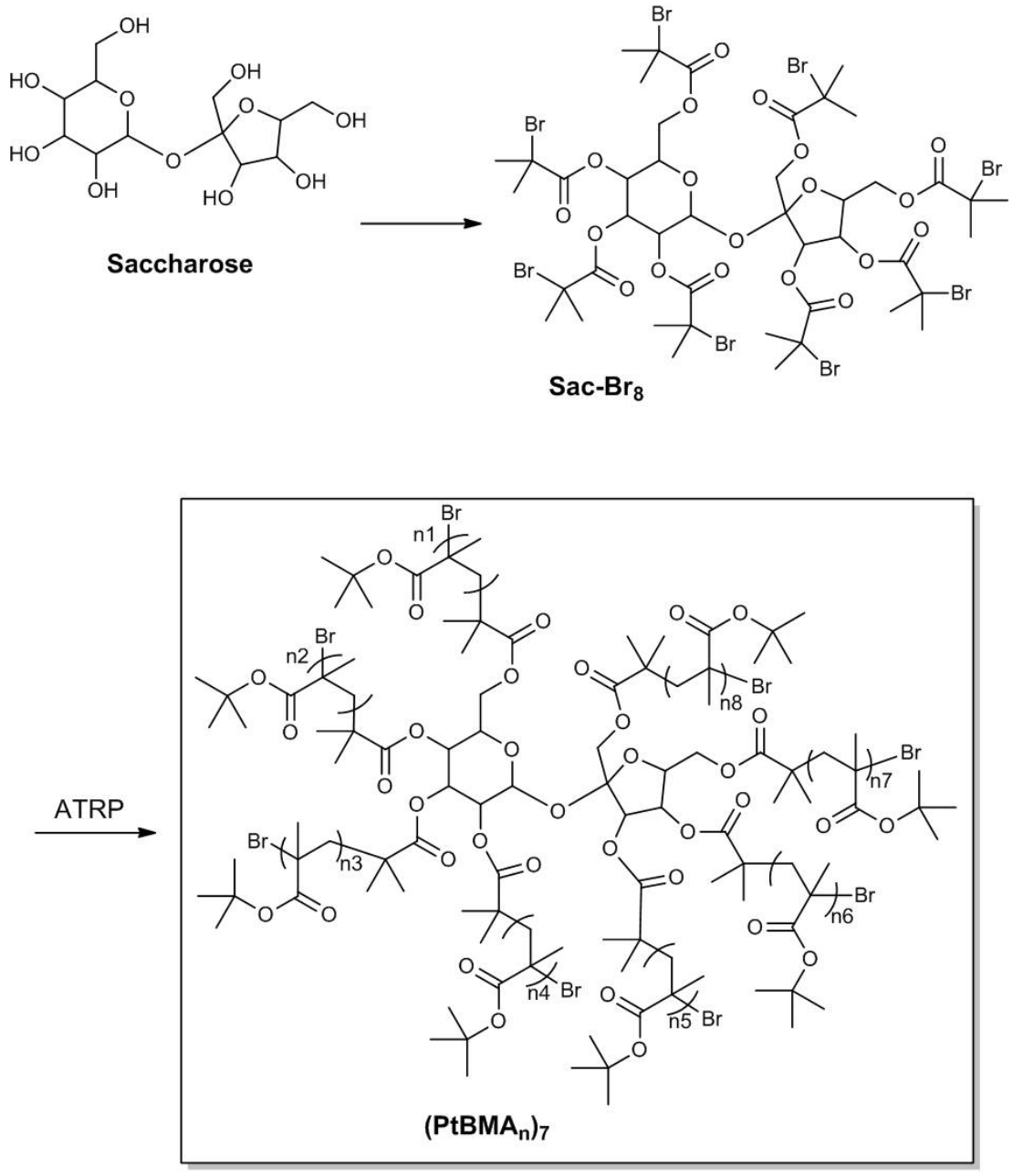

Figure 2-2. Reaction pathway toward tert-butyl methacrylate star oligomers.

2.2.3 Characterization

2.2.3.1 Size Exclusion Chromatography

The molecular weight of purified star oligomers were measured by size exclusion chromatography (SEC) performed on a Waters GPC system (Waters 486 UV detector) by eluting THF (1 cm^3 min^{-1}) at 40°C with a linear polystyrene standard to determine relative molecular weight. Aliquots were purified by filtration through silica using THF as an eluent followed by the evaporation of solvent under vacuum before performing SEC. Final products were tested without further modification.

SEC with a Wyatt DAWN HELEOS multiangle light scattering detector equipped with a 632.8 nm He-Ne laser (GPC/MALS) and Viscotek Model 250 viscosity detector (GPC/viscosity) were used to determine the absolute molecular weights. THF was used as eluent at a flow rate of 1.0 mL/min: column set, 5 μm PSS SDV gel, 103, 105, and 106 Å, 30 cm each. For GPC/viscosity, the refractive index increment of the star oligomer solutions in THF at 25 °C were measured using a PSS DnDC-2010/620 differential refractometer.

2.2.3.2 SAC-Br_8 Initiation Efficiency

Initiation efficiency in multifunctional initiators are limited by steric hindrances.[43] Theoretical degrees of polymerization were calculated from conversion data and compared with Mn absolute to determine an initiation efficiency of 85%.

2.2.4 Dissolution of Star Oligomers by Titration

A 100nm film was obtained through spincoating a five percent solution of star oligomer in propylene glycol methyl ether acetate (PGMEA) on a hexamethyldisilazane (HMDS) primed quartz crystal microbalance (QCM) at 2000

RPM. Excess solvent was removed by baking at 130°C on a hot plate for one minute. The QCM was submerged in a magnetically stirred solution of 2:1 isopropanol (IPA):H_20. Frequency measurements were recorded every 0.5 seconds enabling the thickness of the film to be calculated in real time. The film was allowed to reach an equilibrium dissolution rate prior to the IPA concentration being increased. IPA was titrated into the solution until rapid dissolution was achieved.

2.2.5 Dissolution Modification of Star Oligomers

100 nm films were obtained through spincoating PGMEA solutions containing 20:1 weight ratio of star oligomer and bis(tert-butylphenyl)iodonium nonaflate (BPIN) at 2000 RPM onto a silicon wafer vapor primed with HMDS. Excess solvent was removed by baking at 130°C for one minute.

Following thermal treatment, a 100 keV Leica VB6-HR electron beam tool operated at 57.1 $\mu C/cm^2$ was used to generate acid from the BPIN in the film. A second thermal treatment at 125°C for 30 seconds enabled the acid catalyzed thermal deprotection of the non-polar tert-butyl group in locations where acid had been generated.[17] The resulting solubility change was revealed by developing the film in an IPA:H_2O solution that selectively dissolved only the star oligomers that had undergone chemical deprotection, resulting in a patterned surface.

The film was sputtered with a thin film of Gold / Palladium using a Hummer Au/Pd Sputtering System. Patterned lines and spaces with a half-pitch of 100nm were examined in a LEO 1550 Field Emission Scanning Electron Microscope (SEM) operated at 1.5 keV.

2.3 Results and Discussion

A key goal of this work is to determine the feasibility of preparing star-shaped oligomers with a high degree of reproducibility. The initiation efficiency of SAC-Br_8 was measured at 85%, indicating an average number of arms (f_{avg}) of 6.8 and a median of 7 arms per star. For star p(tBMA) oligomers synthesized from SAC-Br_8, arms should not be greater than 10 monomer units long to obtain $T_g<T_{g,\infty}$. This requirement creates procedural challenges that must be overcome to reproducibly synthesize target molecules. Large deviation from the target arm length between batches would be introduced to the star oligomer if monomer additions occur at a rate greater than the temporal precision in which a reaction can be reliably initiated, carried out and quenched. It is imperative that monomer additions per chain end occur on a time scale no less than one addition every few minutes. Therefore, reducing the polymerization rate is a requirement for synthesizing star oligomers with customizable arm lengths on the order of several monomer units.

2.3.1 ATRP Synthesis of Star Oligomers Modified by Dilution

As a first attempt to achieve reproducible star oligomers synthesized by ATRP, the reaction rate was modified by diluting the reaction volume with solvent for the purpose of slowing the rate of monomer conversion. The relative Initiator : Ligand : Cu(I)Cl : $Cu(II)Cl_2$: Monomer weight ratio was held constant at 1.0 : 8.0 : 5.6 : 2.4 : 400 with a reaction temperature of 60°C. The solution volume was adjusted by adding solvent equal to 2.33 and 10.0 times bulk volume, yielding two reactions with solvent concentrations of 70% and 91% or $[I]_0$ concentrations of 4.7 and 1.4 mmol/L respectively. Aliquots taken during the reaction were analyzed by ^{1}H-NMR and GPC with the results summarized in Table 2-1 and Table 2-2.

Low polydispersity index (PDI) values (1.09 ± 0.04) were measured for all star oligomers, despite low conversion. This can be attributed to the distribution narrowing effect observed in branched polymers, initially explained for a specific case by Schulz and later a general derivation was developed by Flory.[44, 45] Qualitatively, the distribution narrowing can be explained to result from the low probability of all short or all long arms being covalently connected to the same molecule. While the individual arms cannot be measured from aliquots of star oligomer, it is worth noting that the Poisson term [see Equation 2-1][39, 40, 46, 47] predicts an increase in PDI inversely proportional to $\overline{DP}_n$. For the low conversion samples, the significance of the Poisson term increases dramatically. In the lowest conversion sample, the Poisson term is 0.44. This suggests that although the overall molecular weight of star oligomers can be well controlled, one cannot expect to achieve mono-disperse arms.

$$PDI = 1 + \frac{1}{\overline{DP}_n} + \left(\frac{k_p([RX]_0 - [RX])}{k_{deact}[Cu^{II}]}\right)\left(\frac{2}{p} - 1\right) \qquad \text{Equation 2-1}$$

Conversion index [see Equation 2-2][39, 40, 46] is a logarithmic representation of the conversion of monomer that is proportional to the polymerization time for ATRP. This relationship holds true for the star oligomers reported in Table 2-1 and Table 2-2. (Figure 2-3) The separate linear trendlines are a result of changing the amount of solvent between the two reactions. The variables k_p, K_{ATRP} and $[Cu^I]/[Cu^{II}]$ are therefore expected to remain constant. $[P_mX]$ is directly proportional to $[I]_0$ when the rate of initiation and termination is kept much lower than the rates of activation and deactivation.[40] This leads to a simplified relationship between the conversion index and time [see Equation 2-3] that is independent of dilution. Graphing the conversion index, normalized by $[I]_0$, against polymerization time, yields a single trend for both reactions. (Figure 2-4) The normalized conversion indices overlap demonstrating that

Table 2-1. Polymerization of 2,3,4,6,1',3',4',6'-octa-O-(2-bromoisobutyryl)saccharose

entry	$[I]_0$ (mmol/L)	time (min)	conv (%)[a]	$\overline{DP}_n$, theor[b]	$\overline{DP}_{n,arm}$, theor[c]
$(PtBMA_{10})_7$	4.7	30	14.0	65.9	9.7
$(PtBMA_{19})_7$	4.7	60	27.5	129.4	19.0
$(PtBMA_{26})_7$	4.7	90	37.8	177.9	26.2
$(PtBMA_{31})_7$	4.7	120	45.4	213.6	31.4
$(PtBMA_{35})_7$	4.7	150	50.0	235.3	34.6
$(PtBMA_{2})_7$	1.4	30	3.3	15.5	2.3
$(PtBMA_{3})_7$	1.4	40	3.8	17.9	2.6
$(PtBMA_{4})_7$	1.4	50	5.7	26.8	3.9
$(PtBMA_{5})_7$	1.4	60	7.2	33.9	5.0
$(PtBMA_{7})_7$	1.4	75	9.5	44.7	6.6
$(PtBMA_{8})_7$	1.4	90	11.1	52.2	7.7
$(PtBMA_{10})_7$	1.4	105	13.8	64.9	9.6
$(PtBMA_{12})_7$	1.4	120	16.9	79.5	11.7
$(PtBMA_{13})_7$	1.4	145	18.4	86.6	12.7

[a]Conversion measured by ^{1}H-NMR peak integration. [b]Theoretical degree of polymerization calculated by $\overline{DP}_n = (\Delta[M]/(0.85[I]_0)$. [c]Theoretical degree of arm polymerization calculated by $\overline{DP}_n = (\Delta[M]/[I]_0)/f_{avg}$.

Table 2-2. Characterization of 2,3,4,6,1',3',4',6'-octa-O-(2-bromoisobutyryl)-saccharose

entry	Poisson Term	M_n, theor[d] (g/mol)	$M_{n,}$meas[e] (g/mol)	M_w/M_n[e]
$(PtBMA_{10})_7$	0.10	10 900	9 000	1.05
$(PtBMA_{19})_7$	0.05	19 900	14 400	1.09
$(PtBMA_{26})_7$	0.04	26 800	17 700	1.11
$(PtBMA_{31})_7$	0.03	31 900	20 400	1.10
$(PtBMA_{35})_7$	0.03	35 000	22 300	1.14
$(PtBMA_2)_7$	0.44	3 700	2 400	1.11
$(PtBMA_3)_7$	0.38	4 100	2 800	1.11
$(PtBMA_4)_7$	0.25	5 300	3 300	1.10
$(PtBMA_5)_7$	0.20	6 400	3 700	1.10
$(PtBMA_7)_7$	0.15	7 900	4 300	1.11
$(PtBMA_8)_7$	0.13	9 000	4 900	1.12
$(PtBMA_{10})_7$	0.10	10 800	5 300	1.12
$(PtBMA_{12})_7$	0.09	12 800	5 800	1.12
$(PtBMA_{13})_7$	0.08	13 800	6 500	1.13

[d]Theoretical molecular weight calculated by $Mn=(\overline{DP}_{n,theor})(MW_M)+MW_I$. [e]SEC using differential refractive index detection vs linear polystyrene standards.

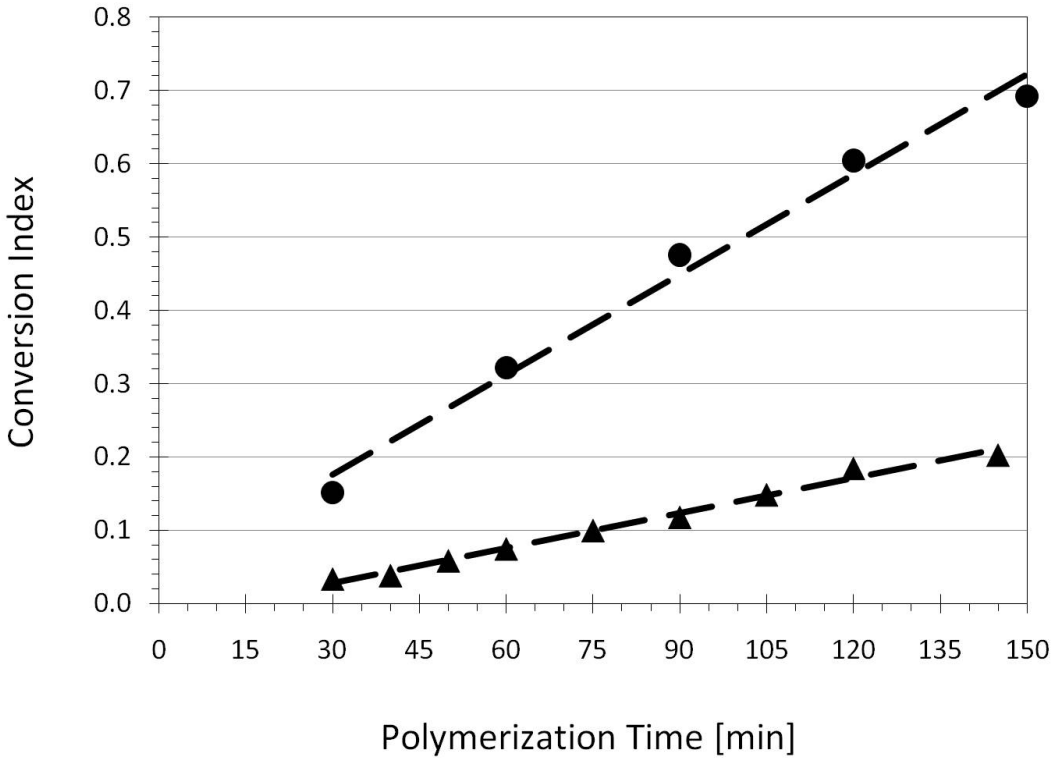

Figure 2-3. The conversion index of monomer as a function of polymerization time for tBMA star oligomers with initial initiator concentrations of 4.7 (●) and 1.4 (▲) mmol/L.

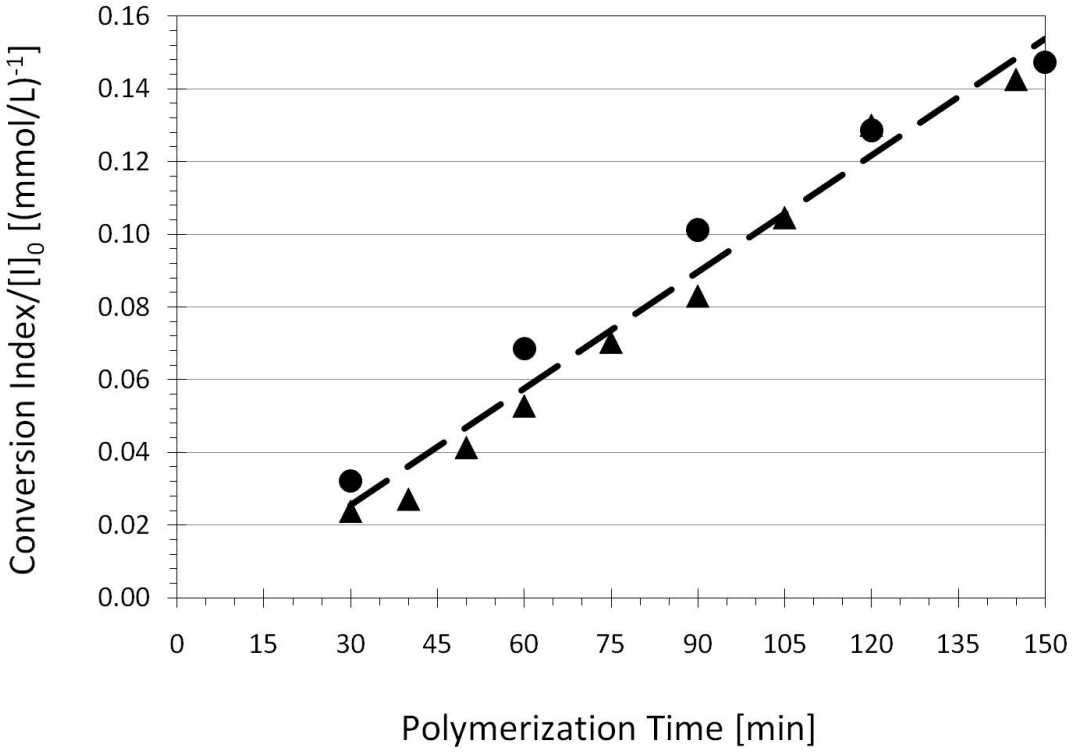

Figure 2-4. Conversion index normalized by $[I]_0$ as a function of polymerization time for tBMA star oligomers with initial initiator concentrations of 4.7 (●) and 1.4 (▲) mmol/L. Trendline is calculated from the combined data set resulting in $\ln([M]_0/[M]_t) \cdot [Cu^{II}] \cdot [Cu^{I}]^{-1} \cdot [I]_0^{-1} \cdot t^{-1} = 4.21 \cdot 10^{-4}$ [$min^{-1} \cdot mmol^{-1} \cdot L$].

this relationship can be extended to dilutions of 1000% without inducing unexpected kinetic behaviors.

$$\ln\left(\frac{[M]_0}{[M]_t}\right) = \frac{k_p K_{ATRP}[P_m X][Cu^I]}{[Cu^{II}]} t \qquad \text{Equation 2-2}$$

$$\ln\left(\frac{[M]_0}{[M]_t}\right) \approx [I]_0 t \qquad \text{Equation 2-3}$$

$$Mn,pred = \left[1 - \left(e^{k_p K_{ATRP}[I]_0[Cu^I]_0 t/[Cu^{II}]_0}\right)^{-1}\right] \frac{[M]_0 MW_{mer}}{[I]_0 I_{eff}} + MW_{init} \qquad \text{Equation 2-4}$$

A linear relationship exists between the M_n measured by SEC and the conversion index, providing further evidence of the living character of these reactions. The measured M_n for all samples falls below the theoretical M_n. This is consistent with previous reports of star polymers that have a lower hydrodynamic radius than equivalent molecular weight linear polymers.[29-34, 48] Therefore, in SEC techniques, such as GPC, that calibrate molecular weight to the hydrodynamic radius of a linear standard, the measured molecular weight of stars will be less than the stars' absolute molecular weight. The difference depends on the star's functionality and the calibration of the GPC.

This study has verified that the rate of monomer addition in ATRP can be reduced sufficiently to prepare low polydispersity, star oligomers. One can vary the rate of monomer conversion linearly with concentration by keeping the ratio between monomer, initiator, catalysts and ligand constant. Equation 2-3 becomes a simple, but powerful tool for tailoring the molecular weight of star oligomers. One need only calculate a conversion that corresponds to the desired molecular weight and then dilute the reaction until the polymerization time reaches a value that gives repeatable results. (Figure 2-5)

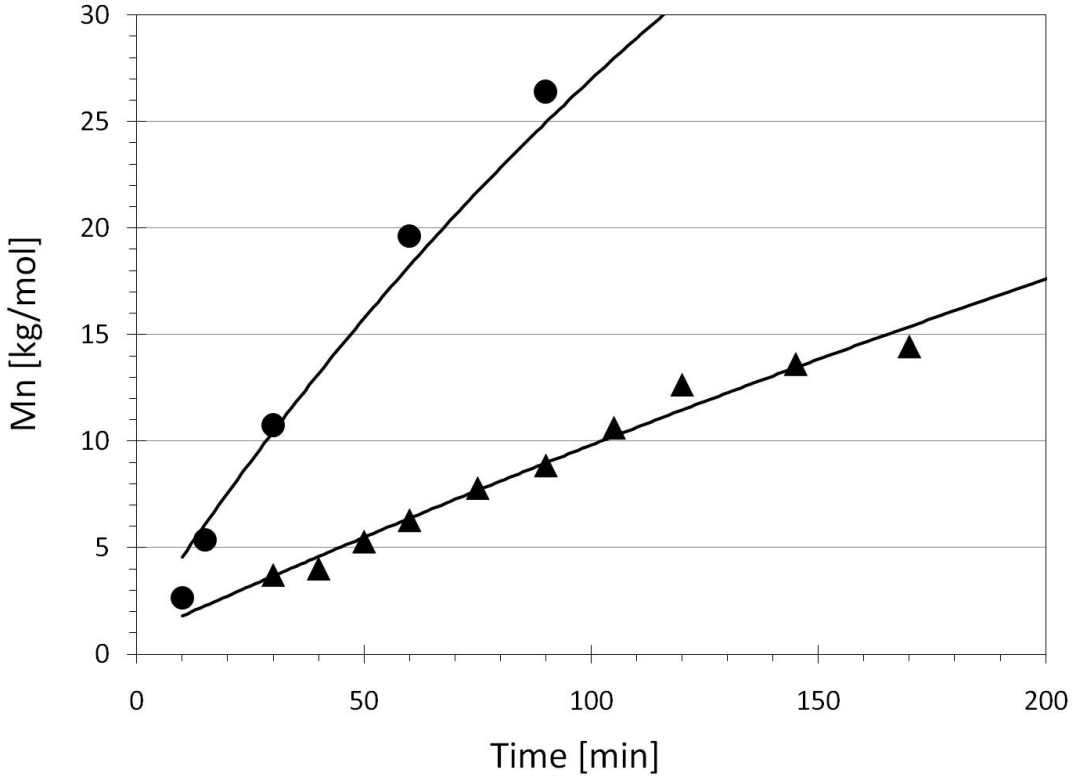

Figure 2-5. Mn is plotted against polymerization time with initial initiator concentrations of 4.7 (●) and 1.4 (▲) mmol/L. Curves show molecular weight calculated from linear conversion index, time best fit lines [see Equation 2-4].

2.3.2 Glass Transition Temperature

T_g is analyzed as a function of molecular weight for all p(tBMA) stars polymerized from SAC-Br_8 that are presented in this publication, in addition to higher molecular weight materials that were prepared for a solution property investigation discussed in a separate publication.[41] (Figure 2-6) The Fox-Flory Equation for T_g [See Equation 2-5][49, 50] is fit to the data by a root mean square calculation, giving the Tg of infinite weight star poly(tBMA)($T_{g,\infty}$) at 111 °C and a Fox-Flory constant (K) of 125 °C·kg/mol.

$$T_g = T_{g,\infty} - K/Mn \qquad \text{Equation 2-5}$$

2.3.3 ATRP Synthesis of Star Oligomers Modified by Reaction Time

Having established that the experimental results are described by Equation 2-3, and gained insight into the star oligomers' thermal behavior, the next goal was to synthesize and isolate star oligomers in larger quantities for more extensive testing.

A consequence of high dilution, low conversion and low molecular weight reaction conditions is that the resulting solution could not be directly precipitated. Following the removal of catalyst by filtration, the solution was concentrated. Excess monomer was successfully removed by dialysis with 1000 Dalton dialysis tubing in 1,4-dioxane, enabling the precipitation of the product in methanol/water.

Absolute molecular weights were measured for the pure products by GPC/MALS and GPC/viscosity. (Table 2-3 and Table 2-4) The quantities dn/dc and [η] were measured individually for each star and both were found to be higher at the region I-II boundary than at the region II-III boundary. In evaluating reproducibility, both materials were found to have an onset polymerized 20 minutes longer than the original experiments but otherwise follow the predicted trend. (Figure 2-7) The additional

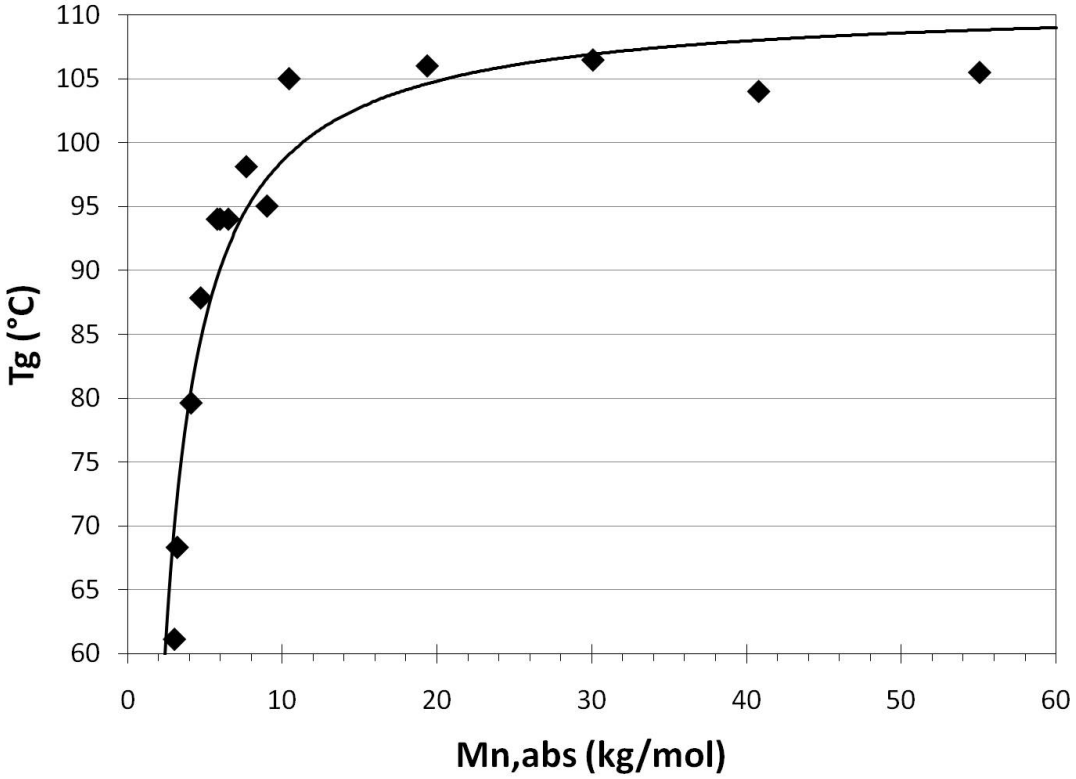

Figure 2-6. Fox-Flory Tg plot for **$(PtBMA_n)_7$**.

Table 2-3. Theoretical and relative molecular weight

			GPC[b]	
entry	time[a] (min)	Predicted Mn (g/mol)	M_n (g/mol)	M_w/M_n
$(PtBMA_4)_7$	60	7 400	5 600	1.3
$(PtBMA_{10})_7$	120	12 700	9 700	1.3

[a]Reaction time in min [b]SEC using differential refractive index detection vs linear polystyrene standards.

Table 2-4. Absolute molecular weight

	GPC/MALS, viscosity			
entry	M_n,abs	M_w/M_n	$[\eta]^c$	dn/dc^d
$(PtBMA_4)_7$	5 400	1.05	7.0	0.113
$(PtBMA_{10})_7$	11 200	1.10	6.1	0.078

[c]In mL/g, integrated from the curve of [η]xMW vs elution volume. [d]In mL/g, from the curve of Δn vs. concentration.

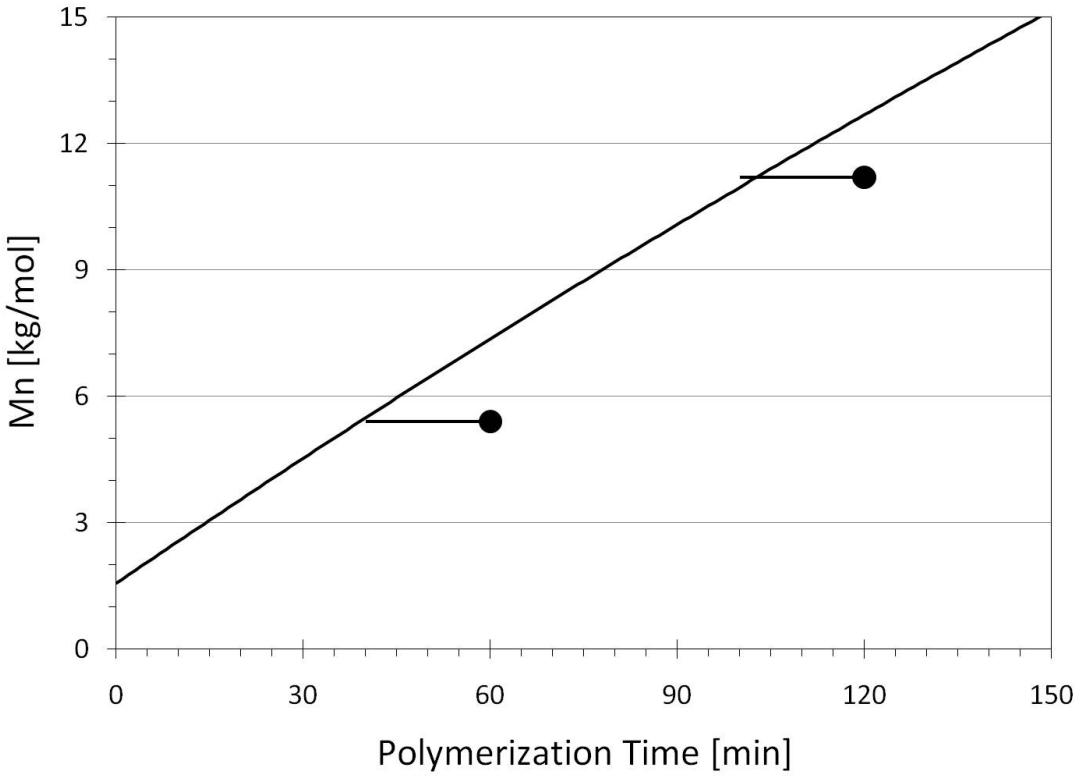

Figure 2-7. Mn_{abs} for $\mathbf{(PtBMA_4)_7}$ and $\mathbf{(PtBMA_{10})_7}$ are plotted against Mn_{pred} (curved line), which is calculated from Equation 2-4 using the value for $\ln([M]_0/[M]_t) \cdot [Cu^{II}] \cdot [Cu^{I}]^{-1} \cdot [I]_0^{-1}$ found in Figure 3, to determine reproducibility. Absolute molecular weight lags the predicted molecular weight by 20 minutes.

onset time stems from the scale-up, which resulted in longer initial heating times, shortening the effective polymerization time. Greater reproducibility will be sought in future work by preheating the reactor prior to the addition of ligand to remove heating error from the procedure.

2.3.4 Dissolution of Star-Oligomer and Star-Polymer

QCM measures a change in mass (Δm) on a quartz oscillator by the corresponding frequency change (ΔF), calculated by the resonant frequency (f_0), area of the quartz crystal (A), quartz density (ρ), and quartz shear modulus (μ). [See Equation 2-6][51] Its sensitivity is on the order of nanograms, prompting its use in a recent study on the dissolution of organic films in solution.[52]

$$\Delta F = -\frac{2f_0^2}{A\sqrt{\rho\mu}}\Delta m \qquad \text{Equation 2-6}$$

The dissolution of the star-shaped oligomer was compared with a similarly synthesized star-shaped polymer, **$(PtBMA_{550})_7$**.[41]Initial IPA:H_2O ratios of 2:1 were used and swelling was allowed to continue to completion until a steady rate dissolution equilibrium was achieved prior to titrating in additional IPA. **$(PtBMA_4)_7$** swelled for 10 minutes before the onset of dissolution at 40% swelling. (Figure 2-8) **$(PtBMA_{550})_7$** swelled for 4 hours before an equilibrium was reached at 225% swelling. This result is in agreement with previous knowledge of polymer relaxation time and chain extension decreasing for lower molecular weight materials.[53]

A critical concentration of IPA was observed for both materials, below which the dissolution rate was constant. (Figure 2-9) At greater concentrations, the dissolution rate increased rapidly with additional IPA. The critical concentration occurred at an IPA:H_2O ratio of 2.35:1 for **$(PtBMA_{550})_7$** but not until 2.7:1 for **$(PtBMA_4)_7$**. This

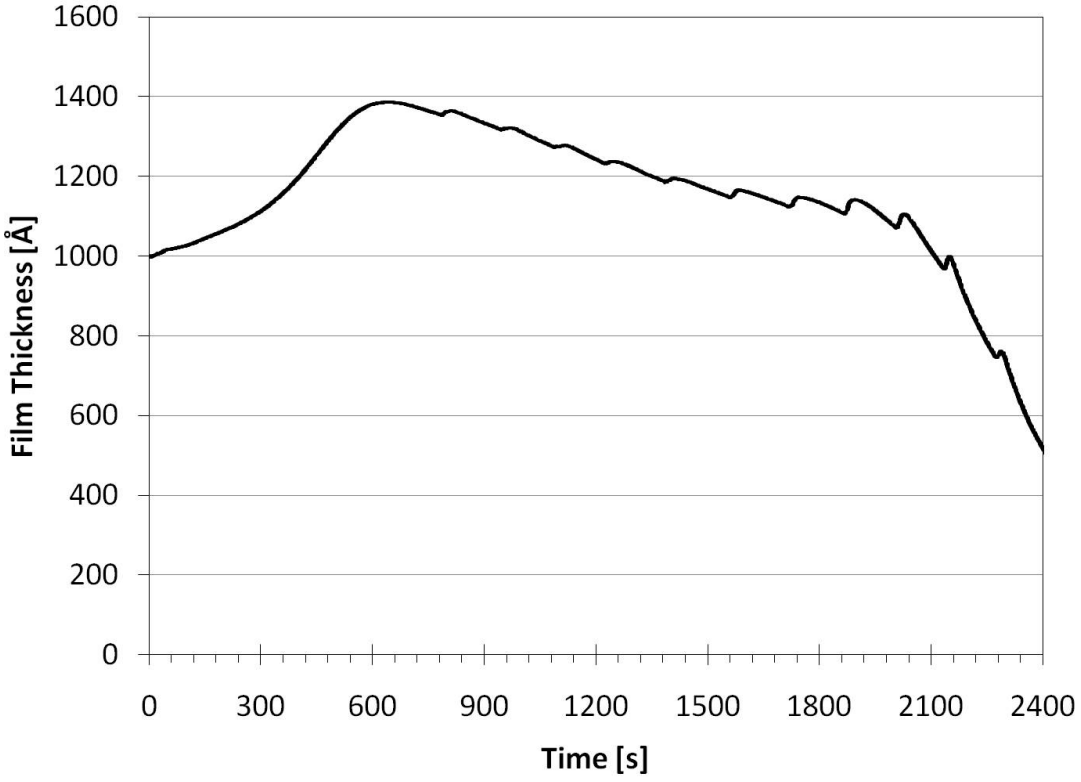

Figure 2-8. QCM thickness titration experiment for **$(PtBMA_4)_7$** in IPA:H_2O. Film achieved 40% swelling after 10 minutes at the initial solvent ratio of 2:1. Periodic thickness increases correspond to the addition of IPA.

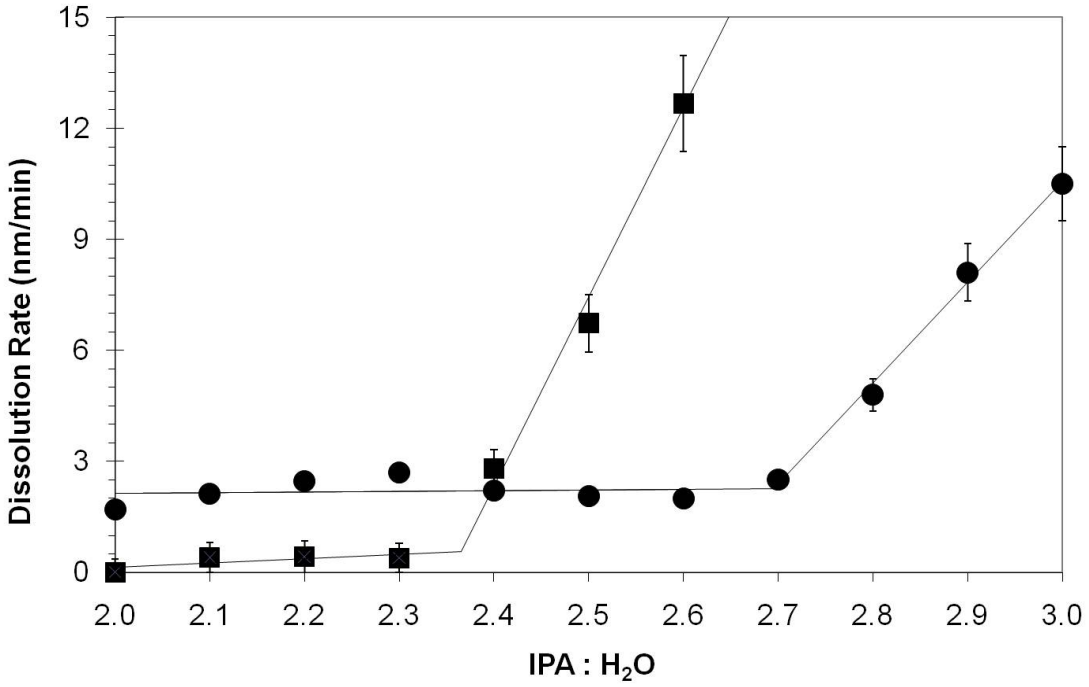

Figure 2-9. Dissolution rates measured by QCM titration for **$(PtBMA_{550})_7$** (■) and **$(PtBMA_4)_7$** (●).

counterintuitive result is likely associated with the increasing influence of the less soluble core on the overall molecule's solubility as molecular weight is decreased in the star oligomer regime. Below the critical concentration, the baseline dissolution rate was negligible for **$(PtBMA_{550})_7$** but 2 nm/min for **$(PtBMA_4)_7$**.

2.3.5 Dissolution Modification of Star Oligomers

The capability to alter the dissolution properties of star-shaped oligomers *in-situ* is lithographically demonstrated. 100 nm lines and spaces in patterns of 2:1, 1:1 and 1:2 were formed by rastering a 100 keV electron beam to generated acid from a BPIN additive in the thin film. Upon heating, the polarity of the star-shaped oligomers in the film was locally increased. This resulted in a solubility switch, increasing the dissolution rate in the exposed lines.[17] The film was developed in a 2:1 IPA:H_2O solution, a concentration at which the star-shaped oligomer was initially insoluble. Positive-tone patterns were formed and imaged with a SEM. (Figure 2-10). Nano-patterned features could not be achieved with the larger star polymer, likely due to a combination of chain entanglements and the swelling behavior observed by QCM. This experiment demonstrates the capability for star-shaped oligomers to react to local stimuli on a size-scale that cannot be achieved with star-shaped polymers.

2.4 Conclusions

A procedure for reproducibly synthesizing star oligomer poly(tBMA) was successfully implemented, relying on a high solvent dilution to control the rate of polymerization. Star oligomers with arms as short as dimers were examined and the Fox-Flory T_g dependence on molecular weight was determined. In addition, an increase in the measured quantities of [η] and dn/dc was found at low molecular weights. Differences between the dissolution behavior of star-shaped oligomers and

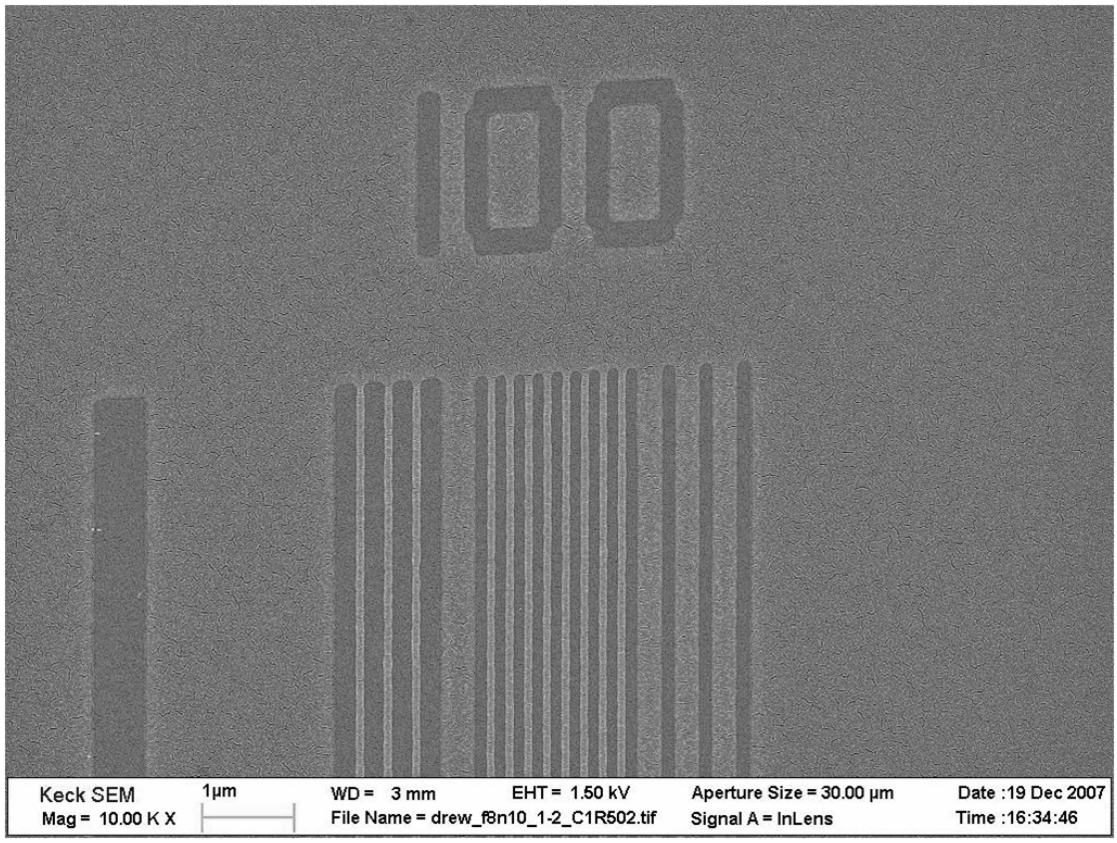

Figure 2-10. SEM of 100 nm half-pitch line spaces test pattern achieved with **$(PtBMA_{10})_7$**. Pattern exposed at 57.1µC/cm^2 with e-beam. 125°C PEB and developed for 1 min in 2:1 IPA:H_2O to reveal positive-tone patterns.

star-shaped polymers were examined with QCM, revealing less swelling and more rapid responses for the lower molecular weight materials. The capability to generate local differences in dissolution behavior was demonstrated lithographically. This capability, which does not exist for high molecular weight star-shaped polymers, indicates that star-shaped oligomers can be used to extend the application and understanding of the star-shaped polymer architecture in new directions.

2.5 Acknowledgement

Financial support from the Semiconductor Research Corporation (GRC-1677.001 and GRC-1675.002) is greatly appreciated. Research was performed in part at the Cornell NanoScale Facility, a member of the Nation Nanotechnology Infrastructure Network and the Cornell Center for Materials Research, which are supported by the National Science Foundation (ECS-0335765 and DMR-0520404). Macromolecular Chemistry I and Macromolecular Chemistry II at the University of Bayreuth are thanked for the generous use of their polymer synthesis and characterization facilities. D.C.F. was supported by a GRC and Applied Materials fellowship.

REFERENCES

1. Likos, C.N. and H.M. Harreis, *Star polymers: from conformations to interactions to phase diagrams.* Condensed Matter Physics, 2002. **29**: p. 173-200.

2. Likos, C.N., *Soft matter with soft particles.* Soft Matter, 2006. **2**: p. 478-498.

3. Likos, C.N., et al., *Star Polymers Viewed as Ultrasoft Colloidal Particles.* Physical Review Letters, 1998. **80**(20): p. 4450-4453.

4. Sutherland, R.J. and R.B. Rhodes, *Dispersant viscosity index improvers*, U.S. Patent, Editor. 1994, Shell Oil Company: United States. p. 1-7.

5. Spinelli, H.J., *Silicone containing acrylic star polymers*. 1991, E. I. du Pont de Nemours and Company. p. 1-9.

6. Hunter, R.J., *Foundations of Colloid Science, Vol. 1*. 1986, New York: Oxford University Press.

7. Grest, G., L.J. Fetters, and J.S. Huang, *Star polymers: experiment, theory, and simulation.* Advances in Chemical Physics, 1996. **94**((Polymeric Systems)): p. 67-163.

8. Hsu, H.-P., W. Nadler, and P. Grassberger, *Scaling of Star Polymers with 1-80 Arms.* Macromolecules, 2004. **37**(12): p. 4658-4663.

9. von Ferber, C. and Y. Holovatch, *Field-theoretical renormalization group analysis for the scaling exponents of star polymers.* Condensed Matter Physics, 2002. **29**: p. 117-136.

10. Dzubiella, J. and A. Jusufi, *Star-polymer-colloid mixtures.* Condensed Matter Physics, 2002. **30**: p. 285-305.

11. Bohrisch, J., et al., *New Polyelectrolyte Architectures.* Advances in Polymer Science, 2004. **165**: p. 1-41.

12. Ganazzoli, F., *Conformations and dynamics of stars and dendrimers: the Gaussian Self-Consistent approach.* Condensed Matter Physics, 2002. **5**(1): p. 37-71.

13. Plamper, F.A., et al., *Synthesis, Characterization and Behavior in Aqueous Solution of Star-Shaped Poly(acrylic acid).* Macromolecular Chemistry and Physics, 2005. **206**: p. 1813-1825.

14. Liechty, W.B., et al., *Polymers for drug delivery systems.* Annual Review of Chemical and Biomolecular Engineering, 2010. **1**: p. 149-173.

15. Adair, J.H., et al., *Recent developments in the preparation and properties of nanometer-size spherical and platelet-shaped particles and composite particles.* Materials Science & Engineering: R: Reports, 1998. **23**(4-5): p. 139-242.

16. Matz, G.F., et al., *Low molecular weight water soluble polymer composition and method of use*, in *PCT Int. Appl.*, W.I.P. Organization, Editor. 2001, Calgon Corporation, USA.

17. Ito, H., *Chemical Amplification Resists for Microlithography.* Advances in Polymer Science, 2005. **172**: p. 37-245.

18. De Silva, A., N.M. Felix, and C.K. Ober, *Molecular glass resists as high-resolution patterning materials.* Advanced Materials, 2008. **20**(17): p. 3355-3361.

19. De Leon-Rodriguez, L.M., et al., *MRI Detection of VEGFR2 in Vivo Using a Low Molecular Weight Peptoid-$(Gd)_8$-Dendron for Targeting.* Journal of the American Chemical Society, 2010. **132**(37): p. 12829-12831.

20. Kato, M., et al., *Polymerization of Methyl Methacrylate with the Carbon Tetrachloride/Dichlorotris-(triphenylphosphine)ruthenium(II)/Methylaluminum Bis(2,6-di-tert-butylphenoxide) Initiating System: Possibility of Living Radical Polymerization.* Macromolecules, 1995. **28**(5): p. 1721-1723.

21. Wang, J.-S. and K. Matyjaszewski, *Controlled/"Living" Radical Polymerization. Atom Transfer Radical Polymerization in the Presence of Transition-Metal Complexes.* Journal of the American Chemical Society, 1995. **117**(20): p. 5614-5615.

22. Wang, J.-L., T. Grimaud, and K. Matyjaszewski, *Kinetic Study of the Homogeneous Atom Transfer Radical Polymerization of Methyl Methacrylate.* Macromolecules, 1997. **30**(21): p. 6507-6512.

23. Sawamoto, M. and M. Kamigaito, *Living radical polymerizations based on transition metal complexes.* Trends in Polymer Science (Cambridge, United Kingdom), 1996. **4**(11): p. 371-377.

24. Haddleton, D.M., et al., *Atom Transfer Radical Polymerization of Methyl Methacrylate Initiated by Alkyl Bromide and 2-Pyridinecarbaldehyde Imine Copper(I) Complexes.* Macromolecules, 1997. **30**(7): p. 2190-2193.

25. Zhang, M. and A.H.E. Müller, *Cylindrical polymer brushes.* Journal of Polymer Science, Part A: Polymer Chemistry, 2005. **43**(16): p. 3461-3481.

26. Sheiko, S.S., B.S. Sumerlin, and K. Matyjaszewski, *Cylindtrical molecular brushes: Synthesis, characterization, and properties.* Progress in Polymer Science, 2008. **33**(7): p. 759-785.

27. Gao, C. and D. Yan, *Hyperbranched polymers: from synthesis to applications.* Progress in Polymer Science, 2004. **29**(3): p. 183-275.

28. Gaynor, S.G. and K. Matyjaszewski, *Step-Growth Polymers as Macroinitiators for "Living" Radical Polymerization: Synthesis of ABA Block Copolymers.* Macromolecules, 1997. **30**(14): p. 4241-4243.

29. Kasko, A.M., A.M. Heintz, and C. Pugh, *The Effect of Molecular Architecture on the Thermotropic Behavior of Poly[11-(4'-cyanophenyl-4"-phenoxy)undecyl acrylate] and Its Relation to Polydispersity.* Macromolecules, 1998. **31**(2): p. 256-271.

30. Kickelbick, G., P.J. Miller, and K. Matyjaszewski, *Multifunctional star initiators for atom transfer radical polymerization.* Polymer Preprints (American Chemical Society, Division of Polymer Chemistry), 1998. **39**(1): p. 284-285.

31. Matyjaszewski, K., et al., *Synthesis of Block, Graft and Star Polymers from Inorganic Macroinitiators.* Applied Organometallic Chemistry, 1998. **12**: p. 667-673.

32. Matyjaszewski, K., et al., *Synthesis and Characterization of Star Polymers with Varying Arm Number, Length and Composition from Organic and Hybrid Inorganic/Organic Multifunctional Initiators.* Macromolecules, 1999. **32**(20): p. 6526-6535.

33. Ueda, J., M. Kamigaito, and M. Sawamoto, *Calixarene-Core Multifunctional Initiators for the Ruthenium-Mediated Living Radical Polymerization of Methacrylates.* Macromolecules, 1998. **31**(20): p. 6762-6768.

34. Ueda, J., et al., *Multifunctional Initiators for the Ruthenium-Mediated Living Radical Polymerization of Methyl Methacrylate: Di- and Trifunctional Dichloroacetates for Synthesis of Multiarmed Polymers.* Macromolecules, 1998. **31**(3): p. 557-562.

35. Muthukrishnan, S., et al., *Synthesis and Characterization of Glycomethacrylate Hybrid Stars from Silsesquioxane Nanoparticles.* Macromolecules, 2005. **38**(26): p. 10631-10642.

36. Plamper, F.A., et al., *Pearl Necklace Architecture: New Threaded Star-Shaped Copolymers.* Macromolecules, 2010. **43**(5): p. 2190-2203.

37. Rein, D., P. Rempp, and P.J. Lutz, *Recent developments in the field of star-shaped polymers.* Makromolekulare Chemie, Macromolecular Symposia, 1993. **67 (EPF Workshop on Anionic Polymerization and Related Processes, 1992)**: p. 237-249.

38. Wang, J.-S., D. Greszta, and K. Matyjaszewski, *Atom transfer radical polymerization (ATRP): A new approach towards well-defined (co)polymers.* Polymeric Materials Science and Engineering, 1995. **73**: p. 416-417.

39. Tang, W. and K. Matyjaszewski, *Kinetic Modeling of Normal ATRP, Normal ATRP with $[Cu^{II}]_0$, Reverse ATRP and SR&NI ATRP.* Macromolecular Theory and Simulations, 2008. **17**: p. 359-375.

40. Goto, A. and T. Fukuda, *Kinetics of living radical polymerization.* Progress in Polymer Science, 2004. **29**: p. 329-385.

41. Weiburger, F., et al., *Solution behavior of poly(tert-butylmethacrylate) star oligomers.* Manuscript in preparation, 2010.

42. Schnitter, M., et al., *Adsorption of linear and star-shaped poly(acrylic acid) to model surfaces formed by amphiphiles at the air/water interface.* Macromolecular Chemistry and Physics, 2000. **201**(13): p. 1504-1512.

43. Heise, A., et al., *Investigation of the Initiation Behavior of a Dendritic 12-Arm Initiator in Atom Transfer Radical Polymerization.* Macromolecules, 2001. **34**(11): p. 3798-3801.

44. Schaefgen, J.R. and P.J. Flory, *Synthesis of multichain polymers and investigation of their viscosities.* Journal of the American Chemical Society, 1948. **70**: p. 2709-18.

45. Schulz, G.V., *The kinetics of chain polymerization. V. The effect of various reaction species on the multimolecularity.* Zeitschrift für physikalische Chemie, 1939. **B43**: p. 25-46.

46. Matyjaszewski, K. and J. Xia, *Atom Transfer Radical Polymerization.* Chemical Reviews, 2001. **101**(9): p. 2921-2990.

47. Matyjaszewski, K., *The importance of exchange reactions in controlled/living radical polymerization in the presence of alkoxyamines and transition metals.* Macromolecular Symposia, 1996. **111**: p. 47-61.

48. Angot, S.K., et al., *Atom Transfer Radical Polymerization of Styrene Using a Novel Octafunctional Initiator: Synthesis of Well-Defined Polystyrene Stars.* Macromolecules, 1998. **31**(21): p. 7218-7225.

49. Fox, T.G., Jr. and P.J. Flory, *Second-order transition temperatures and related properties of polystyrene. I. Influence of molecular weight.* Journal of Applied Physics, 1950. **21**: p. 581-591.

50. Fox, T.G. and P.J. Flory, *The glass temperature and related properties of polystyrene. Influence of molecular weight.* Journal of Polymer Science, 1954. **14**(315-319).

51. Sauerbrey, G., *The use of quartz oscillators for weighing thin layers and for microweighing.* Zeitschrift fuer Physik, 1959. **155**: p. 206-222.

52. De Silva, A., et al., *A fundamental study on dissolution behavior of high-resolution molecular glass photoresists.* Chemistry of Materials, 2008. **20**(23): p. 7292-7300.

53. Rubinstein, M. and R.H. Colby, *Polymer Physics*. 2003: Oxford University Press.

CHAPTER 3. CHEMICALLY AMPLIFIED STAR-SHAPED OLIGOMERS AS 'STAR RESISTS' FOR NEXT GENERATION LITHOGRAPHY

Drew C. Forman, Xavier Andre, Joan K. Bosworth, Priscilla Taylor, John Whang, Marvin Paik, Jin Kyun Lee, and Christopher K. Ober

Materials Science & Engineering

Cornell University, Ithaca, NY 14853

Florian Wieberger and Hans-Werner Schmidt

Macromolecular Chemistry I

University of Bayreuth, Bayreuth, Germany 95440

Andreas Walther, Marietta Böhm, and Axel H. E. Müller

Macromolecular Chemistry II

University of Bayreuth, Bayreuth, Germany 95540

3.0 Abstract

A series of star-shaped oligomer resists consisting of poly(tert-butyl methacrylate) (tBMA) arms and either a tert-butyl cholate, α-D-glucose or saccharose based multifunctional initiators was synthesized via core-first atom transfer radical polymerization (ATRP). The effect of core etch durability on the etch durability of the star resist was studied. Variants on the homopolymer materials were prepared either by reduction of the homopolymers or directly through copolymerization with a lactone ring containing methacrylate to facilitate base development following either electron beam or deep ultraviolet (DUV) exposures. The star architecture was found to induce desirable dry etch durability characteristics indicating potential advantages of this architecture over conventional linear resists, and warranting further study.

3.1 Introduction

Since its inception,[1, 2] the architectural complexity of polymers synthesized by ATRP has advanced from simple linear acrylates and methacrylates[3-5] to cylindrical brushes[6, 7], hyperbranched[8, 9] star polymers[10-16] and highly specialized architectures such as pearl necklaces[17]. A majority of this work has focused on high molecular weight materials, although there exist commercial applications for low molecular weight materials including drug delivery conjugates,[18] nanoparticle dispersions,[19] cosmetics,[20] *in vivo* sensors[21] and lithography[22]. Star polymers, which consist of multiple polymer arms adjoined at a single core branching point, might exhibit superior performance in the field of lithography because, unlike linear materials, the solution properties of polyelectrolyte stars can be adjusted by changing the number of arms.[23-29]

Although the kinetics of ATRP are well understood,[30, 31] synthesizing low molecular weight star polymers presents a significant challenge. In the core-first

approach, polymer arms are grown from multifunctional initiators.[32, 33] A consequence of this strategy is that the molecular weight of the star polymer increases faster than an equivalent linear polymerization, complicating the precision synthesis of star-shaped oligomers. We have recently published an approach that uses a combination of reaction rate reducing factors to reproducibly prepare star-shaped p(tBMA) oligomers with a saccharose core.[34] In examining these materials we have observed that it is possible to achieve desirable thermal and solution properties in the low molecular weight regime.[34, 35] While higher molecular weight star-shaped polymers possess similar properties, they are not suited to lithographic applications where molecular size can limit resolution.[36]

In this chapter we expand the selection of core materials to include glucose and a new tert-butyl cholate multifunctional initiator. (Figure 3-1) Along with the previously reported saccharose core, this trio of cores are used to form a series of star-shaped p(tBMA) oligomers with different numbers of arms. In addition, each core is composed with a different number of carbon rings, a feature that can be exploited to examine the etch durability potential of star-shaped oligomers. Finally, we demonstrate variations on the star-shaped p(tBMA) oligomers that can be developed in an industrial base developer.

3.2 Experimental

3.2.1 Materials

Cholic acid was purchased from AlfaAesar and used as received. 2-Bromo-2-methylpropanoyl bromide, 4-(dimethylamino)pyridine, 2-methacryloyl chloride, triethylamine and 3-hydroxy-4,4-dimethyldihydro-2(3H)-furanone were purchased from Aldrich. AZ® 300 MIF, a 0.26N tetramethylammonium hydroxide (TMAH) base

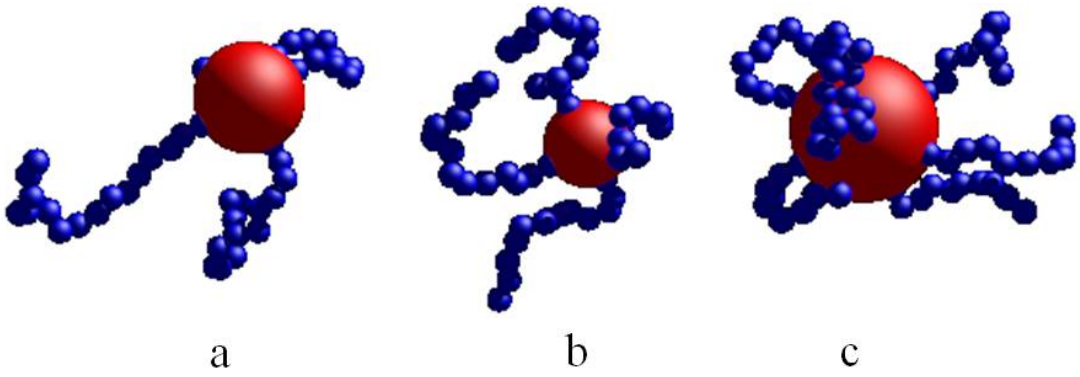

Figure 3-1. Graphical depiction of star-shaped p(tBMA) oligomers comprised of 3, 4 and 7 arms, corresponding to the samples (a) **$(PtBMA_{16})_3$**, (b) **$(PtBMA_{12})_4$** and (c) **$(PtBMA_{10})_7$**. The cores and monomer units are represented by spheres with volumes equal to each component's molecular weight.

developer, was purchased from Fisher. Anhydrous pyridine, CH_2Cl_2 CuCl, $CuCl_2$, $LiAlH_4$ and N,N,N',N",N"-pentamethyldiethylenetriamine (PMDETA) were purchased from Aldrich and used without further purification. The tBMA monomer was purchased from Aldrich and passed through a basic alumina column to remove the inhibitor. Reaction solvents were purchased through Aldrich.

The poly(tBMA) polymers prepared in this chapter are named for their architecture: $(PtBMA_n)_f$ where n is the number average of monomer units per arm and f is the number average of arms per molecule.

3.2.2 Synthesis

3.2.2.1 Preparation of Multifunctional Initiators

The core-first[32] approach and ATRP were selected to synthesize star-shaped poly(tBMA) oligomers. Three multifunctional initiators, with different functionality, were synthesized to serve as the precursors for stars with different numbers of arms. 2,3,4,6,1',3',4',6'-octa-O-(2-bromoisobutyryl)-saccharose (SAC-Br_8), which has eight initiating sites, was prepared from saccharose and 1,2,3,4,6-penta-O-(2-bromoisobutyryl)-α-D-glucose (GLU-Br_5), which contains five initiating sites, was prepared from α-D-glucose.[29] A third initiator, Tris(2-bromoisobutyryl)tert-butyl cholate (tCHO-Br_3), containing four rings and three initiating sites, was prepared by the following procedure.

Tert-butyl cholate was prepared according to the literature method.[37] It should be noted that a different ATRP initiator with four initiating sites was recently published using a different cholic acid derivative.[38]

^{1}H NMR spectra were recorded on a Varian Inova-500 spectrometer at ambient temperature, using the chemical shift of a residual solvent ($CHCl_3$ at δ 7.28 ppm) as an

internal reference. All chemical shifts are quoted in parts per million (ppm) relative to the internal reference and coupling constants *J* are measured in Hz. The multiplicity of the signal is indicated as follows: s (singlet), d (doublet) and m (multiplet). ^{13}C NMR spectra were recorded on a Varian Inova-500 (126 MHz) spectrometer using the central resonance of the triplet of $CDCl_3$ at δ 77.0 ppm. Infrared absorptions were measured for samples on a NaCl window with a Mattson Instruments Galaxy 2020 spectrophotometer. Microanalyses were carried out by Quantitative Technologies, Inc. Mass spectrometry was performed by the Department of Molecular Biology and Genetics, Cornell University. Thermo gravimetric analysis (TGA) was performed on a TA Instruments Q500 at a heating rate of 10 °C min^{-1} under N_2. The T_g of materials were measured on a TA Instruments Q1000 modulated differential scanning calorimeter (DSC) at a heat/cool rate of 10°C min^{-1} under N_2 for heat/cool/heat cycles.

To a magnetically stirred solution of *tert*-butyl cholate[37] (1.00 g, 2.15 mmol) in CH_2Cl_2 (anhydrous, 15 cm^3) were added pyridine (anhydrous, 1.2 g, 15 mmol), 4-(dimethylamino)pyridine (0.079 g, 0.65 mmol) and 2-bromo-2-methylpropanoyl bromide (2.47 g, 10.8 mmol) in ice/water bath. The reaction mixture was stirred for 1 h at 0˚C and kept overnight at room temperature. It was then poured into water (20 cm^3). The bottom layer was recovered, washed with water (20 cm^3), dried over anhydrous $MgSO_4$ and concentrated under reduced pressure. The resulting crude product was purified by flash column chromatography (silica gel, CH_2Cl_2) to give the ester **tCHO-Br$_3$** as a white amorphous solid (0.85 g, 43%); (Found: C, 52.8; H, 6.7. $C_{40}H_{63}Br_3O_8$ requires C, 52.7; H, 7.0); ν_{max}(NaCl window)/cm^{-1} 2973, 2942, 2871, 1729, 1462, 1386, 1279, 1172, 1110, 1009, 905 and 733; δ_H (500 MHz; $CDCl_3$) 0.78 (3 H, s, C*H*$_3$), 0.84 (3 H, d, *J* 6.5, C*H*$_3$), 0.97 (3 H, s, C*H*$_3$), 1.06-1.24 (3 H, m), 1.29-1.42 (3 H, m), 1.44 [9 H, s, C(C*H*$_3$)$_3$], 1.51-1.82 (12 H, m), 1.85 [6 H, s, (C*H*$_3$)$_2$BrC], 1.98 [3 H, s, (C*H*$_3$)$_2$BrC], 2.00 [6 H, s, (C*H*$_3$)$_2$BrC], 2.01 [3 H, s, (C*H*$_3$)$_2$BrC], 2.04-

2.36 (6 H, m), 4.61-4.68 (1 H, m, CH_2CHO), 5.02 (1 H, d, *J* 2.5, CH_2CHO) and 5.18 (1 H, s, CH_2CHO); δ_C (126 MHz; $CDCl_3$) 11.98, 17.52, 22.00, 23.02, 24.44, 25.83, 27.17, 28.09, 28.58, 30.66, 30.70, 30.80, 30.84, 30.93, 30.95, 30.98, 31.16, 32.59, 34.26, 34.35, 34.51, 34.84, 38.19, 40.31, 42.92, 45.25, 47.60, 56.11, 56.18, 56.26, 72.80, 75.06, 80.03, 170.47, 170.56, 170.86 and 173.41; *m*/*z* (ES) 935.2 [$(M+Na)^+$. $C_{40}H_{63}Br_3NaO_8$: requires *M*, 935.2].

3.2.2.2 Preparation of tert-Butyl Methacrylate Star Oligomer Homopolymers

374mg (0.41mmol) of **2**, 8.75g (61.55mmol) tBMA, 234.7mg (1.35mmol) PMDETA, 93.8mg (0.95mmol) CuCl and 54.6mg (0.41mmol) $CuCl_2$ were stirred in 90 mL of acetone under an inert atmosphere. The solution was placed in a 60 °C oil bath for 2 hours.

Additional $CuCl_2$ was added and the reaction quenched in cold water. The solution was concentrated under reduced pressure, taken up in dichloromethane and filtered through silicon powder to remove the copper catalyst. The solution was then concentrated under reduced pressure a second time, taken up in 1,4-dioxane and placed in 1000 Dalton dialysis tubing. Dialysis in one liter of 1,4-dioxane was performed overnight, twice. The contents of the dialysis tubing were concentrated under reduced pressure and precipitated into water/methanol. The precipitate was collected and freeze-dried to obtain star poly(tBMA) with a tert-butyl cholate core **$(PtBMA_{16})_3$**. (Figure 3-2)

Similar procedures were followed with 228mg (0.246mmol) GLU-Br_5 and 240mg (0.154mmol) **SAC-Br_8** substituted for **tCHO-Br_3** to obtain star poly(tBMA) with a glucose core **$(PtBMA_{12})_4$** and star poly(tBMA) with a saccharose core **$(PtBMA_{10})_5$**, respectively. (Figure 3-3 and Figure 3-4)

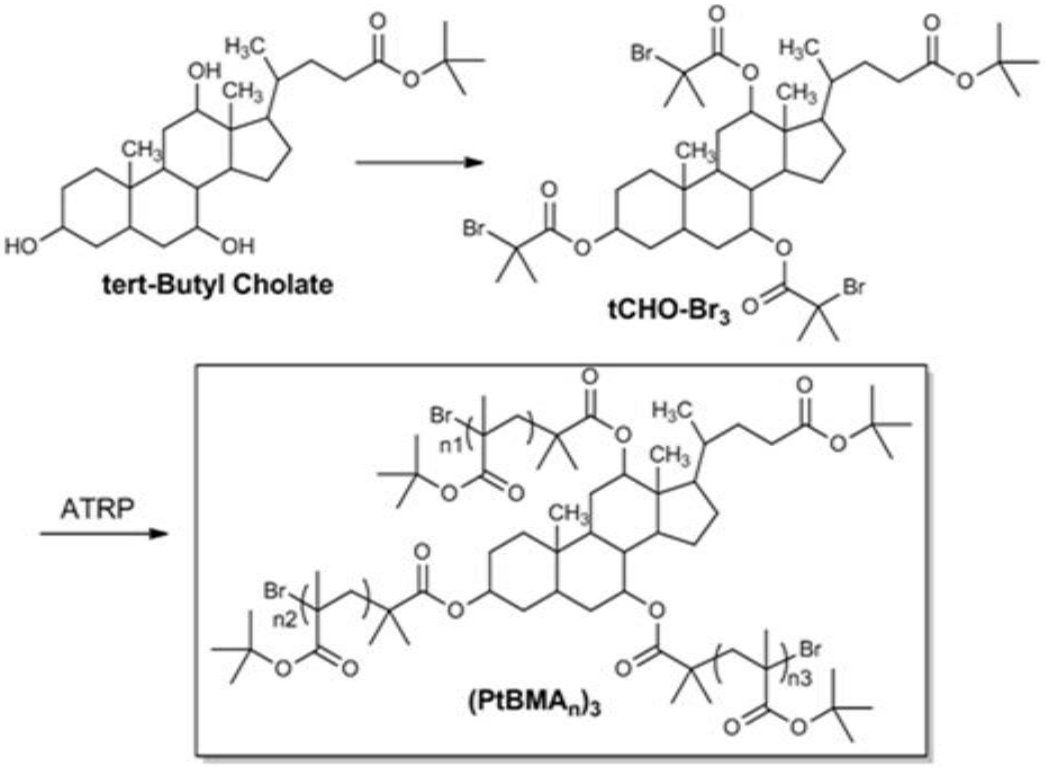

Figure 3-2. Reaction pathway towards three arm tert-butyl methacrylate star oligomers

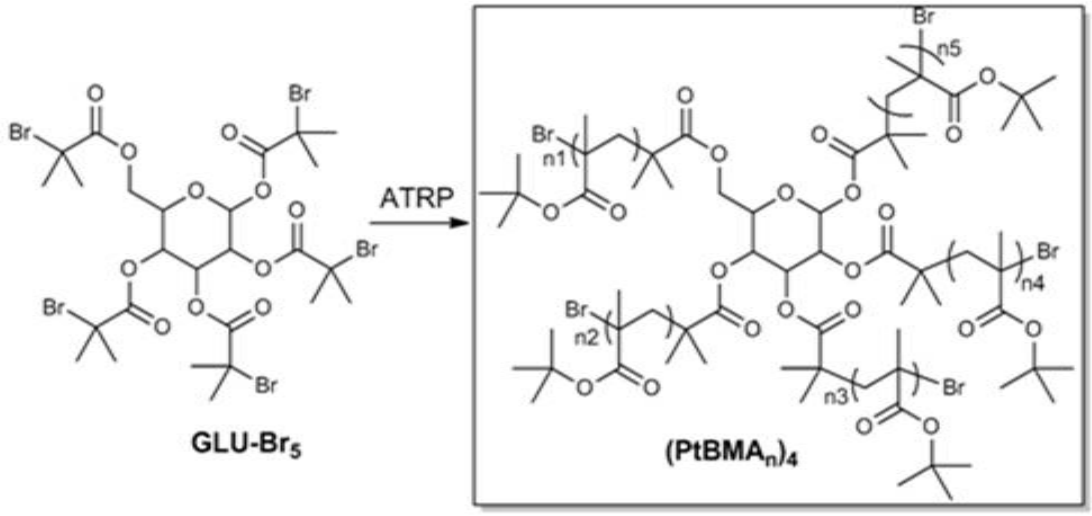

Figure 3-3. Reaction pathway towards four arm tert-butyl methacrylate star oligomers

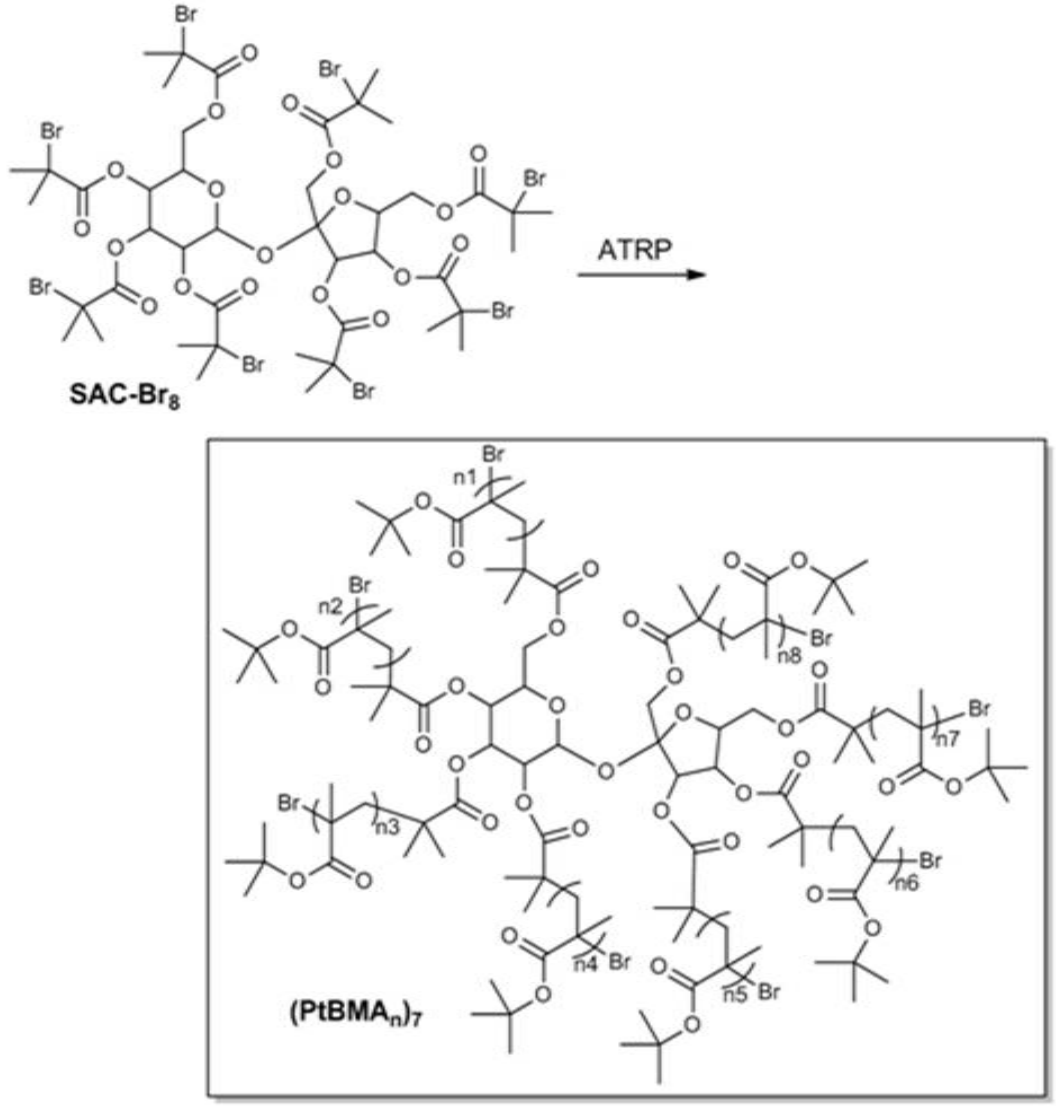

Figure 3-4. Reaction pathway towards five arm tert-butyl methacrylate star oligomers

3.2.2.3 Preparation of Star-Shaped Oligomer Copolymers

Copolymers were achieved by reduction of homopolymers (Figure 3-5) and through copolymerization (Figure 3-6).

Partial reduction of p(tBMA) resulted in a p(tBMA)-co-poly(2-methylprop-2-en-1-ol) (MPO) copolymer. A solution of 0.6 g of star-shaped p(tBMA) oligomer in 6 mL anhydrous THF were stirred under an inert environment. 1.5 mL of 1 M $LiAlH_4$ solution (.45 equivalents) was added dropwise and stirred overnight. The solution was diluted with 50 mL ethyl acetate and washed with aqueous citric acid twice, then extracted with brine and dried over $MgSO_4$, filtered and heated in a vacuum oven to obtain the pure product.

A butyrolactone methacrylate (BLMA) was prepared according to a standard procedure[39] by dropping 2-methacryloyl chloride into an acetonitrile/dry ice cooled methylene chloride solution containing 3-hydroxy-4,4-dimethyldihydro-2(3H)-furanone and triethylamine under an inert atmosphere. The solution was allowed to reach room temperature and stirred for 1 hour. The organics were extracted in ethyl acetate and purified by column chromatography with 3:1 hexanes:ethyl acetate eluent. Copolymerization with tBMA was carried out using the same procedure as the homopolymers, except with a 50/50 monomer feed ratio.

3.2.3 Characterization

The molecular weight of purified star-shaped oligomers were measured by size exclusion chromatography (SEC) performed on a Waters GPC system (Waters 486 UV detector) by eluting THF (1 cm^3 min^{-1}) at 40°C with a linear polystyrene standard to determine relative molecular weight.

SEC with a Wyatt DAWN HELEOS multiangle light scattering detector equipped with a 632.8 nm He-Ne laser (GPC/MALS) and Viscotek Model 250 viscosity detector

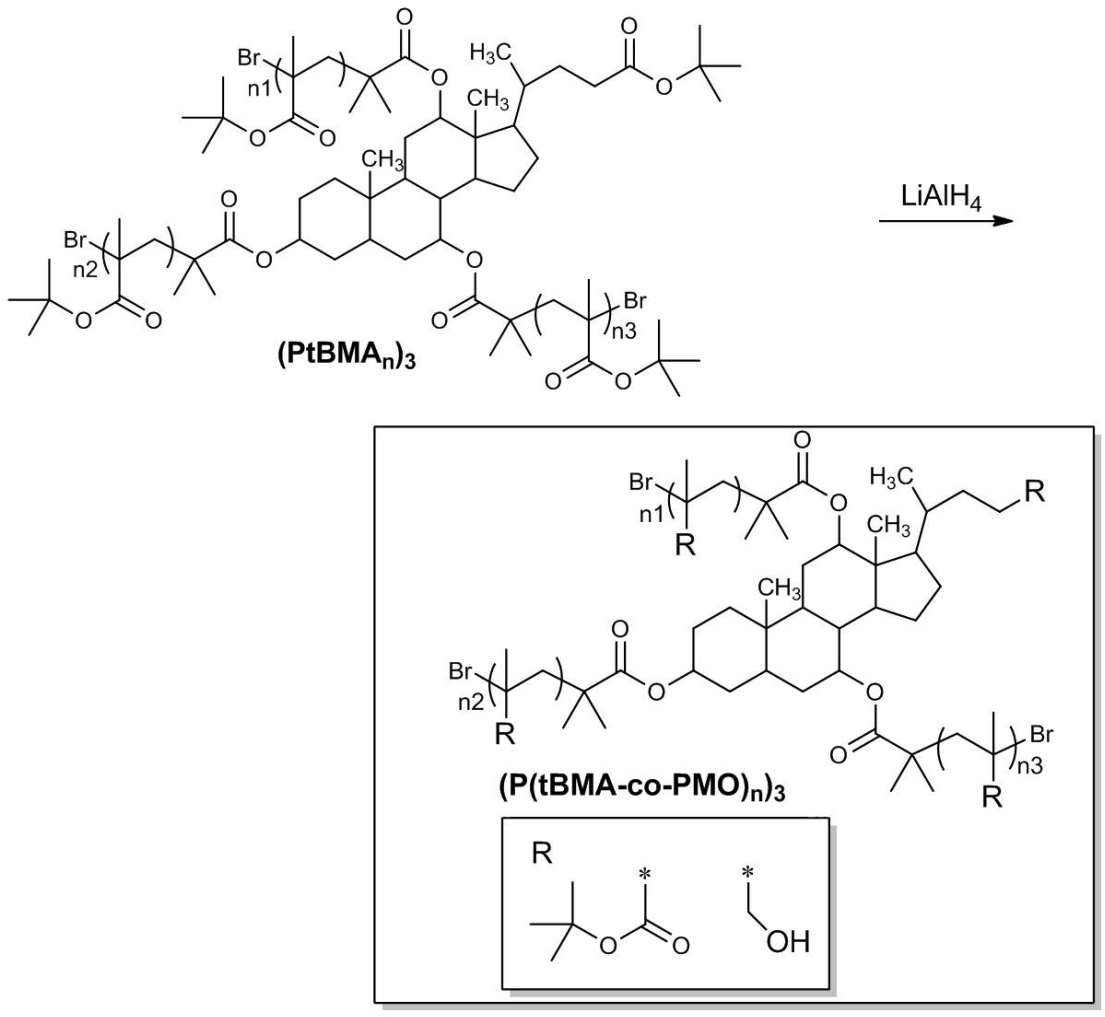

Figure 3-5. Reaction pathway towards p (tBMA)-co-p(MPO) star-shaped oligomers

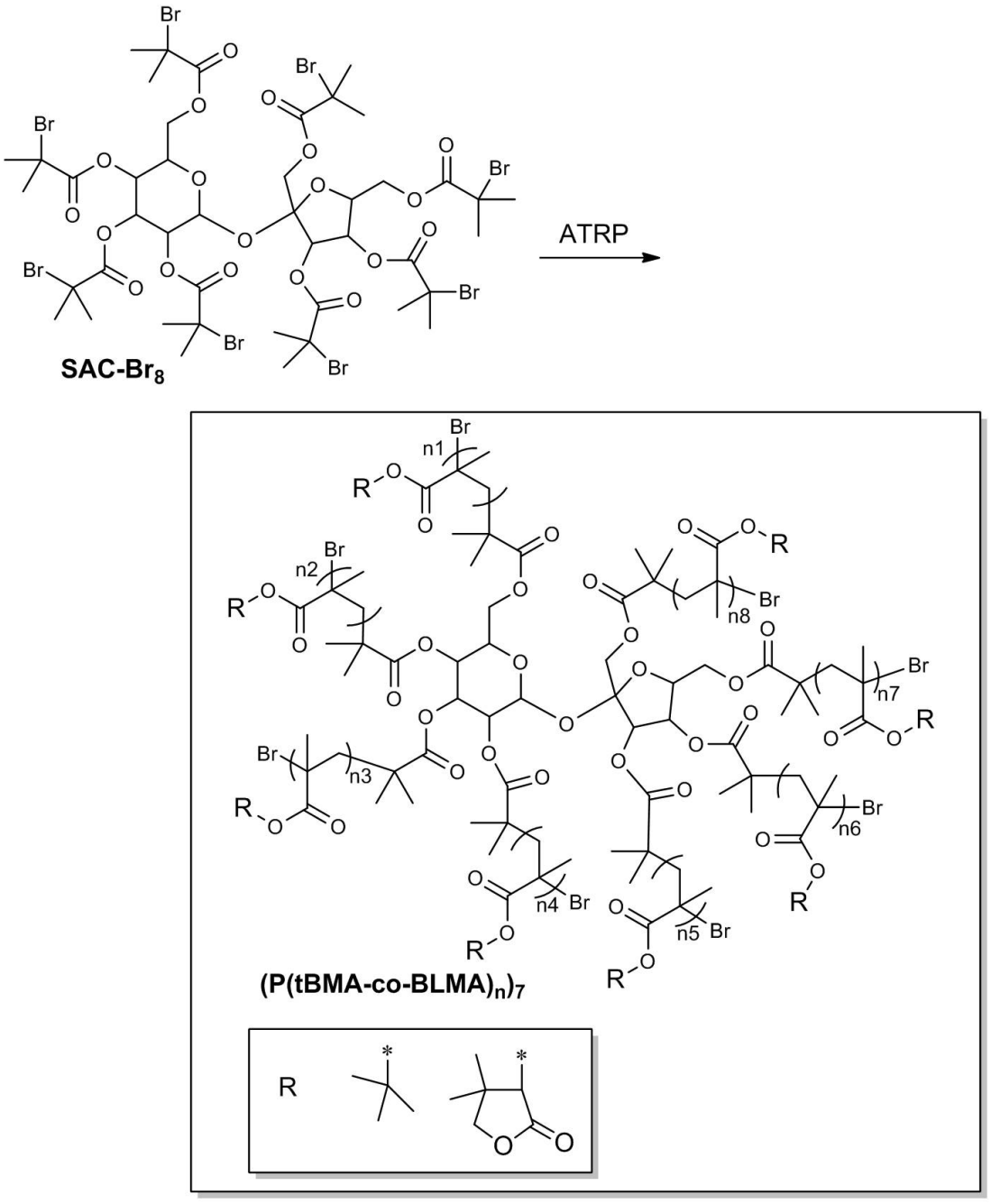

Figure 3-6. Reaction pathway towards p(tBMA)-co-p(BLMA) star-shaped oligomers

(GPC/viscosity) were used to determine the absolute molecular weights. THF was used as eluent at a flow rate of 1.0 mL/min: column set, 5 μm PSS SDV gel, 103, 105, and 106 Å, 30 cm each. For GPC/viscosity, the refractive index increment of the star oligomer solutions in THF at 25 °C were measured to individually for each star using a PSS DnDC-2010/620 differential refractometer.

3.2.4 Lithographic Evaluation

100 nm films were obtained through spincoating five weight percent solutions of polymer containing five weight percent photoacid generator (PAG) in propylene glycol methyl ether acetate at 2000 RPM onto a silicon wafer vapor primed with HMDS. The resulting films underwent a post-apply bake (PAB) for 60 seconds at 105°C. Following thermal treatment the test patterns were exposed in the film at a range of doses, either under 365 nm UV using a GCA Autostep 200 DSW i-line step-and-flash tool and a 100keV Leica VB6-HR electron beam tool. A post exposure bake (PEB) for 30 seconds was followed by development in an isopropanol/water solution to reveal the test patterns. The test patterns were examined under an optical microscope. Fine features were examined by sputtered with a thin film of Gold / Palladium using a Hummer Au/Pd Sputtering System and placing the sample in a LEO 1550 Field Emission Scanning Electron Microscope (SEM) operated at 1.5 kV.

3.2.5 Dry Etch Durability

Thin films were obtained through spincoating. 15 weight percent solutions of stars in ethyl L-lactate were prepared and the solutions spun on unprimed silicon wafers. 15 weight percent solutions of the initiators **tCHO-Br$_3$** and **SAC-Br$_8$** in toluene and a 15 weight percent solution of initiator **GLU-Br$_5$** in acetone/toluene 95/5 were prepared and spincoated on HMDS primed silicon wafers. A 15 weight percent solution of 8

kg/mol poly(hydroxystyrene) (PHOST) from Sigma-Aldrich in propylene glycol methyl ether acetate was prepared and the solution spun onto an unprimed silicon wafer as a control. A 15 weight percent solution of poly(tBMA) from Polysciences, Inc. in ethyl L-lactate was prepared and the solution spun on an unprimed silicon wafer.

A CF_4 RIE was performed on each sample for 1 minute using an Oxford PlasmaLab 80Plus RIE tool. Each sample was etched with a PHOST control and the film thicknesses of the sample and control were measured before and after etching using profilometry to determine the etch rate relative to the PHOST control. Following these measurements the multifunctional initiator thin film samples were tested with a General Area Detector Diffraction System (GADDS) to verify that crystallization had not occurred during the experiment.

3.3 Results and Discussion

The commercial application of polymer photoresists requires a synthetic procedure capable of achieving target molecular weights (typically < 10kg/mol) with a high degree of reproducibility between polymer batches. Introducing the star-shaped polymer architecture for this application necessitates similar overall molecular weights. For a five-arm star, the average arm length must be limited to less than 2 kg/mol, or several monomer units for conventional monomers used in the synthesis of photoresists. This requirement creates procedural challenges that must be overcome to reliably synthesize the target molecules. Large deviation from the target arm length between batches will be introduced to the star oligomer if monomer additions occur at a rate greater than the temporal precision in which a reaction can be reliably initiated, carried out and quenched. It is imperative that monomer additions per chain end occur on a time scale no less than one addition every few minutes. Having recently

pioneered a technique for reproducibly synthesizing star-shaped oligomers, it is now possible to conduct a lithographic investigation.

A basic series of three star-shaped oligomers were synthesized by polymerizing from each multifunctional initiator for 2 hours. The quantity of dn/dc was measured for each star-shaped oligomer and was found to be dependent on the core material. This enabled the determination of absolute molecular weight. (Table 3-1 and Table 3-2) The ratio of monomer to initiating site was held constant for each reaction. However, differences between the multifunctional initiators' solubility and initiation efficiency led to slight differences in the average arm length.

Initiation efficiency was determined by comparing theoretical degree of polymerization from conversion data to the degree of polymerization determined from the absolute molecular weight. Steric hindrances are known to limit initiation efficiency for stars.[40] Both the **GLU-Br$_8$** and **SAC-Br$_5$** initiator were found to have initiation efficiencies close to 85%, resulting in median stars of 4 and 7 arms respectively. The initiator **tCHO-Br$_3$**, which only has three initiating sites, was found to provide more efficient initiation presumably as a result of its lower steric hindrance.

3.3.1 Lithographic Evaluation of Star-Shaped Oligomer Homopolymers

The non-polarity of poly(tBMA) resulted in a film that adhered poorly to the silicon substrate. Poly(tBMA) homopolymer contains only a non-polar acid labile monomer, whereas commercial photoresists contain additional monomer species, including a polar monomer that acts as an adhesion promoter. The lack of an adhesion promoter led to inconsistent film quality. However, uniform films were achieved through repeated spincoating attempts.

The lack of a polar monomer species also proved to be a challenge during the development step. Regardless of exposure dose, the poly(tBMA) homopolymers

Table 3-1. Relative molecular weight

			GPC[b]	
entry	initiator	time[a]	M_n (g/mol)	M_w/M_n
$(PtBMA_{16})_3$	**$tCHO\text{-}Br_3$**	120	6 400	1.3
$(PtBMA_{12})_4$	**$GLU\text{-}Br_5$**	120	5 700	1.3
$(PtBMA_{10})_7$	**$SAC\text{-}Br_8$**	120	9 700	1.3

[a]Reaction time in min [b]SEC using differential refractive index detection vs linear polystyrene standards.

Table 3-2. Absolute molecular weight

entry	GPC/MALS, viscosity			
	M_n,abs (g/mol)	M_w/M_n	$[\eta]^c$	dn/dc^d
$(PtBMA_{16})_3$	7 600	1.10	6.4	0.083
$(PtBMA_{12})_4$	8 200	1.08	4.4	0.064
$(PtBMA_{10})_7$	11 200	1.10	6.1	0.078

[c]In mL/g, integrated from the curve of [η]xMW vs elution volume. [d]In mL/g, from the curve of Δn vs. concentration.

remained insoluble in 0.26N TMAH. The number of chemical switches required to render the poly(tBMA) homopolymers soluble in 0.26N TMAH could not be achieved with standard PAG concentrations and bake times. High-resolution features were achieved by developing in a solution of isopropanol and water. (Figure 3-7)

3.3.2 Lithographic Evaluation of Star-Shaped Oligomer Variants

Demonstrating that star-shaped oligomers can be base developable is an important goal, not only because of the prevalence of base developer throughout the semiconductor industry but also because the capability to reduce the expansion of polyelectrolyte stars might be advantageous to the lithographic process.[29]

Four modified star-shaped oligomers (Table 3-3) were investigated to determine whether the core or the arms were more important in the base development process. Larger versions of the stars initiated from **tCHO-Br$_3$** and **SAC-Br$_8$** were examined to determine if increasing the arm:core ratio could improve base development. Both materials were lithographically tested and, similar to their shorter arm counterparts, patterns could not be achieved through base development alone. This suggested that the strongly non-polar character of the poly(tBMA) homopolymer arms were hindering base development.

(PtBMA$_{16}$)$_3$ was partially reduced via $LiAlH_4$ to **(P(tBMA-co-PMO)$_{16}$)$_3$** increasing the polarity of the star-shaped oligomer's arms. This modification successfully enabled base development in 0.26N TMAH at five weight percent PAG loading in the thin film. (Figure 3-8) Core integrity was verified by measuring the molecular weight before and after reduction.

A separate star-oligomer with increased polarity was directly polymerized from the **SAC-Br$_8$** initiator using a 50/50 feed ratio of tBMA and a BLMA monomer. Base

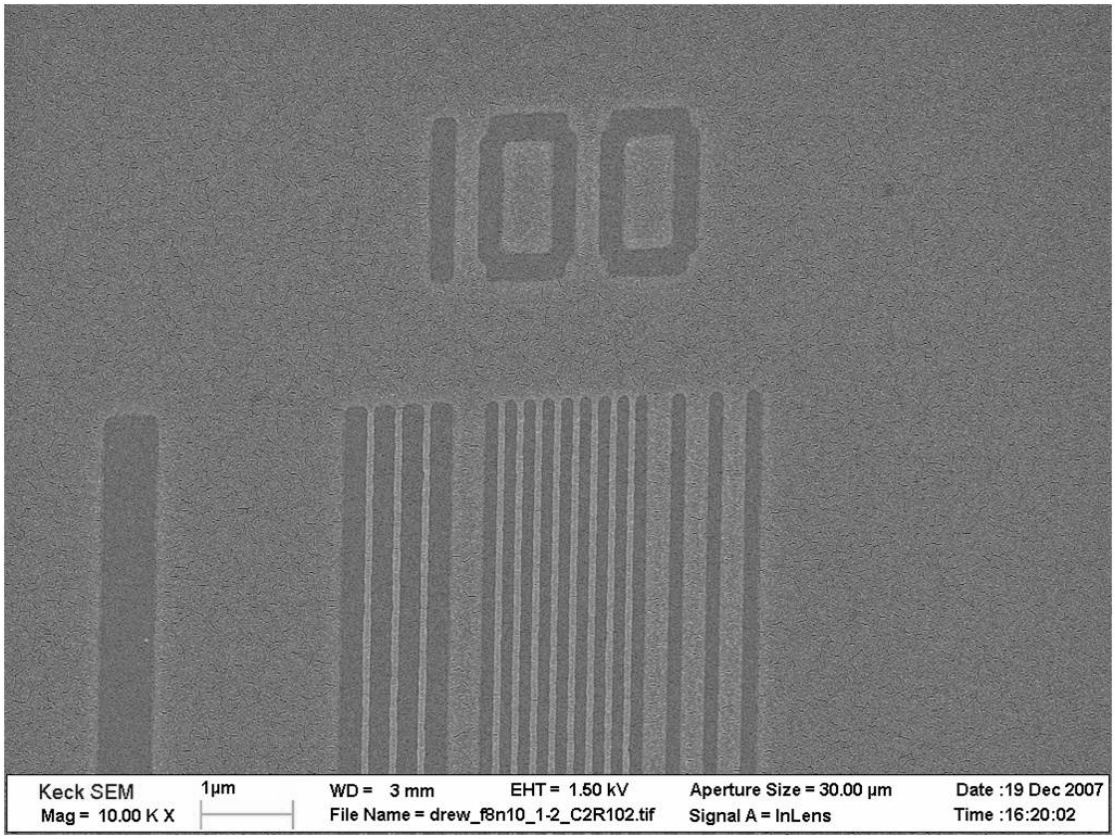

Figure 3-7. SEM of 100 nm half-pitch line spaces test pattern achieved with **$(PtBMA_{10})_7$**. Pattern exposed at 74.3µC/cm^2 with e-beam. 125°C PEB and developed for 1 min in 2:1 isopropanol:water to reveal positive-tone patterns.

Table 3-3. Star-Shaped Oligomer Variants

Entry	Core	Preparation
$(PtBMA_{21})_3$	**$tCHO\text{-}Br_3$**	400 min polymerization
$(PtBMA_{25})_7$	**$SAC\text{-}Br_8$**	400 min polymerization
$(P(tBMA\text{-}co\text{-}PMO)_{16})_3$	**$tCHO\text{-}Br_3$**	Partial reduction
$(P(tBMA\text{-}co\text{-}BLMA)_{10})_7$	**$SAC\text{-}Br_8$**	Copolymerization

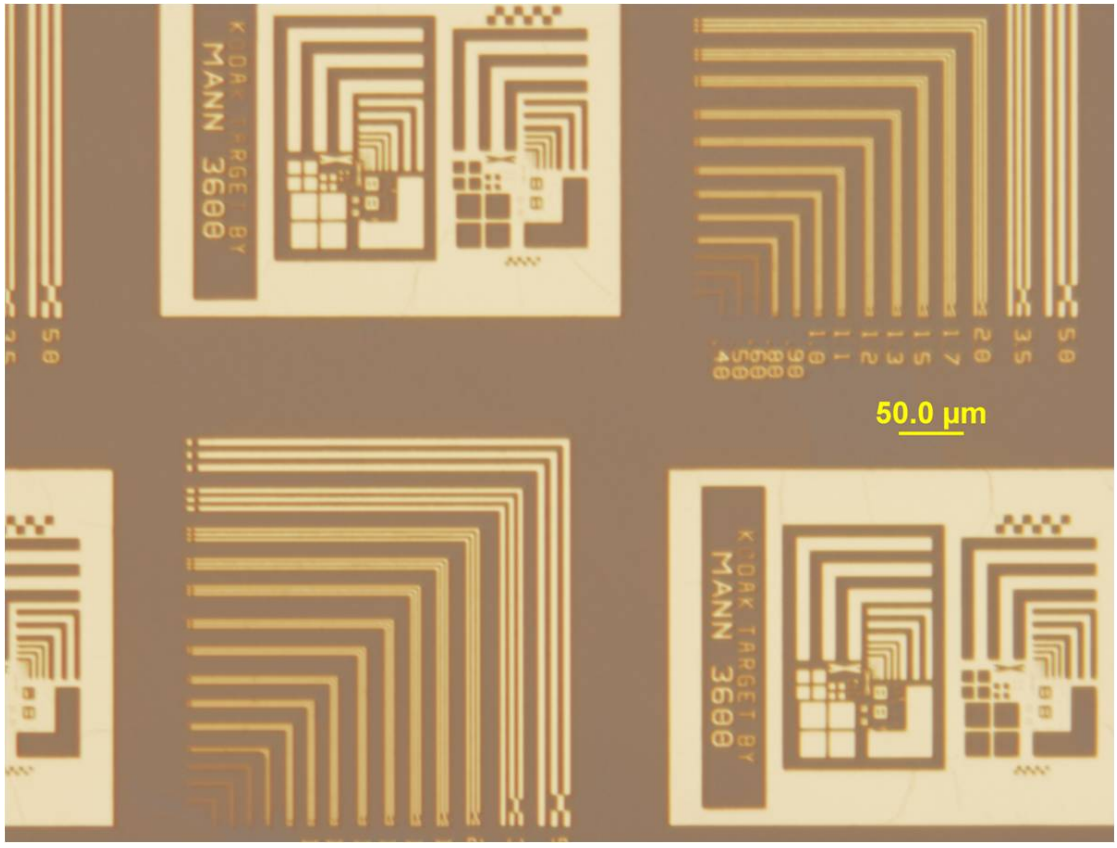

Figure 3-8. Optical micrograph of patterns achieved with **$(P(tBMA\text{-}co\text{-}PM)_{16})_3$**. 3400mJ/cm^2 exposure dose with 365 nm wavelength. PEB for one minute at 125 °C and developed in 0.26N TMAH for five minutes to reveal positive tone patterns.

development was also achieved with this star-oligomer, but only after extended development times. (Figure 3-9)

It is important to note that these materials are not indicative of the ultimate resolution capabilities for star-shaped oligomer resists. They successfully demonstrate that the core does not inhibit base development when the polymeric arms are sufficiently polar. Current work focuses on preparing star-shaped oligomers with arm compositions that are similar to high resolution photoresists targeted at the ArF platform. With such materials, it is possible to make a comparitive study between the resolution and roughness capabilities of linear and star architecture photoresists.[41]

3.3.3 Dry Etch Durability Characteristics of Star Oligomers

Investigating the impact of the multifunctional initiator core on dry etch durability necessitated measuring the etch rate of each core. Uniform films were achieved with **tCHO-Br$_3$** and **SAC-Br$_8$** by spincoating in toluene. GADDS was used to confirm the amorphous character of the films. The core **GLU-Br$_5$** could not be spincoated from toluene but a uniform film was achieved by spincoating from acetone. However, a crystalline ring was observed in the GADDS pattern of the **GLU-Br$_5$** film. It was hypothesized that a small quantity of residual toluene was present in the films of **tCHO-Br$_3$** and **SAC-Br$_8$** that was responsible for inhibiting crystallization. Therefore, a solution of acetone containing five percent toluene was used to spincoat **GLU-Br$_5$**, resulting in a uniform film that was confirmed to be amorphous by GADDS.

The dry etch rates relative to a poly(hydroxystyrene) (PHOST) standard for stars **(PtBMA$_{16}$)$_3$**, **(PtBMA$_{12}$)$_4$** and **(PtBMA$_{10}$)$_7$** are compared in Table 3-4. The weight ratio of the core to arms is similar for all three star-shaped oligomers. The etch rate of all star samples was better than poly(tBMA), which was measured to have an etch rate of 2.3 relative to PHOST. This result was significant because only **tCHO-Br$_3$** had a

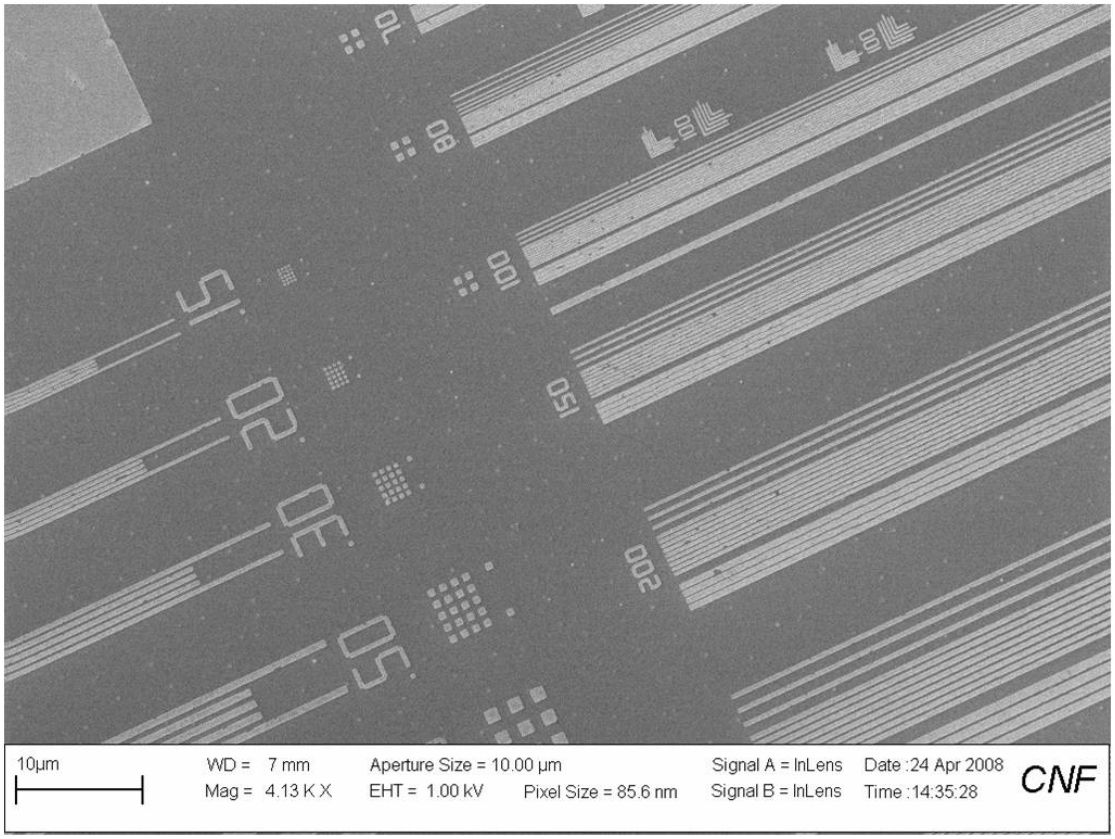

Figure 3-9. SEM of patterns achieved with **$(P(tBMA\text{-}co\text{-}BLMA)_{10})_7$**. 163µC/cm^2 exposure dose with e-beam. PEB for one minute at 125 °C and developed in 0.26N TMAH for 1 hour to reveal positive tone patterns.

Table 3-4. Etch rates of stars and initiators

Star Oligomer	V_{meas}[a]	V_{init}[b]	Θ_{tBMA}[c]	V_{theor}[d]
$(PtBMA_{16})_3$	1.8	1.4	88%	2.2
$(PtBMA_{12})_4$	2.3	3.4	89%	2.4
$(PtBMA_{10})_7$	1.9	2.4	86%	2.3

[a]The etch rate of the sample relative to PHOST. [b]The etch rate relative to PHOST of a film composed entirely of the sample's core. [c]The weight percent of the sample's poly(tBMA) arms. [d]Theoretical etch rate calculated by $V_{theor}=V_{tBMA}*\Theta_{tBMA}+V+*(1-\Theta_{tBMA})$ where $V_{tBMA}=2.3$.

slower etch rate than poly(tBMA), suggesting that the core can only improve, not diminish etch durability.

The etch rate of star **$(PtBMA_{12})_4$**, which was synthesized from the multifunctional initiator with the fastest etch rate, was measured to be the same as poly(tBMA). This result compares with previous reports that aromatic and alicyclic components can quench energy over a distance of several monomer units, reducing the effect of less durable, minor components.[42-44] The etch rate of star **$(PtBMA_{10})_7$**, which had a multifunctional initiator with an etch rate similar to poly(tBMA), exhibited a reduction in etch rate. Crosslinks are known to improve etch durability[45] and theoretical models exist that treat the branching point of stars as crosslinks.[46]

Although star **$(PtBMA_{16})_3$** possesses the fewest number of arms it demonstrates the slowest etch rate due to the presence of a durable core. Blends and copolymers are known to have slower etch rates than the linear combination of their individual components.[45] Despite this, linear approximations, such as the Ohnishi parameter[47] and ring parameter[48] are widely used because their predictions are reasonably accurate. Star **$(PtBMA_{16})_3$** is unusual, not because its etch rate is below the theoretical value calculated from the linear relationship of its two components, but because of the magnitude of the improvement. While the more durable core is the minor component of star **$(PtBMA_{16})_3$**, the molecule etches as if the core were the major component. There is a fivefold increase in the effective contribution of **tCHO-Br_3** on etch behavior.

Increasing the significance of this observation, the spin solvent used to test star **$(PtBMA_{16})_3$** was a non-solvent for tCHO-Br_3**.** It has been reported that using a spin solvent that is a non-solvent for the more durable component will cause segregation of the durable component in the film, lessening the energy quenching effect and adversely impacting the film's etch durability.[49] In star **$(PtBMA_{16})_3$**, the arms were

on average 16 monomer units long, preventing segregation on a scale beyond the energy quenching radius of the core. As a result, star **$(PtBMA_{16})_3$** displays robust etch durability with regard to selection of spin solvent. As further evidence, the etch durability of star **$(PtBMA_{21})_3$** was also measured, and both materials compared to the theoretical etch rate. (Figure 3-10) This suggests that durable cores act as highly efficient etch resistance additives for star oligomers.

3.4 Conclusions

A procedure for reliably synthesizing star oligomer poly(tBMA) from **SAC-Br_8** was extended to the multifunctional initiators **tCHO-Br_3** and **GLU-Br_5**. This produced a series of star-shaped oligomers with 3, 4 and 7 arms as well as significant differences in the relative etch rates of the cores and poly(tBMA) arms. Patterns were obtained by development in an isopropanol and water solution. However, patterning of the poly(tBMA) homopolymers could not be achieved with base developer. Two techniques, the partial reduction of the star oligomers and copolymerization with BLMA, were successfully employed to modify the solubility of the star-oligomers, allowing for base development. Additionally, the star-shaped oligomers were observed to have a potential advantage over linear materials. **$(PtBMA_{16})_3$** exhibited improved etch durability as a result of the higher etch durability of its core. As the core was covalently bonded, segregation of the components could not occur, leading to a highly efficient etch additive. This new strategy for synthesizing photoresist materials will be extended to produce stars with a similar composition to high resolution photoresists, which may lead to additional performance improvements as a result of the star architecture.

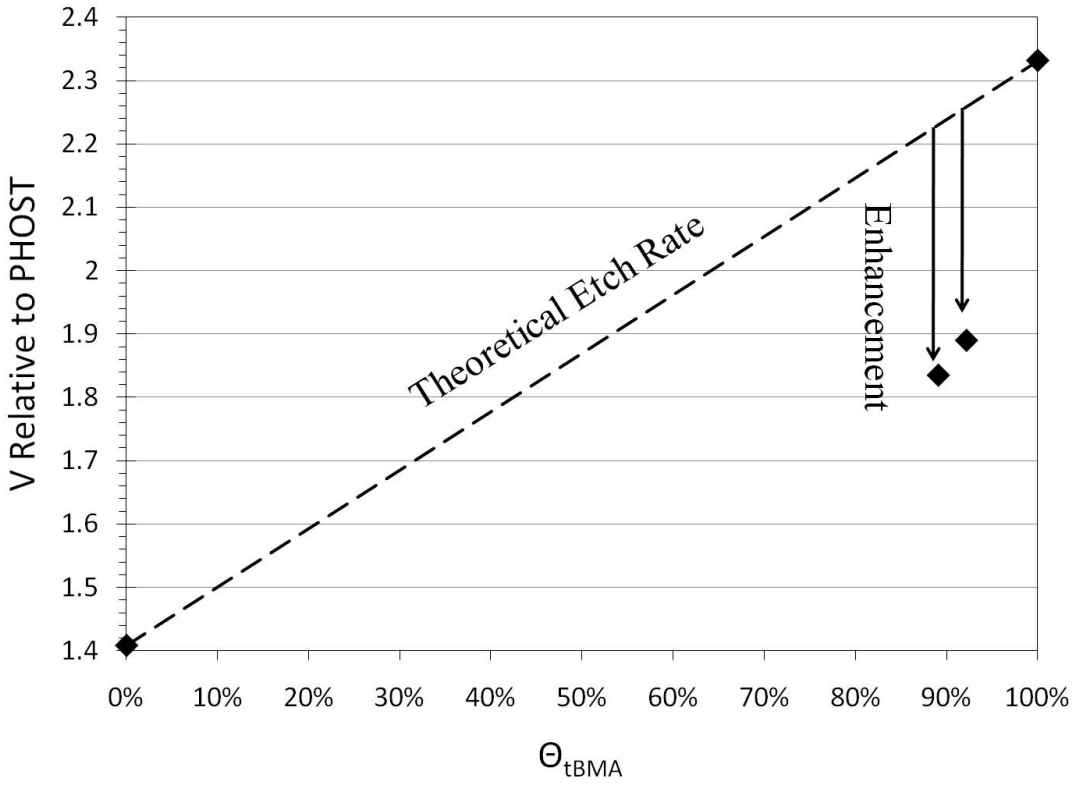

Figure 3-10. Etch rate relative to PHOST for stars **$(PtBMA_{16})_3$**, **$(PtBMA_{21})_3$**, tCHO-Br_3 and poly(tBMA) plotted by tBMA composition. Dashed line calculated from theoretical etch rate.

3.5 Acknowledgement

Financial support from the Semiconductor Research Corporation (GRC-1677.001 and GRC-1675.002) is greatly appreciated. Research was performed in part at the Cornell NanoScale Facility, a member of the Nation Nanotechnology Infrastructure Network and the Cornell Center for Materials Research, which are supported by the National Science Foundation (ECS-0335765 and DMR-0520404). Macromolecular Chemistry I and Macromolecular Chemistry II at the University of Bayreuth are thanked for the generous use of their polymer synthesis and characterization facilities. D.C.F. was supported by a GRC and Applied Materials fellowship.

REFERENCES

1. Kato, M., et al., *Polymerization of Methyl Methacrylate with the Carbon Tetrachloride/Dichlorotris-(triphenylphosphine)ruthenium(II)/Methylaluminum Bis(2,6-di-tert-butylphenoxide) Initiating System: Possibility of Living Radical Polymerization.* Macromolecules, 1995. **28**(5): p. 1721-1723.

2. Wang, J.-S. and K. Matyjaszewski, *Controlled/"Living" Radical Polymerization. Atom Transfer Radical Polymerization in the Presence of Transition-Metal Complexes.* Journal of the American Chemical Society, 1995. **117**(20): p. 5614-5615.

3. Wang, J.-L., T. Grimaud, and K. Matyjaszewski, *Kinetic Study of the Homogeneous Atom Transfer Radical Polymerization of Methyl Methacrylate.* Macromolecules, 1997. **30**(21): p. 6507-6512.

4. Sawamoto, M. and M. Kamigaito, *Living radical polymerizations based on transition metal complexes.* Trends in Polymer Science (Cambridge, United Kingdom), 1996. **4**(11): p. 371-377.

5. Haddleton, D.M., et al., *Atom Transfer Radical Polymerization of Methyl Methacrylate Initiated by Alkyl Bromide and 2-Pyridinecarbaldehyde Imine Copper(I) Complexes.* Macromolecules, 1997. **30**(7): p. 2190-2193.

6. Zhang, M. and A.H.E. Müller, *Cylindrical polymer brushes.* Journal of Polymer Science, Part A: Polymer Chemistry, 2005. **43**(16): p. 3461-3481.

7. Sheiko, S.S., B.S. Sumerlin, and K. Matyjaszewski, *Cylindtrical molecular brushes: Synthesis, characterization, and properties.* Progress in Polymer Science, 2008. **33**(7): p. 759-785.

8. Gao, C. and D. Yan, *Hyperbranched polymers: from synthesis to applications.* Progress in Polymer Science, 2004. **29**(3): p. 183-275.

9. Gaynor, S.G. and K. Matyjaszewski, *Step-Growth Polymers as Macroinitiators for "Living" Radical Polymerization: Synthesis of ABA Block Copolymers.* Macromolecules, 1997. **30**(14): p. 4241-4243.

10. Kasko, A.M., A.M. Heintz, and C. Pugh, *The Effect of Molecular Architecture on the Thermotropic Behavior of Poly[11-(4'-cyanophenyl-4"-phenoxy)undecyl acrylate] and Its Relation to Polydispersity.* Macromolecules, 1998. **31**(2): p. 256-271.

11. Kickelbick, G., P.J. Miller, and K. Matyjaszewski, *Multifunctional star initiators for atom transfer radical polymerization.* Polymer Preprints (American Chemical Society, Division of Polymer Chemistry), 1998. **39**(1): p. 284-285.

12. Matyjaszewski, K., et al., *Synthesis of Block, Graft and Star Polymers from Inorganic Macroinitiators.* Applied Organometallic Chemistry, 1998. **12**: p. 667-673.

13. Matyjaszewski, K., et al., *Synthesis and Characterization of Star Polymers with Varying Arm Number, Length and Composition from Organic and Hybrid Inorganic/Organic Multifunctional Initiators.* Macromolecules, 1999. **32**(20): p. 6526-6535.

14. Ueda, J., M. Kamigaito, and M. Sawamoto, *Calixarene-Core Multifunctional Initiators for the Ruthenium-Mediated Living Radical Polymerization of Methacrylates.* Macromolecules, 1998. **31**(20): p. 6762-6768.

15. Ueda, J., et al., *Multifunctional Initiators for the Ruthenium-Mediated Living Radical Polymerization of Methyl Methacrylate: Di- and Trifunctional Dichloroacetates for Synthesis of Multiarmed Polymers.* Macromolecules, 1998. **31**(3): p. 557-562.

16. Muthukrishnan, S., et al., *Synthesis and Characterization of Glycomethacrylate Hybrid Stars from Silsesquioxane Nanoparticles.* Macromolecules, 2005. **38**(26): p. 10631-10642.

17. Plamper, F.A., et al., *Pearl Necklace Architecture: New Threaded Star-Shaped Copolymers.* Macromolecules, 2010. **43**(5): p. 2190-2203.

18. Liechty, W.B., et al., *Polymers for drug delivery systems.* Annual Review of Chemical and Biomolecular Engineering, 2010. **1**: p. 149-173.

19. Adair, J.H., et al., *Recent developments in the preparation and properties of nanometer-size spherical and platelet-shaped particles and composite particles.* Materials Science & Engineering: R: Reports, 1998. **23**(4-5): p. 139-242.

20. Matz, G.F., et al., *Low molecular weight water soluble polymer composition and method of use*, in *PCT Int. Appl.*, W.I.P. Organization, Editor. 2001, Calgon Corporation, USA.

21. De Leon-Rodriguez, L.M., et al., *MRI Detection of VEGFR2 in Vivo Using a Low Molecular Weight Peptoid-$(Gd)_8$-Dendron for Targeting.* Journal of the American Chemical Society, 2010. **132**(37): p. 12829-12831.

22. Ito, H., *Chemical Amplification Resists for Microlithography.* Advances in Polymer Science, 2005. **172**: p. 37-245.

23. Bohrisch, J., et al., *New Polyelectrolyte Architectures.* Advances in Polymer Science, 2004. **165**: p. 1-41.

24. Dzubiella, J. and A. Jusufi, *Star-polymer-colloid mixtures.* Condensed Matter Physics, 2002. **30**: p. 285-305.

25. Ganazzoli, F., *Conformations and dynamics of stars and dendrimers: the Gaussian Self-Consistent approach.* Condensed Matter Physics, 2002. **5**(1): p. 37-71.

26. Likos, C.N., *Soft matter with soft particles.* Soft Matter, 2006. **2**: p. 478-498.

27. Likos, C.N. and H.M. Harreis, *Star polymers: from conformations to interactions to phase diagrams.* Condensed Matter Physics, 2002. **29**: p. 173-200.

28. Vlassopoulos, D., *Colloidal star polymers: Models for studying dynamically arrested states in soft matter.* Journal of Polymer Science, Part B: Polymer Physics, 2004. **42**(16): p. 2931-2941.

29. Plamper, F.A., et al., *Synthesis, Characterization and Behavior in Aqueous Solution of Star-Shaped Poly(acrylic acid).* Macromolecular Chemistry and Physics, 2005. **206**: p. 1813-1825.

30. Tang, W. and K. Matyjaszewski, *Kinetic Modeling of Normal ATRP, Normal ATRP with $[Cu^{II}]_0$, Reverse ATRP and SR&NI ATRP.* Macromolecular Theory and Simulations, 2008. **17**: p. 359-375.

31. Goto, A. and T. Fukuda, *Kinetics of living radical polymerization.* Progress in Polymer Science, 2004. **29**: p. 329-385.

32. Rein, D., P. Rempp, and P.J. Lutz, *Recent developments in the field of star-shaped polymers.* Makromolekulare Chemie, Macromolecular Symposia, 1993. **67 (EPF Workshop on Anionic Polymerization and Related Processes, 1992)**: p. 237-249.

33. Wang, J.-S., D. Greszta, and K. Matyjaszewski, *Atom transfer radical polymerization (ATRP): A new approach towards well-defined (co)polymers.* Polymeric Materials Science and Engineering, 1995. **73**: p. 416-417.

34. Forman, D.C., et al., *Synthesis, Characterization and Properties of Star-Shaped Poly(tert-Butyl Methacrylate) Oligomers.* Manuscript in preparation, 2010.

35. Weiburger, F., et al., *Solution behavior of poly(tert-butylmethacrylate) star oligomers.* Manuscript in preparation, 2010.

36. Silva, A.D., N.M. Felix, and C.K. Ober, *Molecular glass resists as high-resolution patterning materials.* Advanced Materials, 2008. **20**(17): p. 3355-3361.

37. Bonar-Law, R.P., A.P. Davis, and J.K.M. Sanders, *New procedures for selectively protected cholic acid derivatives. Regioselective protection of the hydroxy group, and tert-butyl esterification of the carboxyl group.* Journal of the Chemical Society, Perkin Transactions 1: Organic and Bio-Organic Chemistry (1972-1999), 1990. **8**: p. 2245-2250.

38. Giguere, G. and X.X. Zhu, *Synthesis and aggregation properties of anionic star-shaped polymers with cholic acid cores and polyacrylate arms.* Journal of Polymer Science, Part A: Polymer Chemistry, 2007. **45**(17): p. 4173-4178.

39. Nozaki, J. and E. Yano, *Evaluation of Alicyclic Methacrylate Resist with a γ-Butyrolactone Protective Group for 193-nm Lithography.* Journal of Photopolymer Science and Technology, 1998. **11**(3): p. 493-498.

40. Heise, A., et al., *Investigation of the Initiation Behavior of a Dendritic 12-Arm Initiator in Atom Transfer Radical Polymerization.* Macromolecules, 2001. **34**(11): p. 3798-3801.

41. Forman, D.C., et al., *Comparison of star and linear ArF resists.* Proceedings of SPIE, 2010. **7639**(Pt. 1, Advances in Resist Materials and Processing Technology XXVII): p. 76390P/1-76390P/8.

42. Koike, M. and A. Danno, *Radiation Effects on Dimethyl-diphenyl Siloxane Copolymer. I. Protective Effect of Phenyl Radical on the Cross-linking.* Journal of the Physical Society of Japan, 1960. **15**: p. 1501-1508.

43. Tsuda, M., S. Oikawa, and K. Kimura, *Potential-Energy Surfaces in the Lower Excited States of Benzene, Dewar-Benzene Isomerization Process.* International Journal of Quantum Chemistry, 1980. **18**(1): p. 157-164.

44. Craighead, H.G., et al., *Contact lithography at 157 nm with a flourine excimer laser.* Journal of Vacuum Science & Technology, B: Microelectronics and Nanometer Structures, 1983. **1**(4): p. 1186-1189.

45. Ueno, N., et al., *Improvement of plasma etching durability of positive working resist by copolymerization, blending, and crosslinking.* Journal of Applied Polymer Science, 1987. **34**(4): p. 1677-1691.

46. Huang, Y., I. Szleifer, and N.A. Peppas, *A Molecular Theory of Polymer Gels.* Macromolecules, 2002. **35**(4): p. 1373-1380.

47. Gokan, H., S. Esho, and Y. Ohnishi, *Dry etch resistance of organic materials.* Journal of the Electrochemical Society, 1983. **130**(1): p. 143-146.

48. Kunz, R.R., et al., *Limits to etch resistance for 193-nm single-layer resists.* Proceedings of SPIE, 1996. **2724**: p. 365-376.

49. Kushida, M., et al., *Energy Quenching Effects on Dry-Etching Durability of Alicyclic-Aliphatic Copolymers and Polymer Blends Enhanced by Polymer-Chain Entanglement.* Japanese Journal of Applied Physics, 2005. **44**(3): p. 1498-1501.

CHAPTER 4. PRECISION SYNTHESIS OF STAR-SHAPED OLIGOMER TERPOLYMERS WITH SACCHAROSE CORES

Drew C. Forman and Christopher K. Ober

Materials Science & Engineering

Cornell University, Ithaca, NY 14853

Florian Wieberger and Hans-Werner Schmidt

Macromolecular Chemistry I

University of Bayreuth, Bayreuth, Germany 95440

Andre Groeschel, Marietta Böhm, Axel H. E. Müller

Macromolecular Chemistry II

University of Bayreuth, Bayreuth, Germany 95540

4.0 ABSTRACT

A series of star-shaped oligomer terpolymers consisting of a saccharose core and α-gamma butyrolactone methacrylate (GBLMA), methyl adamantyl methacrylate (MAMA) and hydroxyl adamantyl methacrylate (HAMA) were prepared via core-first atom transfer radical polymerization (ATRP). The initiator synthesis was modified to reduce the functionality of the multifunctional initiator, enabling the preparation of star oligomers with the same core but different numbers of arms. MAMA homopolymers were synthesized as model materials to determine the initiation efficiency. From this information, the ratio of monomer to initiator was modified to prepare a series of star-shaped oligomer terpolymers with increasing arm size at the same conversion. The quantity of solvent and the initial Cu(I):Cu(II) ratio were modified to reduce the reaction rate so NMR aliquots could be examined throughout the reaction to monitor the rate of conversion. Star-shaped oligomers with average arm lengths as short as 3 monomer units were ultimately achieved. Finally, the capability to combine these techniques to produce star-shaped oligomers with arbitrary arm number and length is demonstrated by the synthesis of three terpolymers, one linear control and two stars with overall number average degree of polymerization ($\overline{DP_n}$) of twenty monomer units.

4.1 Introduction

Star-shaped polymers, which consist of multiple linear polymer arms covalently attached to a central core, have attracted interest in numerous fields due to unique properties that can be achieved by varying the number of arms.[1-3] When a star-shaped polymer has very few arms, the material behaves similar to a linear chain. However, as the number of arms increases, the capability of the arms to interact with neighboring molecules decreases, in essence trading intermolecular for intramolecular interactions,

leading to their description as "ultrasoft colloids."[2] In this regime, star-shaped polymers possess properties significantly altered from their linear counterparts. This has led to stars being used for a range of applications including viscosity index modifiers in oil,[4] oxygen permeability and hardness enhancers in contact lenses,[5] and as additives in coatings, binder in toner and as an encapsulation material for pharmaceuticals.[6, 7] The star-shaped polymer architecture continues to be the focus of both theoretical and experimental studies, which explore the relationship between architecture and thermodynamics, osmotic pressure, molecular size, rheology and polyelectrolyte behavior.[8-13]

There are many areas where the unique properties of the star-shaped architecture could prove beneficial, such as conjugates for drug delivery,[14] nanoparticle dispersion stabilizers,[15] cosmetic dyes,[16] photoresists[17-19] and *in vivo* sensors.[20] A common factor among these applications is the necessity for low molecular weight materials. However, knowledge of the star-shaped polymer architecture is fundamentally limited in the low molecular weight regime. As early as the Daoud-Cotton blob model, assumptions in theoretical studies have been made that treat the core region as negligible.[1, 2] Experimentally, the synthesis of low molecular weight star-shaped polymers is more challenging than that of low molecular weight linear polymers due to the inverse relationship between functionality and the molecular weight of each arm.[21]

ATRP[22, 23] is a versatile polymerization technique that has been used to synthesize polymers as simple as linear acrylates and methacrylates,[24-26] to more complex cylindrical brushes,[27, 28] hyperbranched[29, 30] and star polymers,[31-37] and even highly specialized architectures such as pearl necklaces.[38] Using ATRP, we have previously demonstrated the capability to produce star-shaped oligomers comprised of poly(tert-butyl methacrylate) (tBMA) homopolymers arms and tert-butyl cholate, glucose and

saccharose cores.[19, 21, 39] In this chapter, we address two key challenges facing the preparation of star-shaped oligomers: the preparation of random co-oligomers and the ability to produce star-shaped oligomers with different numbers of arms without changing the core. (Figure 4-1)

While conversion was previously utilized as a process variable, here it is replaced by the Cu(I) : Cu(II) and monomer : initiator ratios. This allows stars with different arm lengths to be prepared at the same conversions, a critical requirement for studying the impact of molecular weight on copolymers. Excepting the unique case of monomer feeds with the same reactivity, preparing random copolymers at different conversions yields different compositions.[40] By targeting a constant conversion, one can produce random copolymers with identical compositions at different molecular weights. This achievement enables a far greater range of materials to be studied as star-shaped oligomers. In addition, the quantity of wasted monomer is reduced as the smallest star-oligomers can now be synthesized at higher conversions.

Our prior work has demonstrated that the core can contribute significantly towards the properties of star-shaped oligomers.[19] This is substantially different than in the case of star-shaped polymers, where the core is generally considered to be negligible aside from its relationship to the material's number of arms. For high molecular weight star-shaped polymers, series of materials with different numbers of arms are synthesized from different cores. A similar scheme cannot be applied to the study of star-shaped oligomers with different numbers of arms, as the effect of core and arm number cannot be readily distinguished. Therefore, we introduce a procedure for preparing multifunctional initiators with different functionality from the same core.

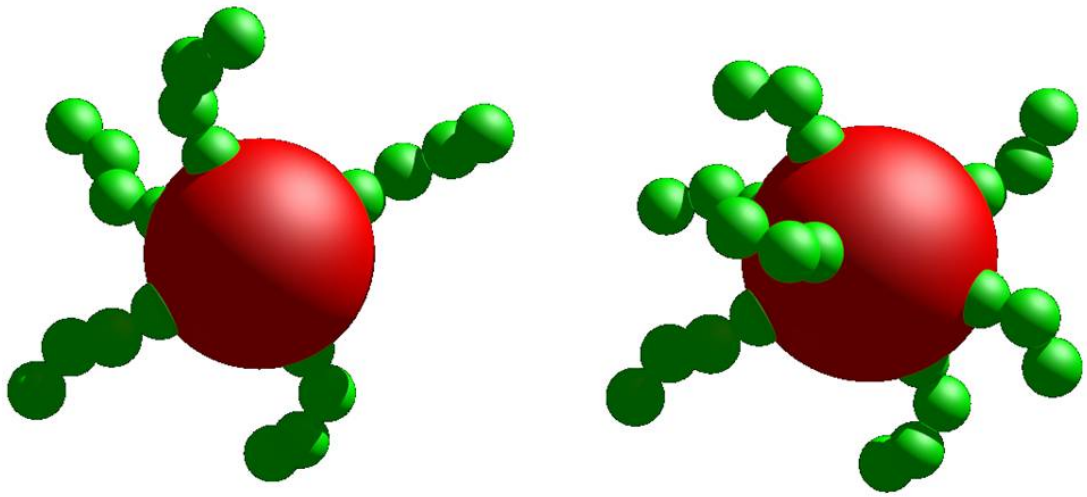

a b

Figure 4-1. Graphical depiction of two star-shaped poly(GBLMA-*co*-MAMA-*co*-HAMA) oligomers with 20 degree of polymerization and saccharose cores but different numbers of arms, corresponding to representative molecules for the samples (a) $((GcMcH)_{3.6})_{5.5}$ and (b) $((GcMcH)_{3.1})_{6.4}$. The core and monomer units are represented by spheres with volumes equal to the molecular weight of the multifunctional initiators (excluding bromine) and the number average molecular weight of the monomers.

4.2 Experimental

4.2.1 Materials

2-bromoisobutyryl bromide, propionyl bromide, 4-(dimethylamino)pyridine, anhydrous pyridine, CH_2Cl_2 CuCl, $CuCl_2$, D(+)-Saccharose and N,N,N',N",N"-pentamethyl-diethylenetriamine (PMDETA), 4-(N,N-dimethylamino)-pyridine were purchased from Aldrich and prepared according to standard procedures. HAMA and MAMA were purchased from Idemitsu Chemicals. GBLMA was purchased from Kuraray. MAMA was passed through a basic alumina column to remove inhibitor. HAMA and GBLMA were used as received.

The GBLMA-*co*-MAMA-*co*-HAMA (GcMcH) statistical terpolymers prepared in this chapter are named for their architecture: $((GcMcH)_n)_f$) where n is the number average of monomer units per arm and f is the number average of arms per molecule.

4.2.2 Synthesis

4.2.2.1 Preparation of Multifunctional Initiators

The core-first[41] approach and ATRP were selected to synthesize star-shaped oligomers. 2,3,4,6,1',3',4',6'-octa-O-(2-bromoisobutyryl)-saccharose (**SAC-Br$_8$**), which has eight initiating sites, was prepared from saccharose as previously published.[13]

A modified version multifunctional initiator with fewer initiating sites (**SAC-Br$_{5.7}$**) was prepared by substituting the 2-bromoisobutyryl bromide with a 50/50 solution of 2-bromoisobutyryl bromide and propionyl bromide. D(+)-Saccharose was dehydrated in a vacuum oven at 80 °C for 1 hour prior to 14.31 g, (41.8 mmol) D(+)-Saccharose being stirred in a solution of 550 mL chloroform and 265 mL pyridine with 4-(N,N-

dimethylamino)-pyridine in catalytic quantities under nitrogen. The solution was cooled with ice and 76.89 g (334.4 mmol) 2-bromoisobutyryl bromide and 45.81 g (334.4 mmol) propionyl bromide were added from a dropping funnel over a period of 3 hours. The solution was brought to room temperature and stirred overnight before undergoing reflux at 75 °C for 3 hours. The solution was diluted with diethyl ether until it became less dense than water and the pyridinium bromide removed by repeated extraction with water, $NaHCO_3$ and NaOH. The organic phase was dried over Na_2SO_4 and concentrated, taken-up in 1,4-dioxane and freeze dried to obtain a solid mixture of products corresponding to a Saccharose based multifunctional initiator with an average of 5.7 initiating sites. (21 g, 40%) (Figure 4-2)

Eight site Saccharose-based initiator **SAC-Br$_8$**: M(+Li^+) = 1541 g·mol-1 by MALDI-TOF MS (DHB:LiCl:initiator 10:1:1). Reduced site Saccharose-based initiator **SAC-Br$_{5.7}$** M(+Li^+) = 1106 (10%), 1199 (31%), 1292 (39%), 1385 (20%) g·mol^{-1} by MALDI-TOF MS (DHB:LiCl: initiator 10:1:1).

4.2.2.2 Preparation of Star Oligomer Terpolymers

A previous procedure for the preparation of star poly(tert-butylmethacrylate) by ATRP was modified as follows: 3.563 g (2.82 mmol) **SAC-Br$_{5.7}$**, 8.75 g (51.4 mmol) GBLMA, 12.15 g (51.9 mmol) MAMA, 5.290 g (22.4 mmol) HAMA, 0.177g (1.79 mmol) CuCl and 1.922 g (14.3 mmol) $CuCl_2$ were stirred in 62 g of anisole under an inert atmosphere. The solution was heated in a 60 °C oil bath before 2.79 g (16.1 mmol) PMDETA was added at time t=0.

Aliquots were removed throughout the reaction and diluted in $CDCl_3$ to monitor the conversion of monomer with ^{1}H-NMR. Peak integration was performed on the vinyl peaks of GBLMA, MAMA, HAMA that occurred at 6.254ppm, 6.109ppm and 6.060ppm, respectively and calibrated to the integration of the anisole peak at 3.780.

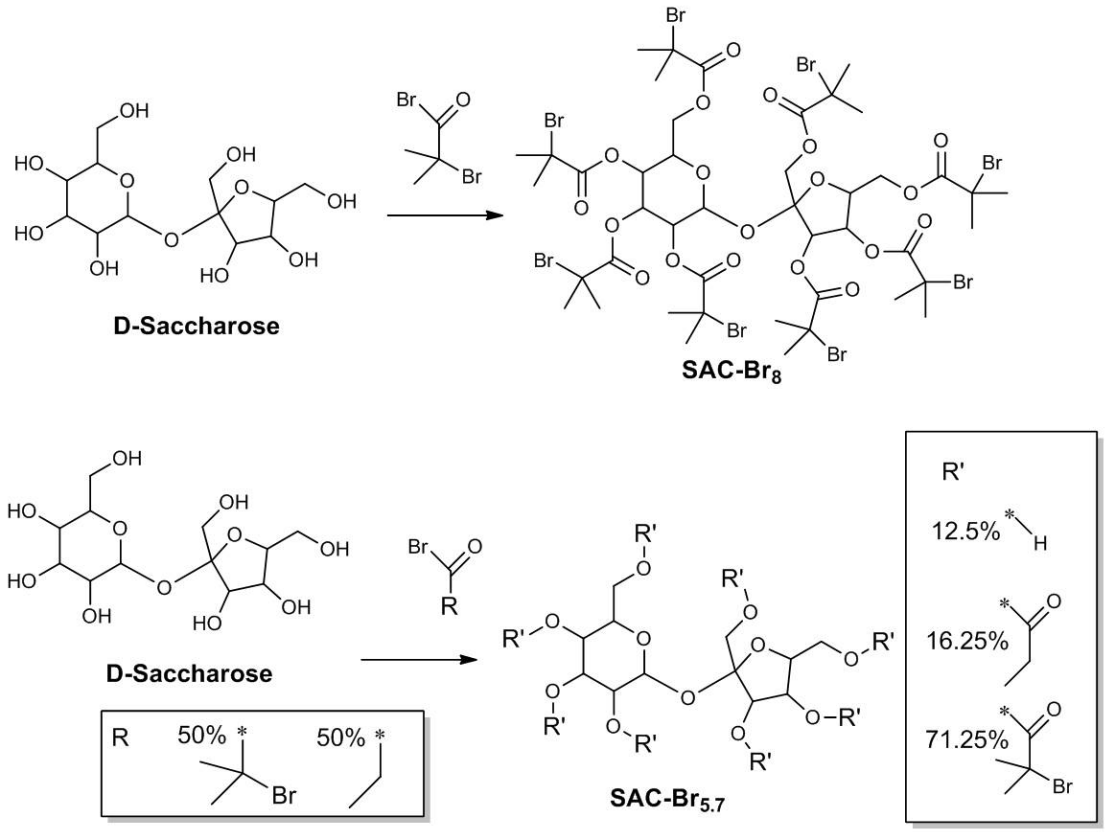

Figure 4-2. Reaction pathway toward saccharose based initiator with reduced functionality.

The logarithmic relationship between conversion and polymerization time was used to determine the end time for 45% conversion at 3 hours. (Equation 4-1)[42-44]

$$\ln\left(\frac{[M]_0}{[M]_t}\right) = \frac{k_p K_{ATRP}[P_m X][Cu^I]}{[Cu^{II}]} t \qquad \text{Equation 4-1}$$

At the calculated end time, a final aliquot was removed to verify the final conversion and the reaction was quenched in liquid nitrogen. Copper catalyst was removed via filtration through silica. The solution was concentrated under reduced pressure while being heated to 70 °C and precipitated in methanol. Following gravity filtration, the resulting powder was taken up in 1,4-dioxane and freeze dried to obtain the star-shaped poly(GcMcH) oligomers as a white amorphous solid. (5.66 g, 38%)

Similar procedures were followed with reactant ratios and polymerization times modified to achieve samples with different arm lengths. (Figure 4-3)

4.2.3 Characterization

The molecular weight of star oligomers was measured by size exclusion chromatography (SEC) performed on a Waters GPC system (Waters 486 UV detector) by eluting THF (1 cm^3 min^{-1}) at 40°C with a linear polystyrene standard to determine relative molecular weight.

SEC with a Wyatt DAWN HELEOS multiangle light scattering detector equipped with a 632.8 nm He-Ne laser (GPC/MALS) and Viscotek Model 250 viscosity detector (GPC/viscosity) were used to determine the absolute molecular weights of MAMA star-shaped oligomers. THF was used as eluent at a flow rate of 1.0 mL/min: column set, 5 μm PSS SDV gel, 103, 105, and 106 Å, 30 cm each. For GPC/viscosity, the refractive index increment of the star oligomer solutions in THF at 25 °C were

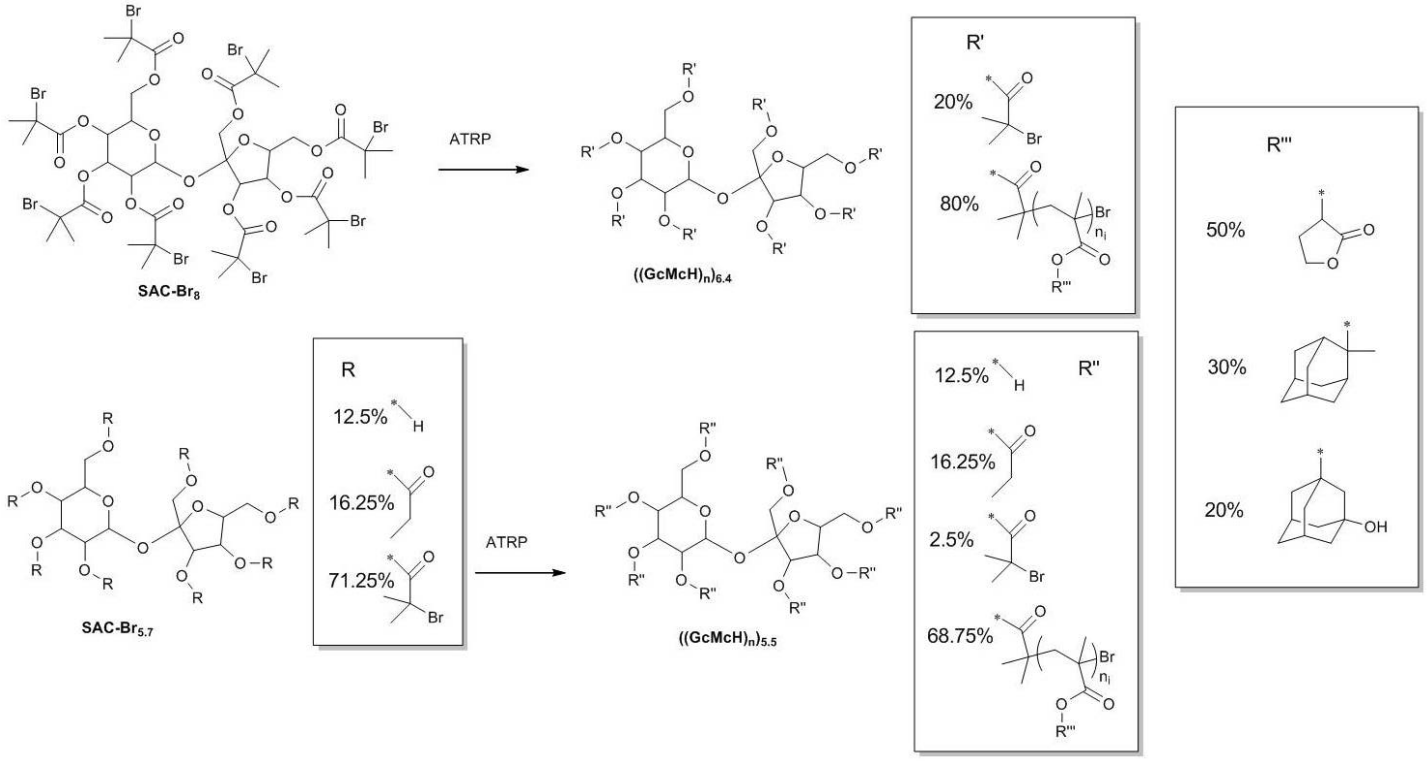

Figure 4-3. Reaction pathway toward star-shaped ter-oligomers

measured using a PSS DnDC-2010/620 differential refractometer.

4.3 Results and Discussion

In order to enable the study of scaling behavior in star-shaped oligomers for a wide range of materials, techniques to reproducibly prepare star-shaped oligomers with identical arm compositions but differing arm number and length must be achieved.

4.3.1 Feed Ratios

For this study a composition of 50% GBLMA, 30% MAMA and 20% HAMA was targeted due to its potential applications.[42] Through repeated experimentation, a feed of 41% GBLMA, 41% MAMA and 18% HAMA was found to achieve the target composition. Composition throughout the polymerization was monitored by observing the vinyl peaks, which corresponded to each monomer, diminish with conversion in ^{1}H-NMR. (Figure 4-4) Excepting the start of the reaction, during which monomer conversion occurred closer to a stochiometric ratio, the composition of the growing polymer remained close to the target composition. Conversion progressed logarithmically with time and no recombination peak was visible in the GPC trace of the final material. (M_w/M_n=1.06) Extrapolation indicated a 50% GBLMA, 30% MAMA and 20% HAMA composition was achieved at 45% conversion. Moving forward, this conversion was targeted for all reported materials.

4.3.2 Multifunctional Initiator Analysis

The composition of the multifunctional initiators was analyzed by MALDI-TOF mass spectrometry (MS) to determine the number of initiating sites per initiator molecule. **SAC-Br$_{5.7}$** is not a single initiator, but rather a mixture of initiators, each with different functionality. Saccharose contains eight possible reaction sites for 2-

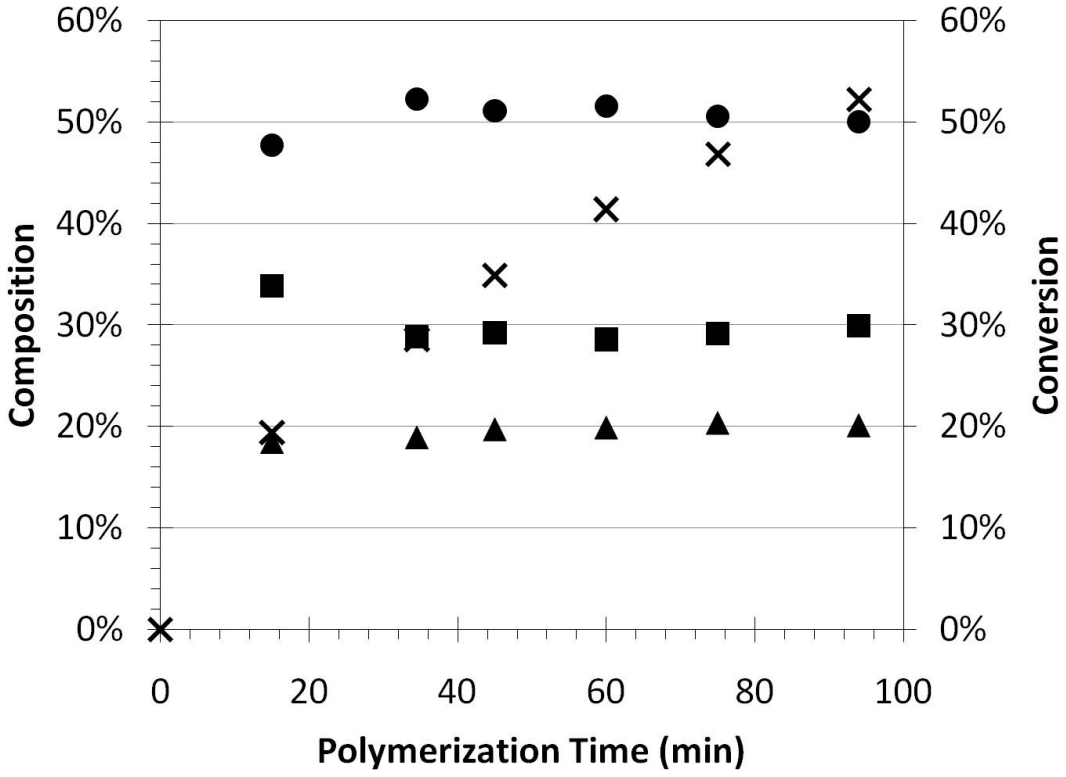

Figure 4-4. Composition evolution with time study. GBLMA (●), MAMA (■) and HAMA (▲) composition are plotted with overall conversion (**X**).

bromoisobutyryl bromide and propionyl bromide. No attempt was made to isolate specific initiators as the number of arms in a star-shaped polymer is generally a statistical average.

Masses were tabulated for all possible configurations of reaction products, where the number of sites reacted with 2-bromoisobutyryl bromide plus the number of sites reacted with propionyl bromide plus the number of unreacted sites must equal eight. The four peaks observed in the MALDI-TOF spectrum occurred at 1106, 1199, 1292 and 1385 g/mol. (Table 4-1) Each of these molecular weights corresponds to a unique configuration of 2-bromoisobutyryl, propionyl and unreacted sites: (4,3,1), (5,2,1), (6,1,1) and (7,0,1), respectively. In every case the molecule contained one unreacted site. Accounting for the differing signal strengths, a mean of 5.7 bromines (or initiating sites) is found for the initiator **SAC-Br$_{5.7}$**. This indicates that the propionyl bromide is less reactive than 2-bromoisobutyryl bromide.

4.3.3 Efficiency of Multifunctional Initiators

Characterizing the number of initiating sites per multifunctional initiator is insufficient to predict the number of arms in stars polymerized from it. An additional knowledge of initiation efficiency is requires as steric hindrances can prevent some sites from initiating.[43] Initiation efficiency (I_{eff}) can be measured from conversion and number average absolute molecular weight. [See Equation 4-2] Obtaining the absolute molecular weight of a copolymer from GPC/MALS is difficult due to compositional fluctuations impacting the dn/dc measurement. Therefore, MAMA homopolymers were prepared from the multifunctional initiators **SAC-Br$_8$** and **SAC-Br$_{5.7}$** to measure the initiation efficiency. (Table 4-2, Table 4-3 and Table 4-4)

$$I_{eff} = \frac{M_{n,abs}}{MW_{monomer}} \left(\frac{\Delta[M]}{[I]_0} \right)^{-1} \qquad \text{Equation 4-2}$$

Table 4-1. MALDI-TOF MS summary for **SAC-Br$_{5.7}$**.

MW (g/mol)	signal intensity[a]	composition	Br[b]
1 106	384	10%	4
1 199	1 135	31%	5
1 292	1 439	39%	6
1 385	723	20%	7

[a]Strength of integrated MALDI-TOF peak. [b]Number of brominated initiating sites determined by tabulation of molecular weight for all possible combinations of unreacted sites, sites reacted with 2-bromoisobutyryl bromide and sites reacted with propionyl bromide.

Table 4-2. Star-shaped MAMA oligomer preparation

initiator	$[M]_0$:$[I]_0$:[PMDETA]:$[Cu^{1+}]_0$:$[Cu^{2+}]_0$	$[I]_0$ (mmol/L)	time (min)
SAC-Br$_8$	47.8 : 1.00 : 5.33 : 0.32 : 5.02	24.8	53
SAC-Br$_{5.7}$	44.7 : 1.00 : 3.98 : 0.44 : 3.54	28.4	95

Table 4-3. Star-shaped MAMA oligomer characterization

initiator	conv[a]	$\overline{DP}_{n,theor}$[b]	dn/dc[c] (ml/g)	$M_{n,abs}$[c] (g/mol)
SAC-Br$_8$	39.4%	18.7	0.1189 ±0.0032	5 000
SAC-Br$_{5.7}$	48.0%	21.3	0.1360 ±0.0026	6 100

[a]Conversion measured by ^{1}H-NMR peak integration. [b]Theoretical degree of polymerization calculated by $\overline{DP}_n = (\Delta[M]/([I]_0)$. [c]Absolute molecular weight measured by GPC/MALS.

Table 4-4. Star-shaped MAMA oligomer initiator efficiency and functionality

initiator	M_w/M_n[c]	$\overline{DP}_n$,abs[d]	I_{eff}[e]	f_{avg}[f]
SAC-Br$_8$	1.05	14.9	80%	6.4
SAC-Br$_{5.7}$	1.10	20.7	97%	5.5

. [c]Absolute molecular weight measured by GPC/MALS. [d]Absolute degree of polymerization calculated by $\overline{DP}_n=(M_n,\text{abs-}MW_{init})/MW_{MAMA}$. [e]Initiator efficiency calculated by $I_{eff}=(\overline{DP}_n,\text{abs}/\overline{DP}_n,\text{theor})$. [f]Average number of arms calculated by $f_{avg}=Br_{avg}\cdot I_{eff}$.

The star-shaped MAMA oligomers yielded initiation efficiencies of 80% and 97% for **SAC-Br$_8$** and **SAC-Br$_{5.7}$**, respectively. This led to stars with an average number of arms (f_{avg}) of 6.4 and 5.5. This sharp difference in initiation efficiency can be attributed to the unreacted site and sites reacted with propionyl bromide decreasing the density of initiation sites. As a result, steric hindrances were insufficient to prevent initiation at most sites.

It is worth noting that we had previously measured the initiation efficiency of **SAC-Br$_8$** with a poly(tBMA) star-shaped oligomer at 85%, resulting in an f_{avg} of 6.8.[21] MAMA is a bulkier monomer than tBMA, resulting in greater steric hindrance, which explains the lower initiation efficiency and fewer number of arms measured with the MAMA star. As substituting tBMA for MAMA only results in a 5% difference in initiating efficiencies, the GBLMA and HAMA monomers used in the terpolymer with MAMA should have a negligible impact on initiation efficiency as their bulkiness is similar to that of MAMA.

4.3.4 ATRP Synthesis of Star-Shaped Oligomers with Modified Arm Lengths

Three star-shaped oligomers, with average arm lengths around 4, 8 and 16 monomer units, were targeted to demonstrate the capability of achieving star-shaped oligomer terpolymers of different arm lengths at the same conversion. The ratio of monomer to initiator was adjusted to yield the desired length when the polymerization approached 45% conversion. Since the reaction time decreases sharply when synthesizing shorter molecules, the ratio of Cu(I) to Cu(II) was decreased for the reactions targeting shorter arms. (Table 4-5 and Table 4-6) Conversions between 40 and 45 percent were achieved for all three reactions by tracking conversion during the reaction with ^{1}H-NMR. Analysis of the final aliquots yielded an overall composition of (51% / 30% / 19%), (50% / 30% / 20%) and (50% / 31% / 19%) (GBLMA /

Table 4-5. Preparation of ter-oligomers initiated from **SAC-Br$_8$**

Entry	$[M]_0$:$[I]_0$:[PMDETA]:$[Cu^{1+}]_0$:$[Cu^{2+}]_0$	$[I]_0$ (mmol/L)	time (min)
((GcMcH)$_{16.3}$)$_{6.4}$	237 : 1.00 : 8.00 : 4.00 : 4.00	9.0	124
((GcMcH)$_{7.8}$)$_{6.4}$	119 : 1.00 : 8.00 : 1.60 : 6.40	17.4	105
((GcMcH)$_{4.1}$)$_{6.4}$	59.3 : 1.00 : 8.00 : 1.60 : 6.40	32.5	27

Table 4-6. Ter-oligomers initiated from **SAC-Br$_8$** characterization

Entry	conv[a]	$\overline{DP}_n$[b]	$\overline{DP}_{n,arm}$[c]
((GcMcH)$_{16.3}$)$_{6.4}$	43.9	104	16.3
((GcMcH)$_{7.8}$)$_{6.4}$	42.0	50.0	7.8
((GcMcH)$_{4.1}$)$_{6.4}$	44.3	26.3	4.1

[a]Conversion measured by ^{1}H-NMR peak integration. [b]Degree of polymerization calculated by $\overline{DP}_n = (\Delta[M]/([I]_0)$. [c]Arm degree of polymerization calculated by $\overline{DP}_{n,arm} = \overline{DP}_n/f_{avg}$.

MAMA / HAMA) for **((GcMcH)$_{16.3}$)$_{6.4}$**, **((GcMcH)$_{7.8}$)$_{6.4}$** and **((GcMcH)$_{4.1}$)$_{6.4}$**, respectively. This successfully demonstrates this technique's strength at preparing copolymers of diverse length, with the same composition.

Examining all of the star-shaped oligomers synthesized from **SAC-Br$_8$**, one can learn to predict the polymerization time. Conversion index [See Equation 4-1][44-46] describes a logarithmic relationship between the conversion of monomer and polymerization time. By normalizing the conversion index with reaction quantities that are proportional to the remaining terms [See Equation 4-3], all three reactions can be shown to follow the same kinetics. (Figure 4-5) This information can then be used to predict how changing each reaction condition will impact the polymerization time required to achieve 45% conversion.

$$\ln\left(\frac{[M]_0}{[M]_t}\right)\cdot\left(\frac{[Cu^{2+}]_0}{[Cu^{1+}]_0[I]_0}\right)\cdot\left(\frac{[M]_0}{[I]_0}\right)\sim t \qquad \text{Equation 4-3}$$

4.3.5 ATRP Synthesis of Star-Shaped Oligomers with Modified Arm Numbers

Two star-shaped oligomers and a linear control were prepared with target $\overline{DP_n}$=20. (Table 4-7 and Table 4-8) This resulted in three oligomeric materials with the same monomer compositions but different architectures. (Figure 4-6) We anticipate that series similar to this one can be used to gain insight into the impact of architecture at low molecular weights for a variety of properties and applications.

The technique's reproducibility can be evaluated through a comparison of the evolution of conversion with time for **(GcMcH)$_{3.1}$)$_{6.4}$** against the predicted value from the previous polymerization using the **SAC-Br$_8$** initiator. A plot of the normalized conversion index results in a slope that is 5.7% lower than the predicted value. (Figure 4-7) This translates into a five minute error. This error can be successfully eliminated

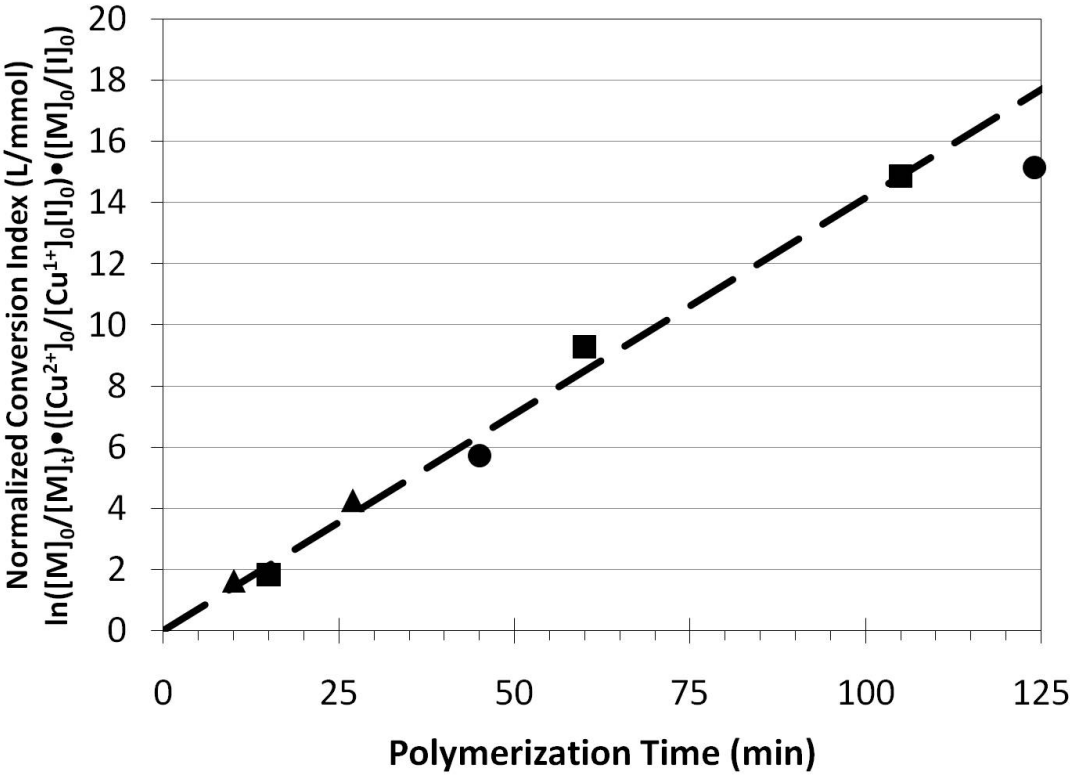

Figure 4-5. Plot of the normalized conversion index versus polymerization time for **((GcMcH)$_{16.3}$)$_{6.4}$** (●), **((GcMcH)$_{7.8}$)$_{6.4}$** (■) and **((GcMcH)$_{4.1}$)$_{6.4}$** (▲). Trendline is calculated from the combined data set resulting in a slope of 0.142 L·mmol^{-1}·min^{-1}.

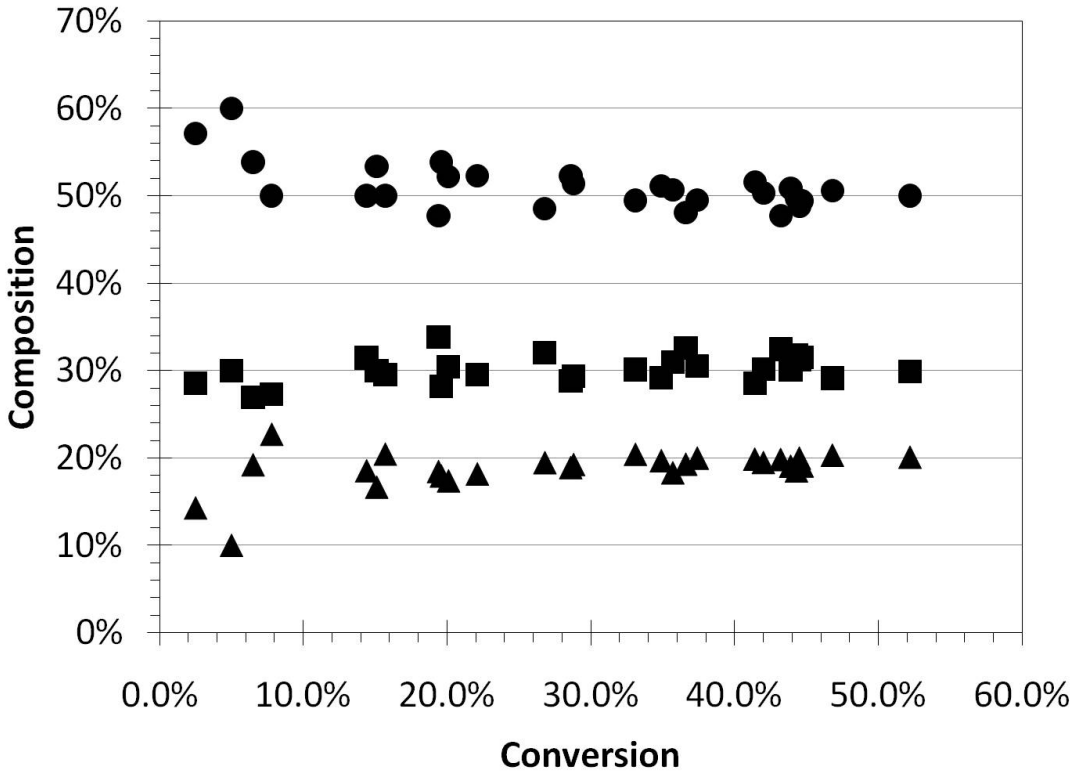

Figure 4-6. A composite plot of composition and conversion for all samples demonstrates equivalent composition between architectures.

Table 4-7. Reactants for ter-oligomers with twenty overall degree of polymerization

Entry	Initiator	$[M]_0$:$[I]_0$:[PMDETA]:$[Cu^{1+}]_0$:$[Cu^{2+}]_0$
$(GcMcH)_{19.2}$	$(CH_3)_2CBrCOOCH_2CH_3$	44.5 : 1.00 : 1.00 : 0.50 : 0.50
$((GcMcH)_{3.6})_{5.5}$	SAC-$Br_{5.7}$	44.5 : 1.00 : 5.70 : 0.63 : 5.07
$((GcMcH)_{3.1})_{6.4}$	SAC-Br_8	44.5 : 1.00 : 8.00 : 0.47 : 7.53

Table 4-8. Ter-ologimers with twenty overall degree of polymerization characterization

Entry	$[I]_0$ (mmol/L)	time (min)	conv[a]	$\overline{DP}_n$[b]	$\overline{DP}_n$,arm[c]
$(GcMcH)_{19.2}$	39.5	59	43.2%	19.2	16.3
$((GcMcH)_{3.6})_{5.5}$	32.9	180	44.5%	19.8	7.8
$((GcMcH)_{3.1})_{6.4}$	31.4	100	44.7%	19.9	4.1

[a]Conversion measured by ^{1}H-NMR peak integration. [b]Degree of polymerization calculated by $\overline{DP}_n = (\Delta[M]/([I]_0)$. [c]Arm degree of polymerization calculated by $\overline{DP}_n,arm = \overline{DP}_n/f_{avg}$.

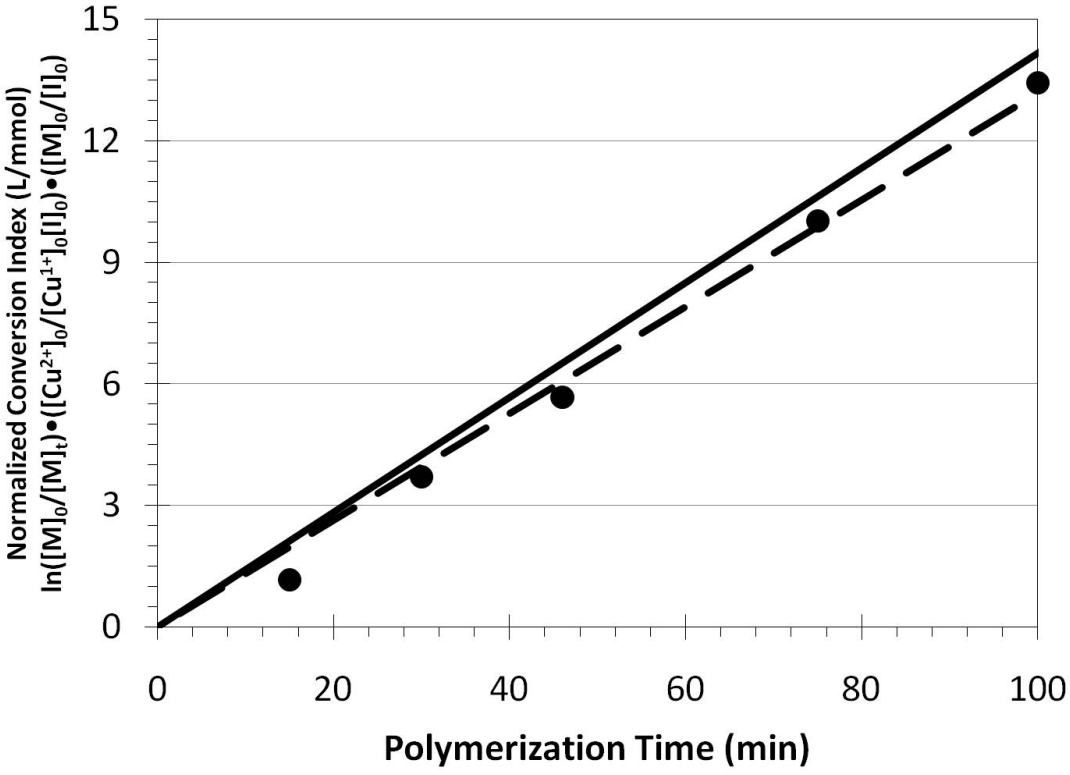

Figure 4-7. Plot of normalized conversion index versus time for **$((GcMcH)_{3.1})_{6.4}$** (●). Trendline (dashed) has a slope 5.7% lower than the predicted value (solid line) found in Figure 4-5.

by measuring the normalized conversion index throughout the reaction, as was done here. As a result, the 5.7% difference between the actual and predicted conversion rates was known prior to the conclusion of the reaction. As a result, the reaction was quenched at 100 minutes instead of the predicted 96 minutes. This resulted in a 44.7% conversion and a molecule with $\overline{DP_n}$=19.9. This demonstrates the capability to target star-shaped ter-oligomers with a precision of 0.1 monomer units.

Slightly less precision is achieved for the polymerization of the other two star-shaped ter-oligomers with target $\overline{DP_n}$=20, although 19<$\overline{DP_n}$<20 is still achieved. The cause stems from differences in the conversion rates for each initiator. All of the star-shaped ter-oligomers synthesized from **SAC-Br$_8$** followed the same linear trend between normalized conversion index and polymerization time. However, changing the initiator results in a substantial change to the slope. (Figure 4-8) Whereas **((GcMcH)$_{3.1}$)$_{6.4}$** had a slope of $1.34 \cdot 10^{-1}$ mmol^{-1}·L·min^{-1}, the conversion **((GcMcH)$_{3.6}$)$_{5.5}$** progressed at a rate of $3.54 \cdot 10^{-1}$ mmol^{-1}·L·min^{-1} and **(GcMcH)$_{19.2}$** had a rate of $1.12 \cdot 10^{-1}$ mmol^{-1}·L·min^{-1}. Although all three initiators are comprised of the same initiating group, other differences including the number of initiating sites and the solubility of the initiator factor into the polymerization kinetics.

In order to achieve the highest levels of precision, the conversion rate must be determined for each initiator. Dilution and catalyst ratios can then be altered from this information to achieve a reaction of sufficient duration to take multiple ^{1}H-NMR samples during polymerization to eliminate the remaining uncertainty. For the star-shaped ter-oligomers **((GcMcH)$_{3.1}$)$_{6.4}$** and **((GcMcH)$_{3.6}$)$_{5.5}$** the reactions were of sufficient length to precisely determine the conversion rate prior to quenching. This resulted in a degree of polymerization within 1% of the target for both molecules. The reaction time for **(GcMcH)$_{19.2}$** was not sufficiently long to measure the conversion rate

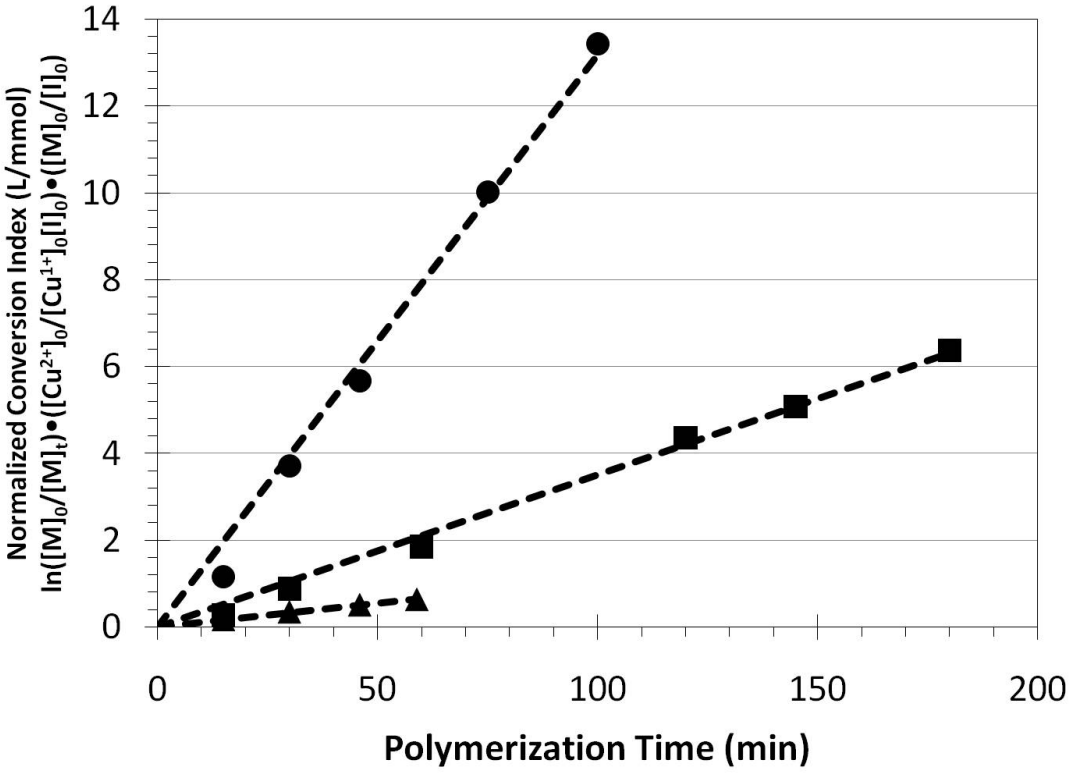

Figure 4-8. Plot of normalized conversion index versus time for **((GcMcH)$_{3.1}$)$_{6.4}$** (●), **((GcMcH)$_{3.6}$)$_{5.5}$** (■) and **(GcMcH)$_{19.2}$** (▲). Different slopes are observed because each oligomer is polymerized from a different initiator.

with the same precision. However, the measurement of the conversion rate was still accurate enough to achieve the oligomer within 1 $\overline{DP_n}$ of the target.

4.4 Conclusions

This work greatly expands both the precision and range of materials that can be prepared as star-shaped oligomers. Random co-oligomers were synthesized with the same composition for average arm lengths of 3.1, 4.1, 7.8 and 16.3 monomer units by modifying the ratios of $[M]_0/[I]_0$ and $[Cu^{1+}]_0/[Cu^{2+}]_0$. In addition, a technique for preparing multifunctional initiators with reduced functionality was introduced. Star-shaped ter-oligomers with the same core but different numbers of arms were successfully synthesized with a $\overline{DP_n}$=20 with a 1% error. These capabilities will now enable studies on the impact of arm number and arm length in the star-shaped oligomer regime for a wide range of materials and properties.

4.5 Acknowledgement

Financial support from the Semiconductor Research Corporation (GRC-1677.001 and GRC-1675.002) is greatly appreciated. Research was performed in part at the Cornell NanoScale Facility, a member of the Nation Nanotechnology Infrastructure Network and the Cornell Center for Materials Research, which are supported by the National Science Foundation (ECS-0335765 and DMR-0520404). Macromolecular Chemistry I and Macromolecular Chemistry II at the University of Bayreuth are thanked for the generous use of their polymer synthesis and characterization facilities. D.C.F. was supported by a GRC and Applied Materials fellowship. The contribution of raw materials by Rohm and Haas is appreciated.

REFERENCES

1. Likos, C.N. and H.M. Harreis, *Star polymers: from conformations to interactions to phase diagrams.* Condensed Matter Physics, 2002. **29**: p. 173-200.

2. Likos, C.N., *Soft matter with soft particles.* Soft Matter, 2006. **2**: p. 478-498.

3. Likos, C.N., et al., *Star Polymers Viewed as Ultrasoft Colloidal Particles.* Physical Review Letters, 1998. **80**(20): p. 4450-4453.

4. Sutherland, R.J. and R.B. Rhodes, *Dispersant viscosity index improvers*, U.S. Patent, Editor. 1994, Shell Oil Company: United States. p. 1-7.

5. Spinelli, H.J., *Silicone containing acrylic star polymers*. 1991, E. I. du Pont de Nemours and Company. p. 1-9.

6. Hunter, R.J., *Foundations of Colloid Science, Vol. 1*. 1986, New York: Oxford University Press.

7. Grest, G., L.J. Fetters, and J.S. Huang, *Star polymers: experiment, theory, and simulation.* Advances in Chemical Physics, 1996. **94**((Polymeric Systems)): p. 67-163.

8. Hsu, H.-P., W. Nadler, and P. Grassberger, *Scaling of Star Polymers with 1-80 Arms.* Macromolecules, 2004. **37**(12): p. 4658-4663.

9. von Ferber, C. and Y. Holovatch, *Field-theoretical renormalization group analysis for the scaling exponents of star polymers.* Condensed Matter Physics, 2002. **29**: p. 117-136.

10. Dzubiella, J. and A. Jusufi, *Star-polymer-colloid mixtures.* Condensed Matter Physics, 2002. **30**: p. 285-305.

11. Bohrisch, J., et al., *New Polyelectrolyte Architectures.* Advances in Polymer Science, 2004. **165**: p. 1-41.

12. Ganazzoli, F., *Conformations and dynamics of stars and dendrimers: the Gaussian Self-Consistent approach.* Condensed Matter Physics, 2002. **5**(1): p. 37-71.

13. Plamper, F.A., et al., *Synthesis, Characterization and Behavior in Aqueous Solution of Star-Shaped Poly(acrylic acid).* Macromolecular Chemistry and Physics, 2005. **206**: p. 1813-1825.

14. Liechty, W.B., et al., *Polymers for drug delivery systems.* Annual Review of Chemical and Biomolecular Engineering, 2010. **1**: p. 149-173.

15. Adair, J.H., et al., *Recent developments in the preparation and properties of nanometer-size spherical and platelet-shaped particles and composite particles.* Materials Science & Engineering: R: Reports, 1998. **23**(4-5): p. 139-242.

16. Matz, G.F., et al., *Low molecular weight water soluble polymer composition and method of use*, in *PCT Int. Appl.*, W.I.P. Organization, Editor. 2001, Calgon Corporation, USA.

17. Ito, H., *Chemical Amplification Resists for Microlithography.* Advances in Polymer Science, 2005. **172**: p. 37-245.

18. De Silva, A., et al., *A fundamental study on dissolution behavior of high-resolution molecular glass photoresists.* Chemistry of Materials, 2008. **20**(23): p. 7292-7300.

19. Forman, D.C., et al., *Chemically Amplified Star-Shaped Oligomers as 'Star Resists' for Next Generation Lithography.* Manuscript in preparation, 2010.

20. De Leon-Rodriguez, L.M., et al., *MRI Detection of VEGFR2 in Vivo Using a Low Molecular Weight Peptoid-$(Gd)_8$-Dendron for Targeting.* Journal of the American Chemical Society, 2010. **132**(37): p. 12829-12831.

21. Forman, D.C., et al., *Synthesis, Characterization and Properties of Star-Shaped Poly(tert-Butyl Methacrylate) Oligomers.* Manuscript in preparation, 2010.

22. Kato, M., et al., *Polymerization of Methyl Methacrylate with the Carbon Tetrachloride/Dichlorotris-(triphenylphosphine)ruthenium(II)/Methylaluminum Bis(2,6-di-tert-butylphenoxide) Initiating System: Possibility of Living Radical Polymerization.* Macromolecules, 1995. **28**(5): p. 1721-1723.

23. Wang, J.-S. and K. Matyjaszewski, *Controlled/"Living" Radical Polymerization. Atom Transfer Radical Polymerization in the Presence of Transition-Metal Complexes.* Journal of the American Chemical Society, 1995. **117**(20): p. 5614-5615.

24. Wang, J.-L., T. Grimaud, and K. Matyjaszewski, *Kinetic Study of the Homogeneous Atom Transfer Radical Polymerization of Methyl Methacrylate.* Macromolecules, 1997. **30**(21): p. 6507-6512.

25. Sawamoto, M. and M. Kamigaito, *Living radical polymerizations based on transition metal complexes.* Trends in Polymer Science (Cambridge, United Kingdom), 1996. **4**(11): p. 371-377.

26. Haddleton, D.M., et al., *Atom Transfer Radical Polymerization of Methyl Methacrylate Initiated by Alkyl Bromide and 2-Pyridinecarbaldehyde Imine Copper(I) Complexes.* Macromolecules, 1997. **30**(7): p. 2190-2193.

27. Zhang, M. and A.H.E. Müller, *Cylindrical polymer brushes.* Journal of Polymer Science, Part A: Polymer Chemistry, 2005. **43**(16): p. 3461-3481.

28. Sheiko, S.S., B.S. Sumerlin, and K. Matyjaszewski, *Cylindtrical molecular brushes: Synthesis, characterization, and properties.* Progress in Polymer Science, 2008. **33**(7): p. 759-785.

29. Gao, C. and D. Yan, *Hyperbranched polymers: from synthesis to applications.* Progress in Polymer Science, 2004. **29**(3): p. 183-275.

30. Gaynor, S.G. and K. Matyjaszewski, *Step-Growth Polymers as Macroinitiators for "Living" Radical Polymerization: Synthesis of ABA Block Copolymers.* Macromolecules, 1997. **30**(14): p. 4241-4243.

31. Kasko, A.M., A.M. Heintz, and C. Pugh, *The Effect of Molecular Architecture on the Thermotropic Behavior of Poly[11-(4'-cyanophenyl-4"-phenoxy)undecyl acrylate] and Its Relation to Polydispersity.* Macromolecules, 1998. **31**(2): p. 256-271.

32. Kickelbick, G., P.J. Miller, and K. Matyjaszewski, *Multifunctional star initiators for atom transfer radical polymerization.* Polymer Preprints (American Chemical Society, Division of Polymer Chemistry), 1998. **39**(1): p. 284-285.

33. Matyjaszewski, K., et al., *Synthesis of Block, Graft and Star Polymers from Inorganic Macroinitiators.* Applied Organometallic Chemistry, 1998. **12**: p. 667-673.

34. Matyjaszewski, K., et al., *Synthesis and Characterization of Star Polymers with Varying Arm Number, Length and Composition from Organic and Hybrid Inorganic/Organic Multifunctional Initiators.* Macromolecules, 1999. **32**(20): p. 6526-6535.

35. Ueda, J., et al., *Multifunctional Initiators for the Ruthenium-Mediated Living Radical Polymerization of Methyl Methacrylate: Di- and Trifunctional Dichloroacetates for Synthesis of Multiarmed Polymers.* Macromolecules, 1998. **31**(3): p. 557-562.

36. Ueda, J., M. Kamigaito, and M. Sawamoto, *Calixarene-Core Multifunctional Initiators for the Ruthenium-Mediated Living Radical Polymerization of Methacrylates.* Macromolecules, 1998. **31**(20): p. 6762-6768.

37. Muthukrishnan, S., et al., *Synthesis and Characterization of Glycomethacrylate Hybrid Stars from Silsesquioxane Nanoparticles.* Macromolecules, 2005. **38**(26): p. 10631-10642.

38. Plamper, F.A., et al., *Pearl Necklace Architecture: New Threaded Star-Shaped Copolymers.* Macromolecules, 2010. **43**(5): p. 2190-2203.

39. Wieberger, F., et al., *Solution behavior of poly(tert-butylmethacrylate) star oligomers.* Manuscript in preparation, 2010.

40. Odian, G., *Principles of Polymerization, Fourth Edition*. 2004, Hoboken, New Jersey: John Wiley & Sons, Inc.

41. Rein, D., P. Rempp, and P.J. Lutz, *Recent developments in the field of star-shaped polymers.* Makromolekulare Chemie, Macromolecular Symposia, 1993. **67 (EPF Workshop on Anionic Polymerization and Related Processes, 1992)**: p. 237-249.

42. Chochos, C.L., et al., *Hyberbranched Polymers for Photolithographic Applications - Towards Understanding the Relationship between Chemical Structure of Polymer Resin and Lithographic Performance.* Advanced Materials, 2009. **21**: p. 1121-1125.

43. Heise, A., et al., *Investigation of the Initiation Behavior of a Dendritic 12-Arm Initiator in Atom Transfer Radical Polymerization.* Macromolecules, 2001. **34**(11): p. 3798-3801.

44. Tang, W. and K. Matyjaszewski, *Kinetic Modeling of Normal ATRP, Normal ATRP with $[Cu^{II}]_0$, Reverse ATRP and SR&NI ATRP.* Macromolecular Theory and Simulations, 2008. **17**: p. 359-375.

45. Goto, A. and T. Fukuda, *Kinetics of living radical polymerization.* Progress in Polymer Science, 2004. **29**: p. 329-385.

46. Matyjaszewski, K. and J. Xia, *Atom Transfer Radical Polymerization.* Chemical Reviews, 2001. **101**(9): p. 2921-2990.

CHAPTER 5. A COMBINATORIAL STUDY ON POST-EXPOSURE BAKE TEMPERATURE IN CHEMICALLY AMPLIFIED, STAR-SHAPED RESISTS

Drew C. Forman and Christopher K. Ober

Materials Science & Engineering

Cornell University, Ithaca, NY 14853

Florian Wieberger, Tristan Kolb, and Hans-Werner Schmidt

Macromolecular Chemistry I

University of Bayreuth, Bayreuth, Germany 95440

5.0 Abstract

A combinatorial temperature gradient stage enable the study of different post-exposure bake (PEB) temperatures on a single wafer. The roughness behavior of four star-shaped resists or "star resists" and an analogous linear resist control were examined on wafers with 925 combinations of PEB temperatures and doses. Optimal PEB temperatures were observed that minimized both the roughness and pattern blur of the resists. Power spectral density (PSD) analysis was performed along the optimal PEB temperatures to provide spatial roughness information. A unique, high frequency smoothing behavior was found in the best performing resist, indicating a potential conformational advantage in that material.

5.1 Introduction

As transistor miniaturization progresses the effect of roughness on critical dimension (CD) variations become increasingly detrimental as a consequence of shorter gate length and transistor width.[1, 2] As roughness from the resist sidewall is transferred to the substrate during the etch process,[3] understanding and minimizing photoresist roughness may be instrumental towards maintaining low defectivity as progress is made along the International Technology Roadmap for Semiconductors (ITRS).[4] Monte Carlo simulations have predicted that changes to the resist architecture should result in decreased roughness,[5] but physical experiments have lagged behind[6] in part because roughness is highly dependent on both the photoresist and its processing.[7, 8]

In many other fields, studies in star-shaped polymers, which consist of multiple linear polymer arms covalently attached to a central core, have revealed improvements to polymer properties as the number of arms is varied.[9-11] Star-shaped polymers with very few arms behave similarly to a linear chain. However, as the number of arms is

increased, the capability of the arms to interact with neighboring molecules decreases, leading to an "ultrasoft colloid" regime.[10] Essentially, intermolecular interactions are traded in favor of intramolecular interactions. Consequently, stars are used for a range of applications including viscosity index modifiers in oil,[12] oxygen permeability and hardness enhancers in contact lenses,[13] and as additives in coatings, binder in toner and as encapsulation materials in pharmaceuticals.[14, 15]

However, these applications, and many theoretical and experimental studies,[16-21] involve star-shaped polymers that are too large for high resolution lithography. We have recently demonstrated the capability to synthesize low molecular weight star-shaped polymers[22-24] that may prove beneficial for a number of applications including drug delivery,[25] nanoparticle dispersion stabilizers,[26] cosmetic dyes,[27] and *in vivo* sensors,[28] in addition to photoresists.[29-31] In photoresists, we have demonstrated that these "star resists" can form smoother features compared with analogous linear materials.[32]

In this work, we take advantage of recently developed combinatorial techniques[33] to fully explore the effect of post-exposure bake temperature on the resulting sidewall roughness of four star resists with the same composition but different arm lengths. (Figure 5-1) In addition to investigating line edge roughness (LER), the length independent roughness metric, infinite LER (LER_{inf}),[1, 2] is examined combinatorially along with the spatial roughness parameters:[1, 2, 34-37] correlation length (ξ) and roughness exponent (α). Finally, power spectral density (PSD) analysis[1, 38, 39] is performed to gain insight into observed smoothing.

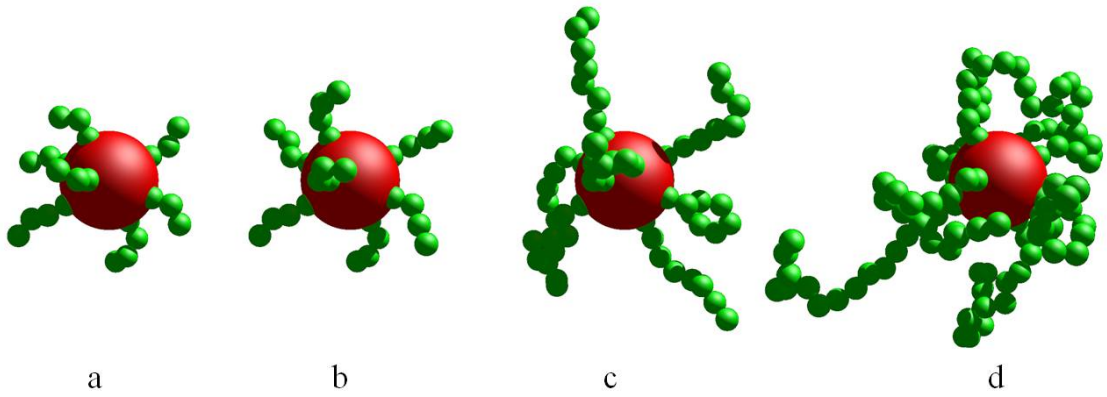

Figure 5-1. Graphical depiction of number average star-shaped poly(α-gamma butyrolactone methacrylate – co – methyl adamantyl methacrylate – co – hydroxyl adamantyl methacrylate) teroligomer corresponding to star resists (a) **$((GcMcH)_{3.1})_{6.4}$**, (b) **$((GcMcH)_{4.1})_{6.4}$**, (c) **$((GcMcH)_{7.8})_{6.4}$** and (d) . The core and monomer units are represented by spheres with volumes set by the molecular weights of the saccharose initiator (excluding bromine) and the monomers (number average).

5.2 Experimental

5.2.1 Materials

Four experimental star resists were synthesized from the same saccharose based multifunctional initiator, which was measured to yield a blend of stars with an average number of arms equal to 6.4. Reaction conditions were modified based on the known kinetics model [See Equation 5-1][40-42] to grow arms with the same mol. percent composition: 50% α-gamma butyrolactone methacrylate (GBLMA), 30% methyl adamantyl methacrylate (MAMA), and 20% hydroxyl adamantyl methacrylate (HAMA) but different arm lengths, as previously described.[24] The GBLMA-*co*-MAMA-*co*-HAMA (GcMcH) statistical terpolymers are named for their architecture: $((GcMcH)_n)_f$) where n is the number average of monomer units per arm and f is the number average of arms per molecule. (Table 5-1)

$$\ln\left(\frac{[M]_0}{[M]_t}\right) = \frac{k_p K_{ATRP}[P_mX][Cu^I]}{[Cu^{II}]}t \qquad \text{Equation 5-1}$$

The base additive triethylamine, photoacid generator (PAG) triephenylsulfonium perfluorobutanesulfonate (TPS-Nf), spin solvent propylene glycol methyl ether acetate (PGMEA), and developer AZ® 726 MIF, a 0.26N tetramethylammonium hydroxide containing substrate wetting surfactants, were purchased from Aldrich and used as received.

Table 5-1. Resist characterization summary

Entry	$\bar{f}$ [a]	$\bar{n}$ [b]	$\overline{DP_n}$ [c]	M_n [d]
$((GcMcH)_{3.1})_{6.4}$	6.4	3.1	20	5 600
$((GcMcH)_{4.1})_{6.4}$	6.4	4.1	26	6 900
$((GcMcH)_{7.8})_{6.4}$	6.4	7.8	50	11 700
$((GcMcH)_{16.3})_{6.4}$	6.4	16.3	104	22 700
$(GcMcH)_{19.2}$	1	19.2	19	4 100

[a]Average number of arms per star. [b]Average number of monomer units per arm. [c]Average degree of polymerization. [d]Average molecular weight. All quantities are number average.

5.2.2 Lithography

5.2.2.1 Preparation of Resist Films

A solution consisting of 5 mg/mL PAG in PGMEA containing base in a 1.0:0.3 PAG:base stochiometric ratio was prepared. 50 mg/mL batches of each resist were prepared from the same solution to ensure equal quantities of PAG and base. 100mm silicon wafers were primed with hexamethyldisilazane vapor in a YES-LPIII vapor priming oven. Resist films were applied through spincasting at 3000 RPM for 1 minute with an acceleration of 3000 RPM/s. Following spin coating, a post apply bake was performed at 130 °C for five minutes.

5.2.2.2 Exposure

Exposures were carried out on a JEOL JBX-9300FS, 100kV electron beam at a current of 2nA with a scan pitch of 6nm and a full width half max beam size of 4.3nm. Half-pitches from 12nm to 144nm in 12nm steps were included in a test pattern consisting of 1:1 line-spaces in a 4 micron by 3 micron rectangle that was repeated five times for each half-pitch in a 60 micron by 60 micron area. A proximity correction was applied with the program Layout BEAMER using electron scattering simulation data from the program Sceleton. Exposures were performed in a 5x5 dose matrix starting from a base dose of 224 $\mu C/cm^2$ with a 1.1x step size. The center to center spacing between doses was 250 microns. The dose matrix was repeated 37 times across the wafer, in an array perpendicular to the large flat, with a spacing of 1.7 mm between matrices. The e-beam was operated using an overlap mode, such that each pattern was exposed twice at half the intended dose.

5.2.2.3 Combinatorial Post-Exposure Bake

A combinatorial thermal gradient stage was machined from $0^{3/8}$ in. thick aluminum. A single piece of aluminum, $8^{1/4}$ in. wide and $20^{1/2}$ in. long, serves as the main stage. Four additional pieces of aluminum were welded to the final 5 in. on one end of the stage, creating a four sided ice bath with an open top $8^{1/4}$ in. tall, 5 in. long and $8^{1/2}$ in. wide that acts as a heat sink. A drainage hole was drilled $2^{1/4}$ in. from the top to prevent changes to the volume/surface area of the heat sink from ice melting. This resulted in a constant heat sink with a 3.13 L volume and a surface area of 825 cm^2. The final $5^{1/2}$ in. on the opposite end of the stage was placed in contact with a hot plate at 220 °C, surface area 293 cm^2, creating a thermal gradient 10 in. long. During the operation of the thermal gradient stage, ice was continuously loaded into the heat sink to replace melting ice. (Figure 5-2)

A Fisher Scientific Traceable Infrared Thermometer Gun with adjustable emissivity (ε) was manually used to record the temperature of an infrared opaque silicon wafer (ε=0.73) placed with its primary flat 1 in. from the hot plate and the opposite end 5 in. from the heat sink. Average temperature readings were recorded at 1, 2, 3, 4, 5, 6, 7 and 8 cm from the large flat until a stable temperature was achieved. At this time, the infrared opaque wafer was removed and replaced with an exposed wafer. After all four wafers were subsequently baked for 30 sec. each, the infrared opaque wafer was replaced and the temperature measured again. This set of before and after temperatures were used to compute the linear temperature gradient. (Figure 5-3)

5.2.2.4 Development

Development was carried out on a Hamatech-Steag wafer processor using 726 MIF developer and a 60 second double puddle recipe.

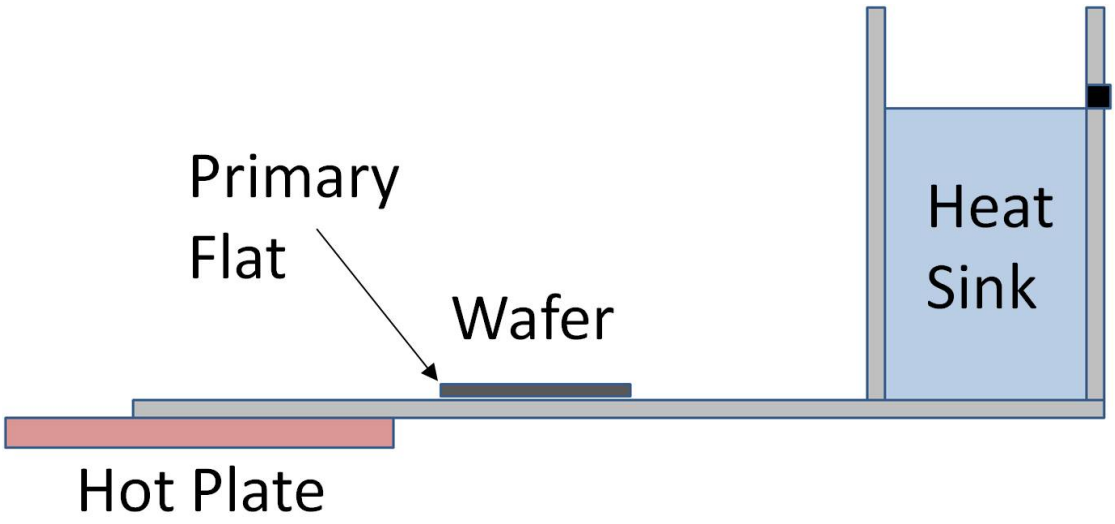

Figure 5-2. Schematic of thermal gradient stage

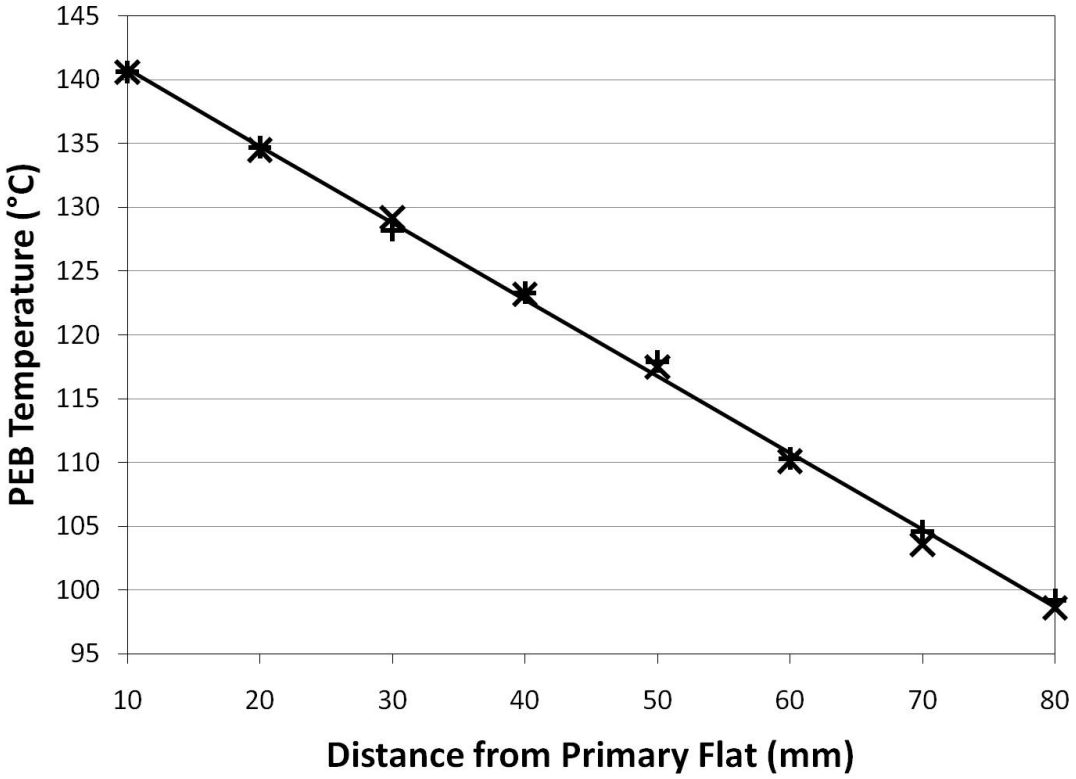

Figure 5-3. Temperature measured before (+) and after (X) PEB. Linear best fit (solid line) calculated from the combined average of before and after temperature readings. Calculated temperature at primary flat: 146.8 °C. Calculated gradient: 6.02 °C/cm.

5.2.3 Characterization

5.2.3.1 Scanning Electron Microscopy (SEM)

Wafers were sputtered using a Hummer Au/Pd sputtering system and placed in a LEO 1550 Field Emission SEM operated at 1.5kV. Images of 96nm half-pitch line-spaces were recorded in a line integration mode (N=10) at a magnification of 40k stored at a 3072 x 2304 resolution, yielding 15 lines, 2.27 μm in length with a pixel size of 0.985 nm.

5.2.3.2 Roughness Measurements

Roughness was measured from electron micrographs of patterned and developed photoresists using the software SuMMIT. A Gaussian prefilter, 6 pixels wide, was applied in the direction perpendicular to the lines and a threshold of 0.5 was used to identify the line edge. The spatial roughness parameters, correlation length and roughness exponent, were calculated from the line edge height-height correlation function. Upon identifying the optimal PEB temperature for each resist, a compound analysis was performed on five sets of patterns, processed identically, to obtain 150 line edges for PSD analysis and final roughness exponent and correlation length measurements.

5.2.4 Linear Comparison

A linear control, **(GcMcH)$_{19.2}$**, was synthesized as previously described[24] and evaluated in a manner analogous to the star resists.

5.3 Results and Discussion

During the PEB step of the lithographic processes, acid diffusion and the deprotection reaction depend on both the bake temperature and time. It is trivial to set the temperature of a hot plate. However, ensuring that multiple samples are heated, transferred to a cooling stage and cooled for the same length of time is substantially more difficult in a laboratory environment. Consequently, when conventional procedures are used to evaluate the effect of small PEB temperature changes, it can be difficult to determine whether roughness observations are caused by temperature or an error in heating and cooling time. The combinatorial technique avoids this uncertainty by examining multiple temperatures on a single wafer, ensuring heating and cooling time consistency between different temperatures on the wafer.

Conventional procedures use a fully iterative process, whereby results from an initial experiment are evaluated and used to make procedural modifications for subsequent experiments. In combinatorial work, all experimental conditions are processed simultaneously. In this case, an iterative process is confined to the SEM evaluation to reduce operation time. SEM images of the test patterns were recorded for every dose at a given PEB temperature. However, only one temperature, every few degrees, was evaluated. After measuring the roughness from these recorded images, a second step of SEM evaluation occurs. With the roughness data from the initial analysis, the temperature range of interest was narrowed. Test pattern images were recorded using a smaller temperature step size in this narrower range. This process was repeated until the best roughness was identified along with the roughness of the immediately higher and lower temperatures to confirm the presence of a minimum. As a result of this combinatorial process, the optimal PEB temperature could be identified in a shorter amount of time and with greater certainty due to the removal of heating and cooling time variations.

5.3.1 LER_{inf} Evaluation

A general trend was observed for all data; as the dose was increased from the clearing dose for a given PEB temperature, the CD of features decreased. The additional dose results in greater acid generation, causing additional deprotection reactions at the same PEB temperature. A blur distance was calculated from the difference between the exposed half-pitch (HP) and the feature CD for every dose and PEB temperature.

As each SEM image contained 30 line edges but only 15 line widths, roughness evaluation was performed using the LER_{inf} metric. Contour maps, depicting LER_{inf} as a function of PEB temperature and blur were calculated from the recorded data using a Delaunay triangulation. (Figure 5-4, Figure 5-5, Figure 5-6 and Figure 5-7) An optimal PEB temperature can be defined by the temperature at which low roughness can be achieved with minimal blur. This occurs at 98 °C for **$((GcMcH)_{3.1})_{6.4}$**, 101 °C for **$((GcMcH)_{4.1})_{6.4}$**, 102 °C for **$((GcMcH)_{7.8})_{6.4}$**, and 126 °C for **$((GcMcH)_{16.3})_{6.4}$**. The optimal PEB temperature was found to increase with molecular size. At these temperatures, the star **$((GcMcH)_{4.1})_{6.4}$** achieved the lowest roughness.

It should be noted that the largest star, **$((GcMcH)_{16.3})_{6.4}$**, was found to have its process window shrink considerably below the reported temperatures. No processing conditions were observed that enabled 96 nm half-pitch resolution in **$((GcMcH)_{16.3})_{6.4}$** at the optimal PEB temperatures of the other star resists. This was not caused by underexposure, as collapsed patterns were observed at higher doses.

The optimal PEB of the other stars was observed between 98 and 102 °C. While PEB heating and cooling times could not be held constant between different wafers in the experimental set-up, it is unlikely that a heating or cooling difference on the order of one second could account for a 4 °C shift. A more satisfactory explanation comes from the relationship between glass transition temperature and molecular weight. At

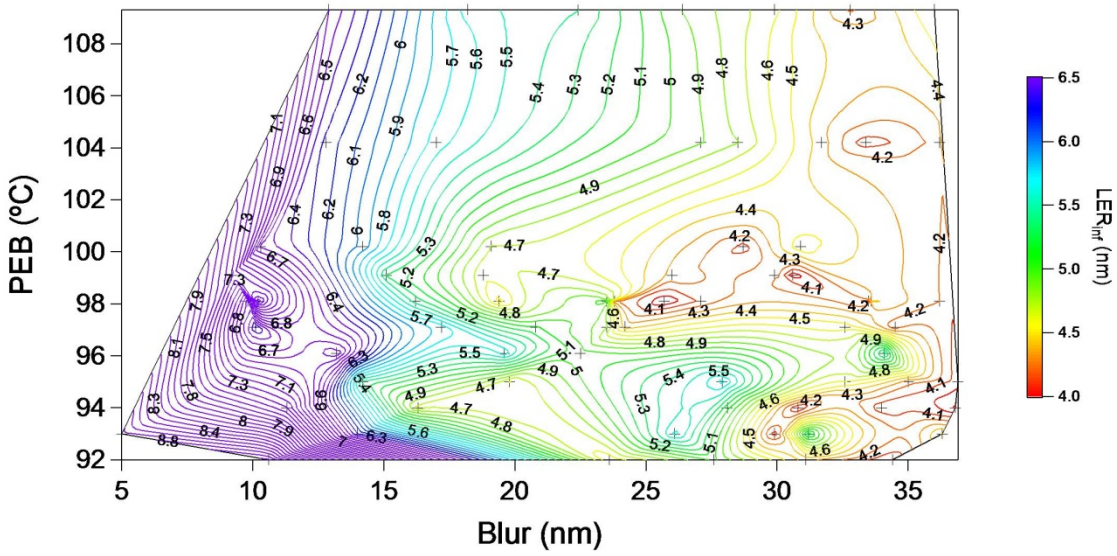

Figure 5-4. Contour plot depicting LER_{inf} as a function of PEB temperature and pattern blur (half pitch minus critical dimension) for **$((GcMcH)_{3.1})_{6.4}$**.

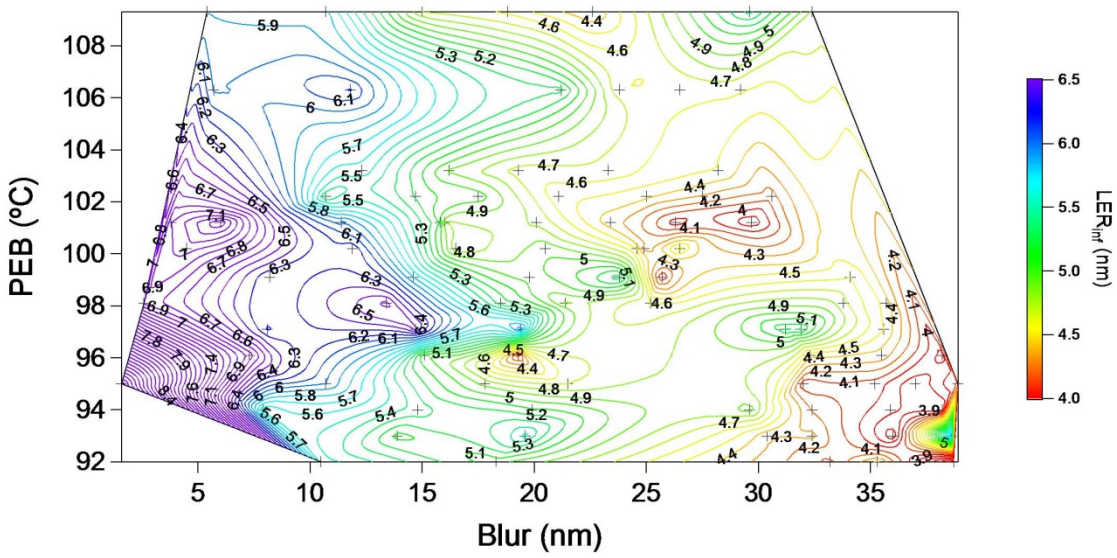

Figure 5-5. Contour plot depicting LER_{inf} as a function of PEB temperature and pattern blur (half-pitch minus critical dimension) for **$((GcMcH)_{4.1})_{6.4}$**.

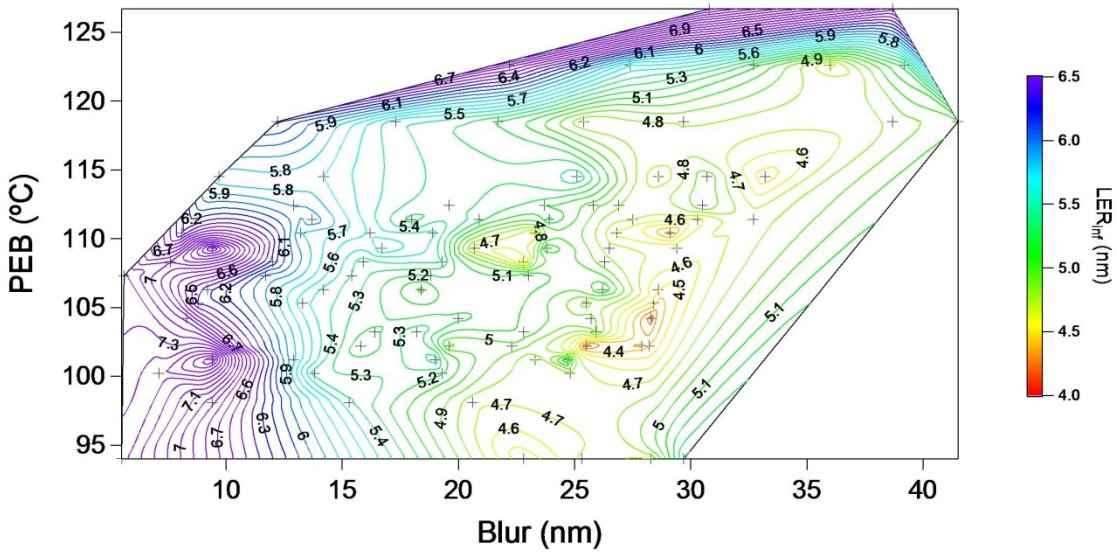

Figure 5-6. Contour plot depicting LER_{inf} as a function of PEB temperature and pattern blur (half-pitch minus critical dimension) for **$((GcMcH)_{7.8})_{6.4}$**.

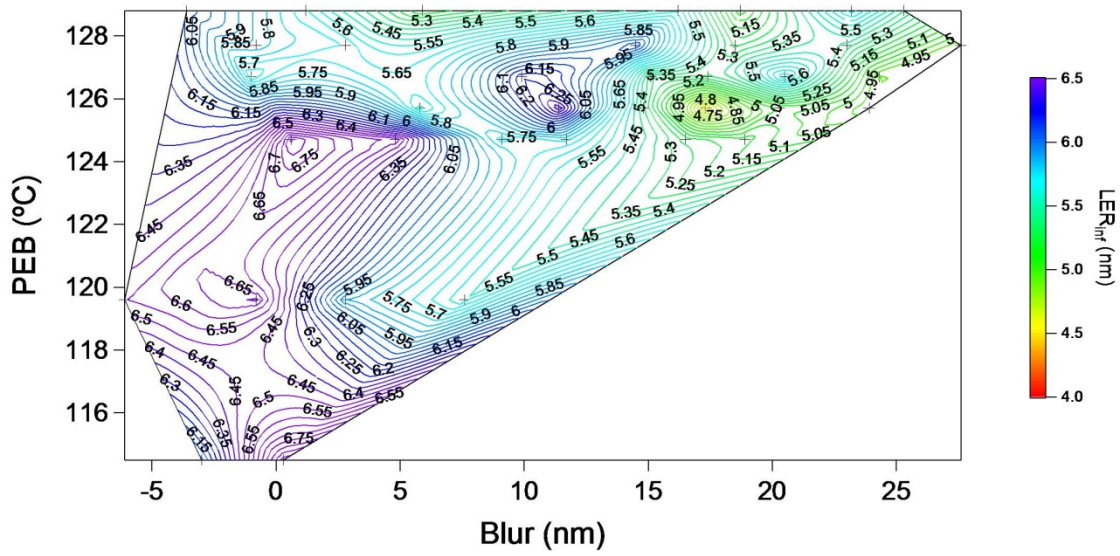

Figure 5-7. Contour plot depicting LER_{inf} as a function of PEB temperature and pattern blur (half-pitch minus critical dimension) for **$((GcMcH)_{16.3})_{6.4}$**.

low molecular weights, glass transition temperature decreases.[43] Consequently, acid can diffuse through a low molecular weight resist more rapidly at a given temperature. This is consistent with the observation that optimal PEB temperature decreased with decreasing molecular weight.

As PEB temperature increases, dose is decreased in all four resists. This result is expected, as dose is responsible for acid generation; with higher temperature, less acid is required to bring about sufficient deprotection for a chemical switch. Roughness has been modeled as partially stemming from localized differences in the deprotection of photoresist[44] At PEB temperatures above the optimal PEB, roughness is increased because smaller quantities of acid result in greater statistical deviations in the localized acid concentration. As temperature decreases more acid must be generated, improving acid concentration statistics and leading to lower roughness. However, this is accompanied by a decrease in the acid diffusion length and available deprotection energy. Therefore, the optimal PEB temperature is a minimum between a higher temperature region where roughness is dominated by statistical differences in acid generation and a lower temperature region where roughness is dominated by statistical differences in deprotection.

5.3.2 Reaction-Diffusion Front

Blur can be interpreted as the progression of the reaction-diffusion front in a chemically amplified resist. However, it is important to note that its progression is dependent on a combination of factors, including acid diffusion, the deprotection reaction, extent of deprotection required to induce a solubility switch for a given resist, and acid trapping mechanisms including, but not limited to, base neutralization.[45] A diffusion coefficient for the reaction-diffusion front can be calculated from blur by simplifying to one dimensional diffusion: $Blur/2=\sqrt{2Dt}$. However, there is no

correlation between this diffusion coefficient and the diffusion coefficient of acid through the resist. (Figure 5-8 and Figure 5-9)

Blur comparisons must be made at a constant exposure dose, as dose alters that initial acid concentration. The plot of logarithmic diffusion coefficient versus inverse temperature plot clearly demonstrates that the reaction-diffusion front does not follow Arrhenius behavior. An acid trapping mechanism (the base additive) impedes the diffusion coefficient's increase with temperature beyond short length scales. However, neither the direct comparison of blur and temperature, nor the pseudo-Arrhenius interpretation of the reaction-diffusion front, yield any fundamental insight to the optimal PEB temperature. For additional understanding one must look to spatial roughness.

5.3.3 Spatial Roughness

The standard roughness metrics of LER and LWR (as well as LER_{inf} and LWR_{inf}) are measures of statistical deviation from a mean.[1] They do not include spatial information describing where that deviation occurs. Below the correlation length, roughness can be characterized as a self-similar fractal with a fractal dimension equal to 2-α. Roughness saturates towards a fractal dimension of one above the correlation length, leading to an overall behavior that is consistent with a self-affine fractal.[36]

The spatial roughness parameters were calculated from the HHCF of 150 line edges for each data point at the optimal PEB temperatures. Plotting the spatial roughness against pattern blur reveals two trends. (Figure 5-10 and Figure 5-11) As previously reported, the roughness exponent is dependent on the deprotected composition at the line edge and is therefore invariant to most processing parameters except development.[8] The behavior of the star resists is consistent with those findings, although a general downwards trend is observed at high degrees of blurring

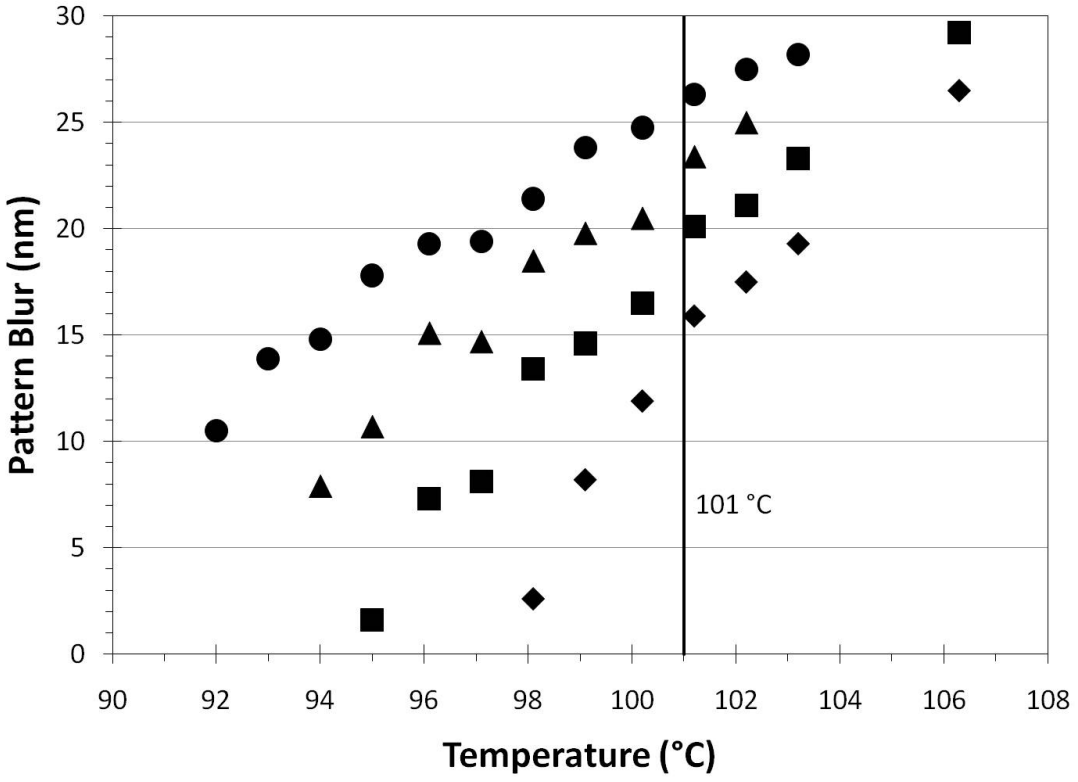

Figure 5-8. Blur-temperature plots for resist $((GcMcH)_{4.1})_{6.4}$ at an exposure dose of 1029 (♦), 1132 (■), 1245 (▲), and 1370 (●) μC/cm^2. Plot of pattern blur versus PEB temperature.

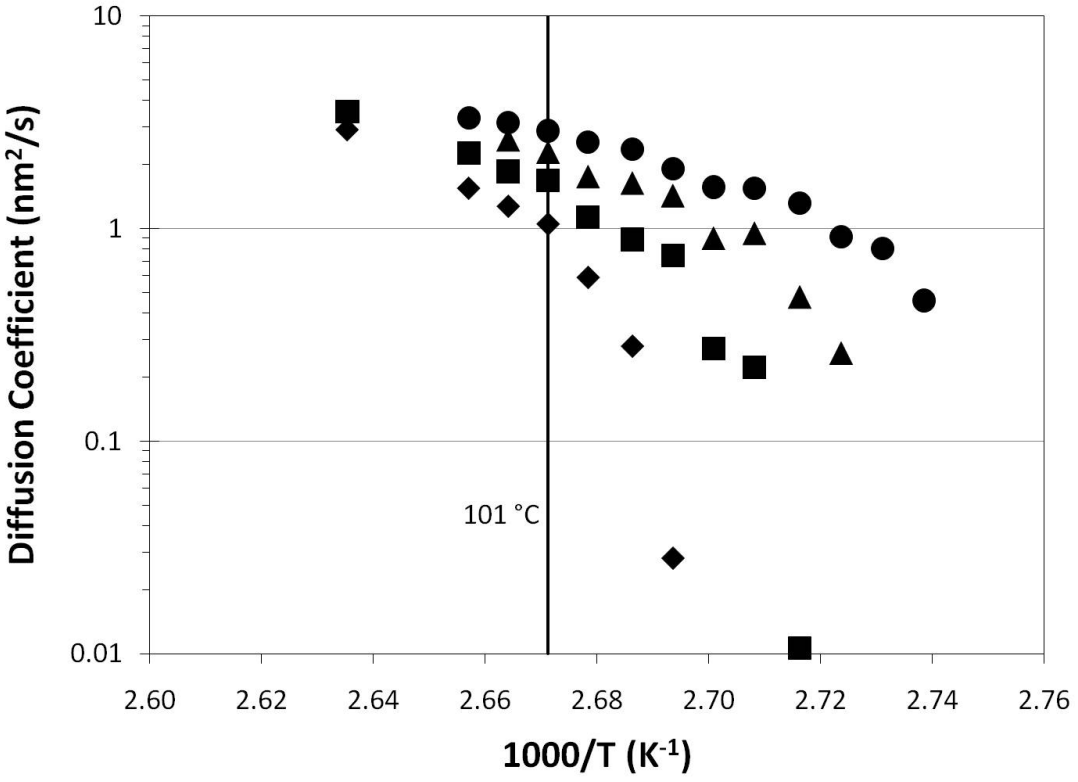

Figure 5-9. Blur-temperature plots for resist $((GcMcH)_{4.1})_{6.4}$ at an exposure dose of 1029 (♦), 1132 (■), 1245 (▲), and 1370 (●) μC/cm^2. Logarithmic diffusion coefficient versus inverse temperature plot for the reaction-diffusion front is not Arrhenius due to acid trapping mechanisms.

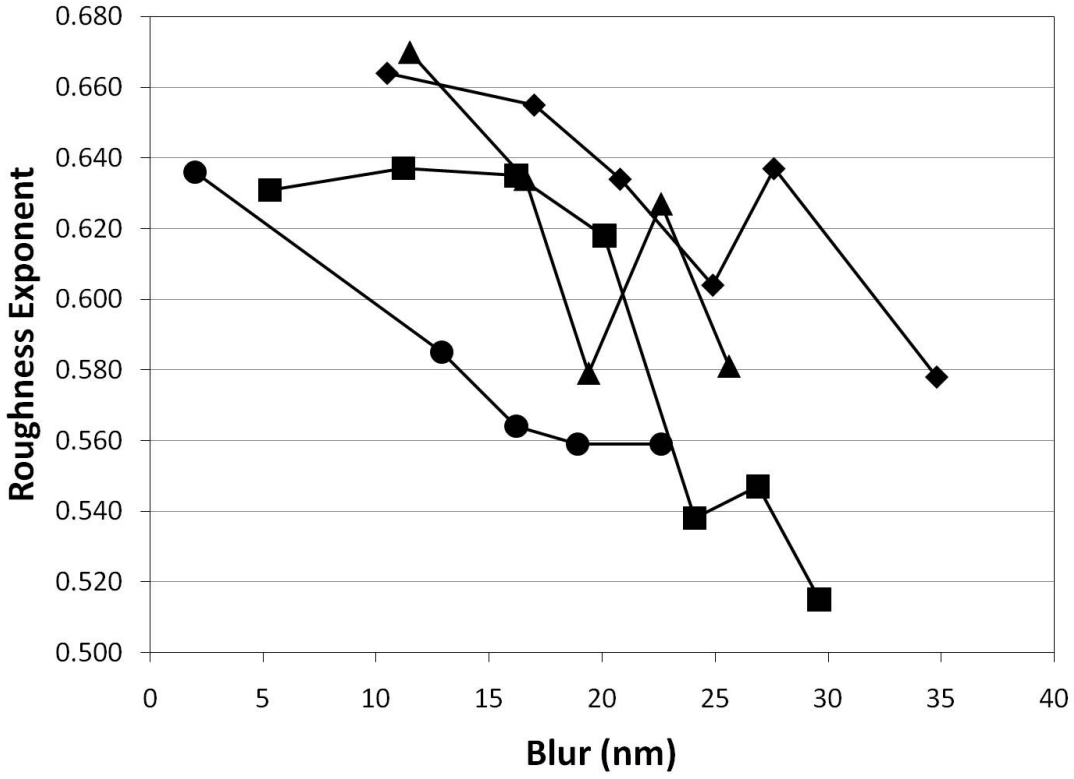

Figure 5-10. Roughness exponent is plotted against blur at the optimal PEB temperatures for $((GcMcH)_{16.3})_{6.4}$ (●), $((GcMcH)_{7.8})_{6.4}$ (▲), $((GcMcH)_{4.1})_{6.4}$ (■), and $((GcMcH)_{3.1})_{6.4}$ (♦). Lines are to guide the eyes.

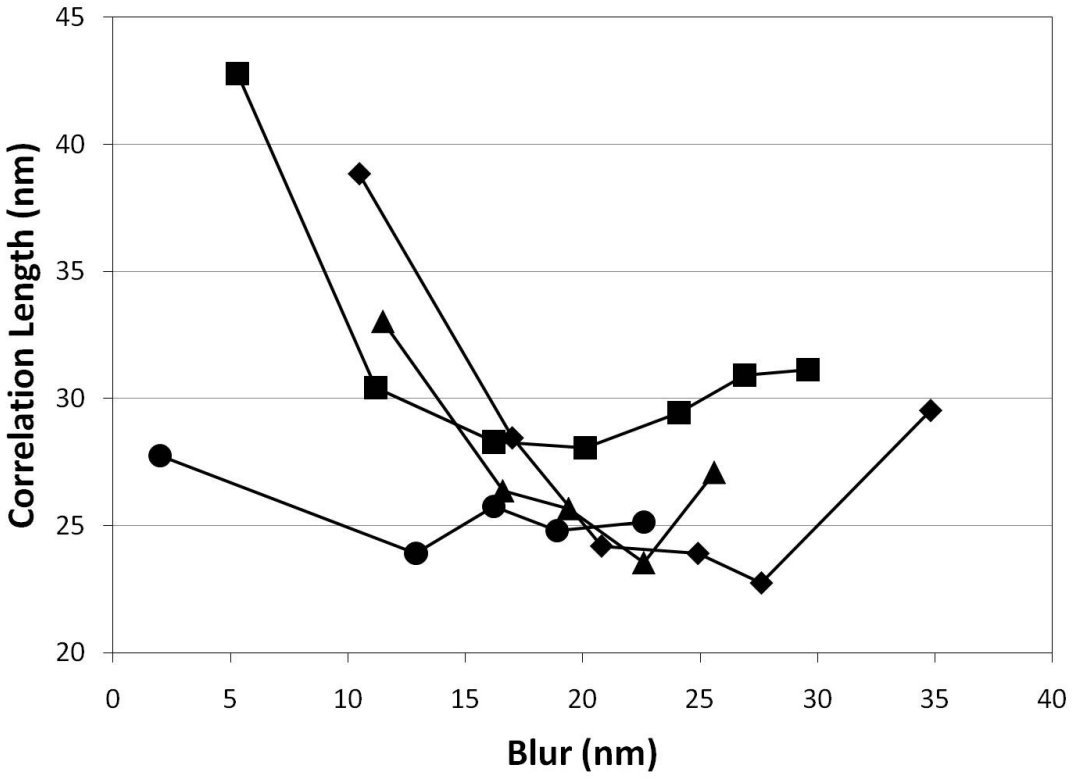

Figure 5-11. Correlation length is plotted against blur at the optimal PEB temperatures for $((GcMcH)_{16.3})_{6.4}$ (●), $((GcMcH)_{7.8})_{6.4}$ (▲), $((GcMcH)_{4.1})_{6.4}$ (■), and $((GcMcH)_{3.1})_{6.4}$ (♦). Lines are to guide the eyes.

as the resists approach pattern collapse. Furthermore, aside from the largest star, the roughness exponents of the resists are in close agreement. Correlation length has a much stronger dependence on the processing conditions. The star resists express a minimum correlation length at moderate blur. Correlation length increases significantly when the resist is on the verge of under- or over-exposure. Similar minimum correlation lengths are observed for all four star resists except, surprisingly, the lowest roughness resist, which has a correlation length 4nm higher than the other resists.

A PSD analysis can provide further spatial information by dividing roughness into its component spatial frequencies. Examining the PSD of the star resists over a range of pattern blurs reveals that the primary smoothing as the star resists blur occurs at low frequencies. (Figure 5-12, Figure 5-13, Figure 5-14 and Figure 5-15)

A unique, high frequency smoothing was observed as pattern blurring increased in **$((GcMcH)_{4.1})_{6.4}$**. Comparing **$((GcMcH)_{4.1})_{6.4}$** with the other star resists blurred a similar amount, reveals that this high frequency smoothing is the reason **$((GcMcH)_{4.1})_{6.4}$** has the lowest roughness. (Figure 5-16) Interestingly, the two smallest resists, **$((GcMcH)_{3.1})_{6.4}$** and the linear control **$(GcMcH)_{19.2}$**, do not exhibit the best roughness. The PSD of **$((GcMcH)_{3.1})_{6.4}$** is a close match with **$((GcMcH)_{7.8})_{6.4}$**, while the linear control has spatial roughness similar to the much larger **$((GcMcH)_{16.3})_{6.4}$**.

In order to examine the role of temperature on this high frequency smoothing, multiple SEM images were collected for the temperatures one degree higher and lower than the optimal PEB for **$((GcMcH)_{4.1})_{6.4}$**. PSD analysis reveals a strong temperature dependence in the high frequency smoothing. (Figure 5-17) If the PEB temperature is raised or lowered by even a single degree, high frequency roughness worsens. This effect is far more significant than the changes in low frequency roughness. Pattern blur is observed to change by 1 nm/°C.

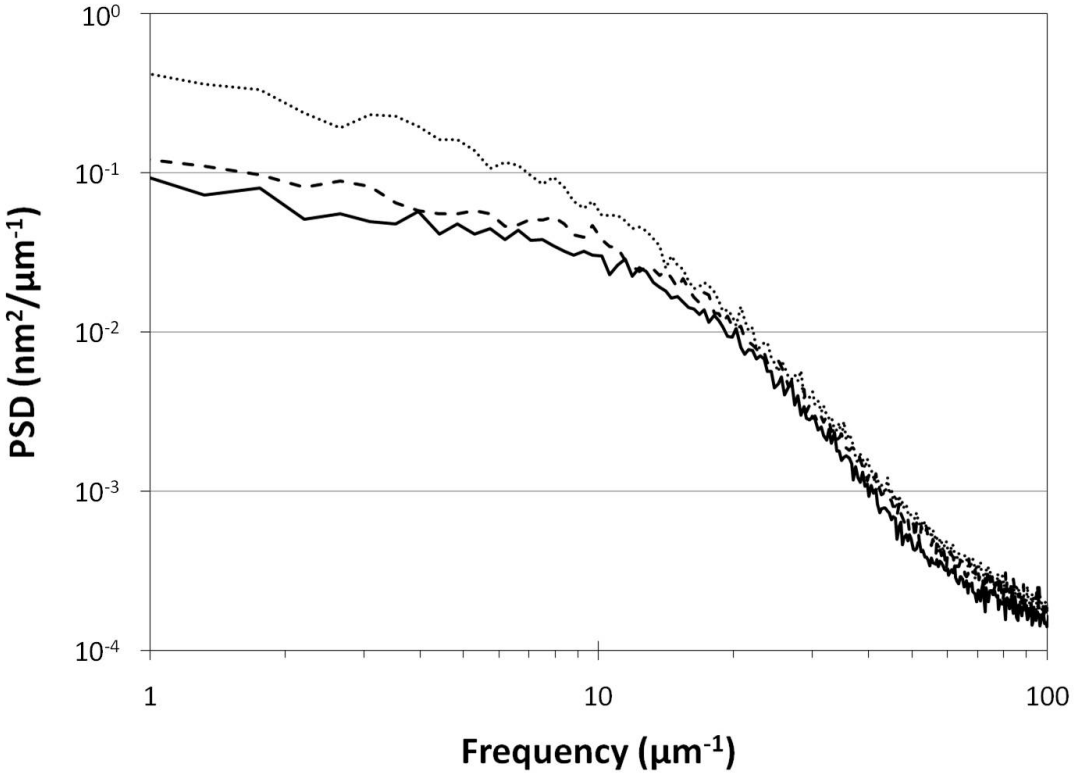

Figure 5-12. PSD analysis of 150 line edges for star resists at their optimal PEB. **$((GcMcH)_{3.1})_{6.4}$** with pattern blur of 10.5 (dot), 20.8 (dash), and 27.6 (solid) nm.

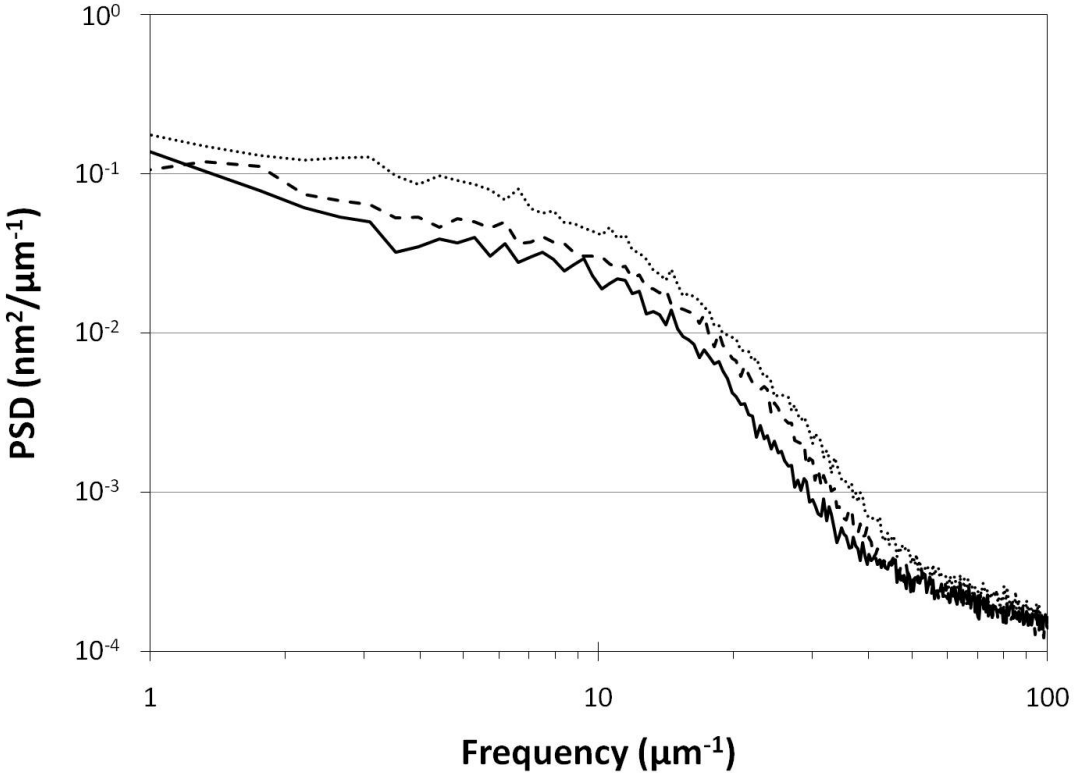

Figure 5-13. PSD analysis of 150 line edges for star resists at their optimal PEB. **$((GcMcH)_{4.1})_{6.4}$** with pattern blur of 11.2 (dot), 20.1 (dash), and 29.6 (solid) nm.

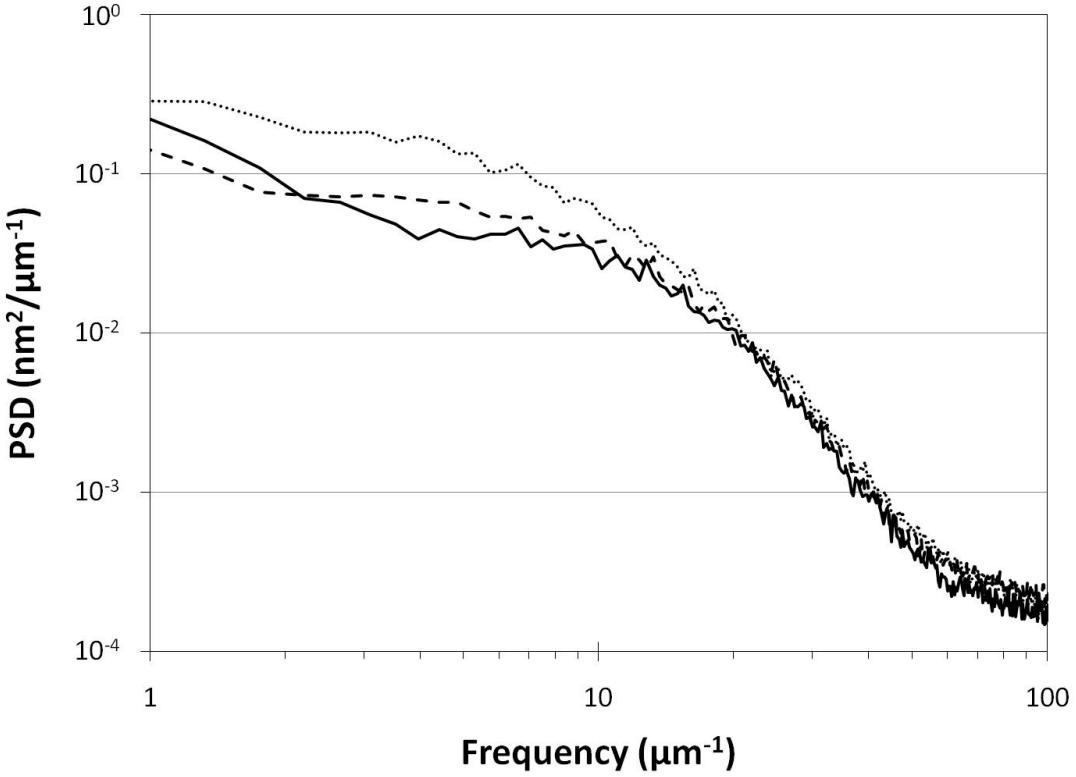

Figure 5-14. PSD analysis of 150 line edges for star resists at their optimal PEB. **$((GcMcH)_{7.8})_{6.4}$** with pattern blur of 11.5 (dot), 19.4 (dash), and 25.6 (solid) nm.

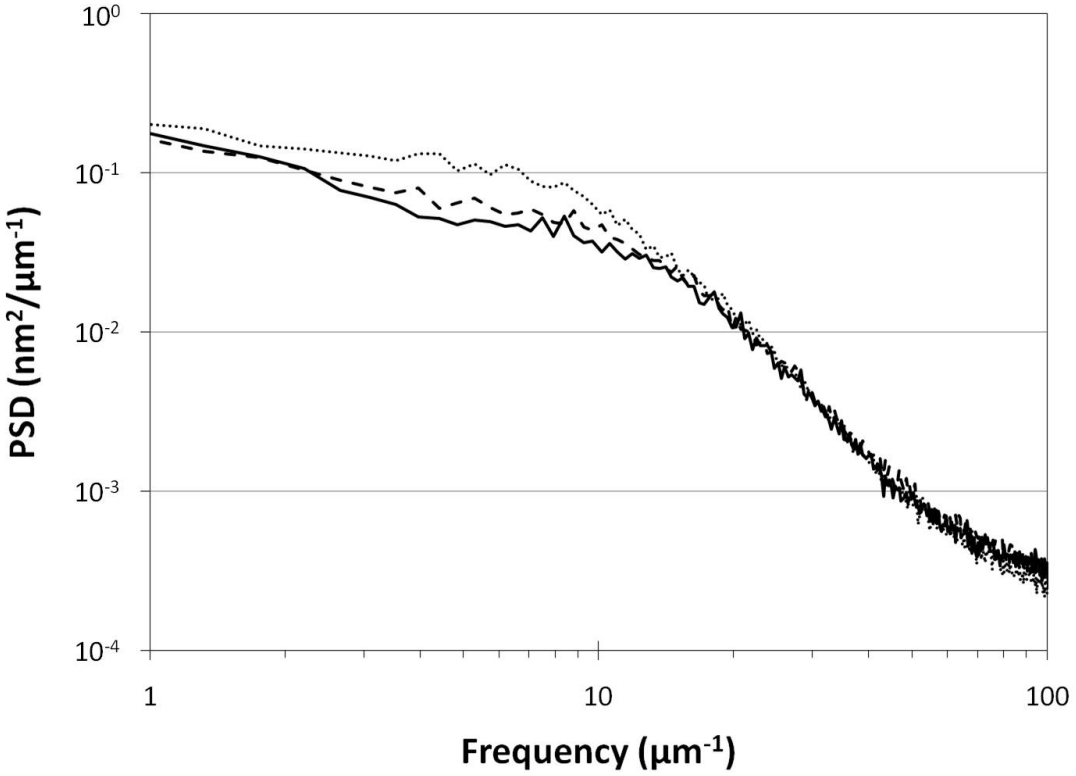

Figure 5-15. PSD analysis of 150 line edges for star resists at their optimal PEB. **$((GcMcH)_{16.3})_{6.4}$** with pattern blur of 2.0 (dot), 16.2 (dash), and 22.6 (solid) nm.

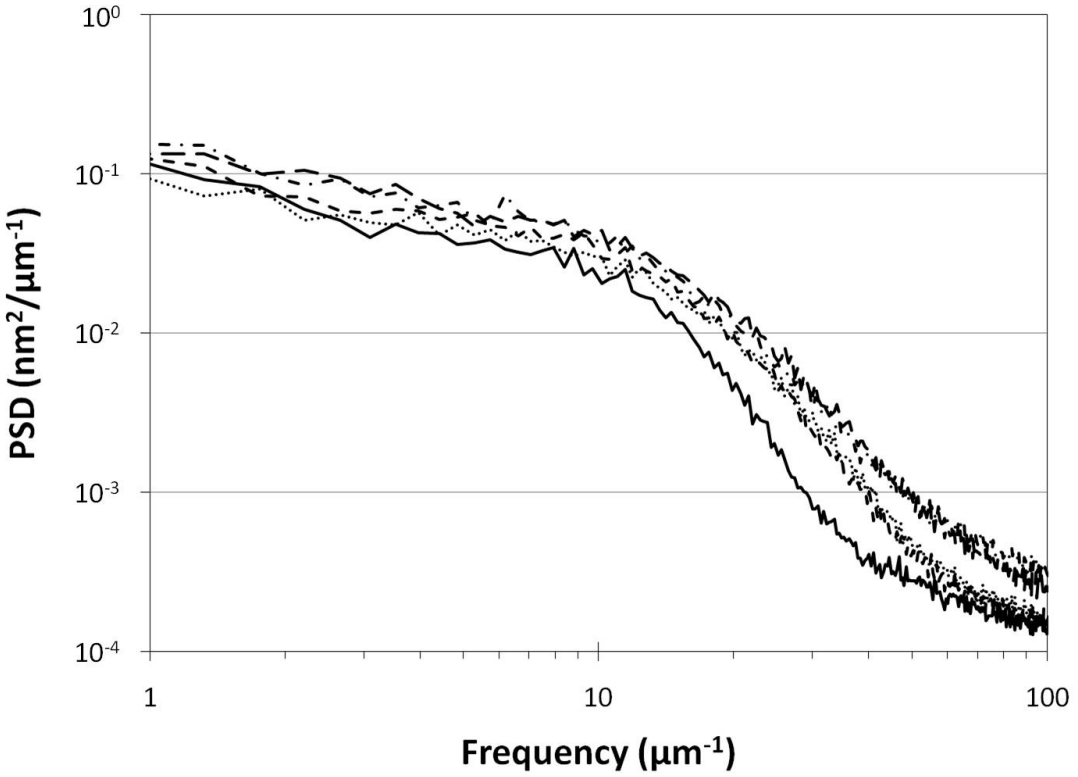

Figure 5-16. PSD analysis of 150 line edges at the optimal PEB for **((GcMcH)$_{16.3}$)$_{6.4}$** (dash-dot), **((GcMcH)$_{7.8}$)$_{6.4}$** (dash), **((GcMcH)$_{4.1}$)$_{6.4}$** (solid) **((GcMcH)$_{3.1}$)$_{6.4}$** (dot), and **(GcMcH)$_{19.2}$** (long dash). Pattern blur is 18.9, 22.6, 26.9, 27.6, and 27.6 nm respectively.

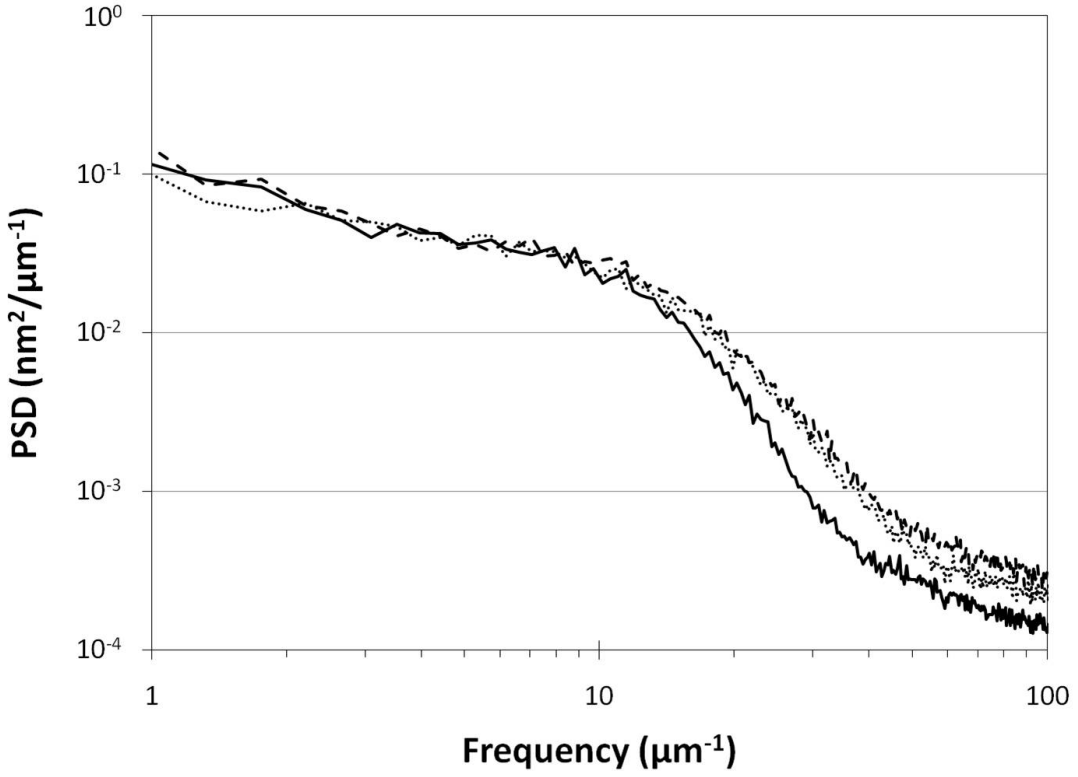

Figure 5-17. PSD analysis of 150 line edges for resist **$((GcMcH)_{4.1})_{6.4}$** exposed with the same dose with PEB temperatures one degree below the optimal PEB, 100 °C (dot), at the optimal PEB, 101 °C (solid), and one degree above the optimal PEB, 102 °C (dash).

5.3.4 Sources of High Frequency Smoothing

Having determined that the best performing resist, **((GcMcH)$_{4.1}$)$_{6.4}$**, displayed unique high frequency smoothing in its spatial roughness, it is important to explore potential causes.

The most obvious difference between the resists is molecular weight. It is understood how roughness can decrease with molecular weight.[7] However, there exists a practical lower limit as the resist's glass transition temperature decreases at low molecular weights.[43] While it is likely that there is a decrease in glass transition temperature between the star resists, it could not be measured as even the smallest star had a glass transition temperature higher than its decomposition temperature (around 150 °C). Molecular weight and glass transition temperature can account for the subtle differences in the optimal PEB of stars **((GcMcH)$_{3.1}$)$_{6.4}$**, **((GcMcH)$_{4.1}$)$_{6.4}$**, and **((GcMcH)$_{7.8}$)$_{6.4}$**. However, as the glass transition temperature of even the smallest star was still above 150 °C, it is difficult to conceptualize how molecular weight arguments could adequately explain high frequency smoothing in **((GcMcH)$_{4.1}$)$_{6.4}$** but not the smaller **((GcMcH)$_{3.1}$)$_{6.4}$**.

An additional difference between the resists is composition. In this experiment the composition of the star resist arms was held constant. However, as the saccharose core was identical for all stars, the overall composition of GBLMA, MAMA and HAMA shifted as molecular weight decreased. (Table 5-2) The percentage of the acid labile group MAMA decreases with resist size, as the core becomes responsible for an increasing percentage of the resist's composition. Consequently there are less sites available for deprotection. In a conventional resist, reducing the number of non-polar sites would improve the resist's sensitivity. The opposite trend is observed in these materials as the increasing influence of the non-polar core overwhelms the decrease in acid labile groups.

Table 5-2. Overall resist composition

Entry	Initiator[a]	GBLMA[a]	MAMA[a]	HAMA[a]
$((GcMcH)_{3.1})_{6.4}$	27.6%	30.0%	26.3%	16.1%
$((GcMcH)_{4.1})_{6.4}$	22.4%	32.3%	28.5%	16.8%
$((GcMcH)_{7.8})_{6.4}$	13.2%	36.7%	30.3%	19.8%
$((GcMcH)_{16.3})_{6.4}$	6.8%	39.9%	32.5%	20.8%
$(GcMcH)_{19.2}$	4.7%	37.9%	35.5%	21.9%

[a]Reported in weight percentage.

It is possible that a minimum in polarity occurs at **((GcMcH)$_{4.1}$)$_{6.4}$**. It may be necessary to synthesize a large number of resists, with many different compositions at each size, to completely disprove such a possibility. However, as with molecular weight, it is difficult to imagine a polarity difference between **((GcMcH)$_{4.1}$)$_{6.4}$** and the slightly smaller **((GcMcH)$_{3.1}$)$_{6.4}$** that is sufficiently large that it could satisfactorily explain high frequency smoothing in one and not the other. In addition, were a combination of polarity and low molecular weight responsible for the high frequency smoothing, one would expect to observe this phenomenon in a polar, low molecular weight resist, such as the linear control **(GcMcH)$_{19.2}$**. As this behavior was not observed in the linear control, one must conclude another cause for the high frequency smoothing. (Figure 5-18)

The final difference between the resists is arm length. Of all the possibilities discussed, only arm length, and its impact on intermolecular interactions, offers an explanation for the observation of high frequency smoothing in **((GcMcH)$_{4.1}$)$_{6.4}$** but not **((GcMcH)$_{3.1}$)$_{6.4}$**. Stated simply, if the arms are too short there will be an insufficient barrier to prevent core-core interactions. Oppositely, as the arm length increases so too does the arm-arm interaction between resist molecules. Simulations of larger stars with many more arms have shown that it is possible for stars to assume a conformation where their cores couple, essentially behaving as a molecule that is twice as large.[18, 46] It is therefore plausible that the conformation of **((GcMcH)$_{4.1}$)$_{6.4}$** exists at an intermolecular interaction minimum, allowing the sidewall revealed upon development to more closely match the deprotection profile and enabling high frequency smoothing. The similar spatial roughness of **((GcMcH)$_{3.1}$)$_{6.4}$** and **((GcMcH)$_{7.8}$)$_{6.4}$**, which is twice the molecular weight, supports this coupling hypothesis. Confirmation of this argument will require molecular simulations of the resist conformations, which are beyond the scope of the current work. At this time,

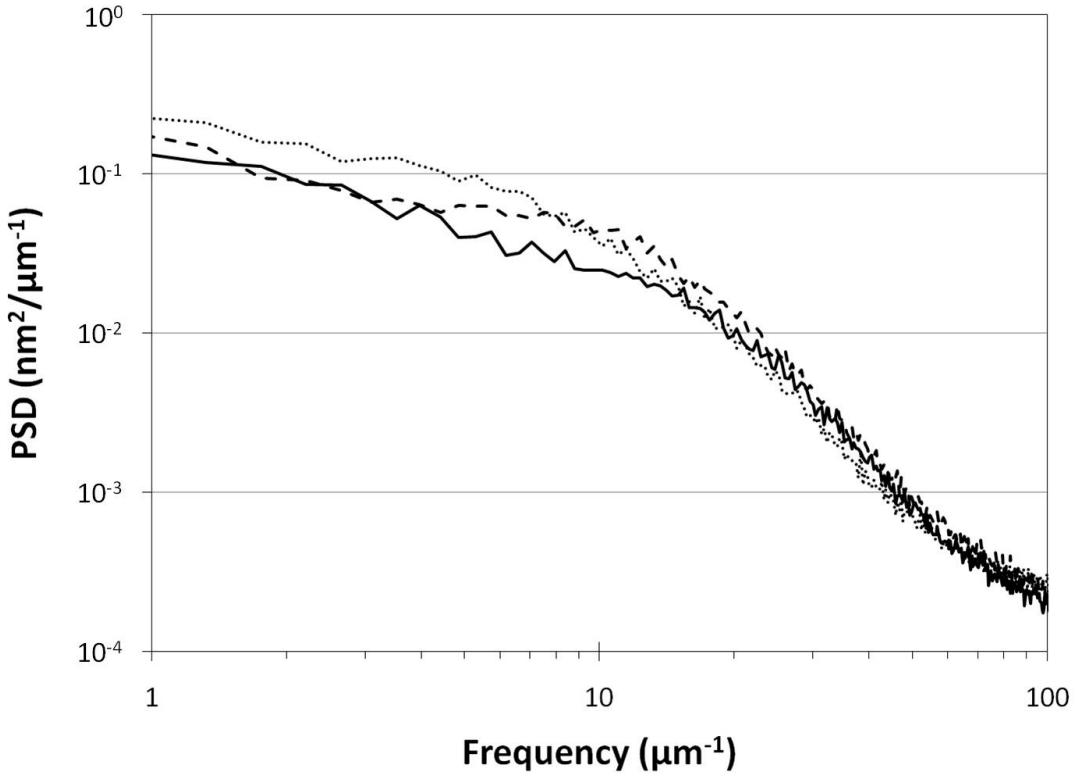

Figure 5-18. PSD analysis of 150 line edges for linear control $(GcMcH)_{19.2}$ with 7.6 (dot), 23.8 (dash), and 40.3 (solid) nm of pattern blurring.

such simulations have only been carried out for star polymers more than an order of magnitude larger than the star resists.[9, 10, 20]

5.3.5 Statistical Comparison of Linear and Star Resists

Having examined 150 line edges for each set of processing conditions at the optimal PEB temperatures, it is possible to make a statistical comparison between the performance of the linear and star resists. (Figure 5-19) At similar amounts of pattern blur, the star resist is smoother than the linear resist. Even by increasing the pattern blur substantially, the linear material is unable to match the roughness of the star. As a final comparison the best SEM of the star resist **$((GcMcH)_{4.1})_{6.4}$** is displayed alongside the best SEM of the linear control at the same blur, clearly demonstrating a smoother line edge. (Figure 5-20 and Figure 5-21) The star resist has a LWR of 4.7 nm and LER of 3.1 nm while the linear resist has a LWR of 6.3 nm and LER of 4.4 nm, all 3σ.

5.4 Conclusions

A combinatorial temperature gradient enabled the study of roughness and PEB temperature on a single wafer eliminating errors in PEB heating and cooling times. A PEB temperature was found for the star resists that minimized roughness and pattern blur. This optimal PEB trended towards lower temperatures as the size of the star decreased, likely as a result of decreasing glass transition temperature. The star resist **$((GcMcH)_{4.1})_{6.4}$** was found to exhibit the best roughness. Using PSD analysis to investigate spatial roughness revealed the source of this improvement stemmed from a unique, high frequency smoothing in that resist. This behavior was found to increase with pattern blur caused by higher exposure doses and to decrease as a result of temperature fluctuations around the optimal PEB. The high frequency smoothing was not observed in the other star resists or in the linear resist control. Molecular

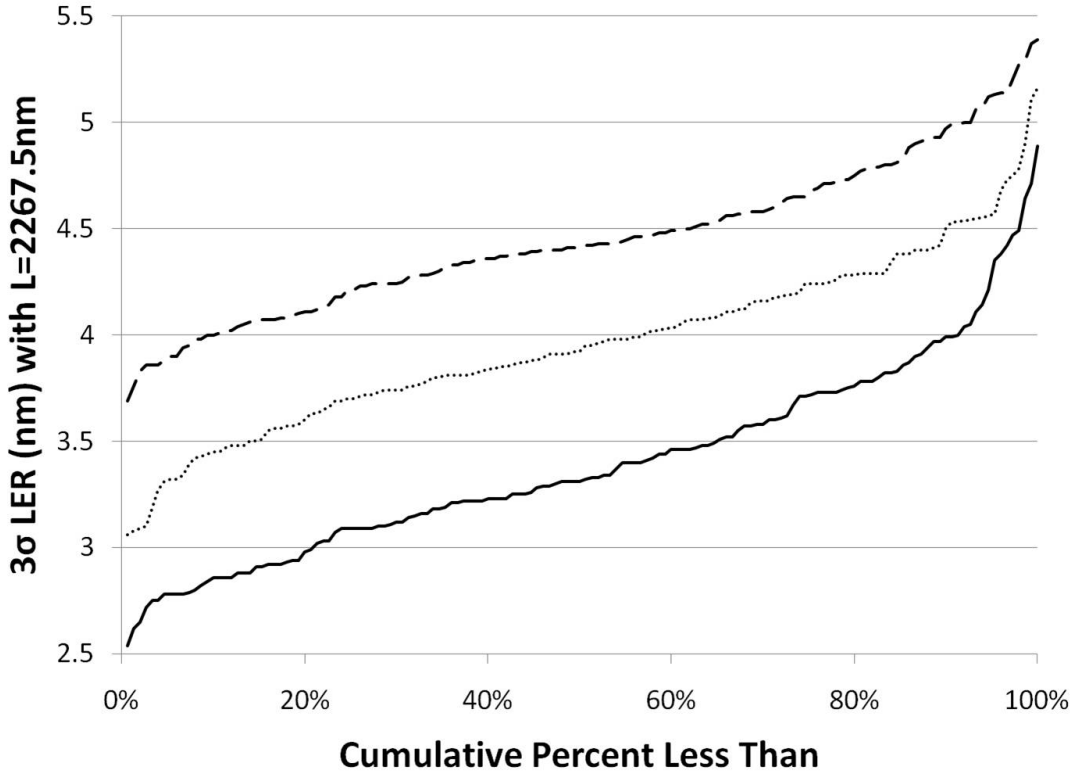

Figure 5-19. Cumulative percent less than plot of LER for star resist $((GcMcH)_{4.1})_{6.4}$ with 26.9 nm of pattern blur (solid) and the linear control $(GcMcH)_{19.2}$ with 27.6 (dash) and 40.3 (dot) nm of pattern blur.

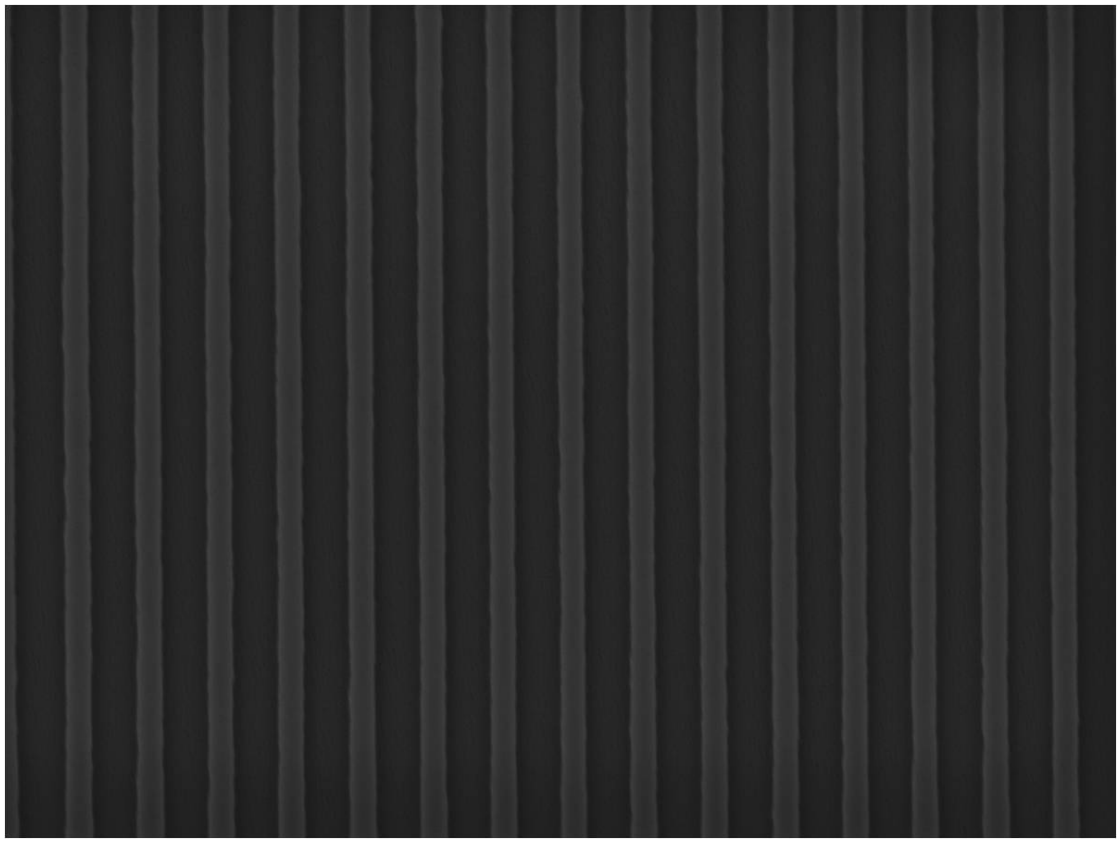

Figure 5-20. SEM of l/s test patterns of star resist with 26.9 nm of pattern blur. Original images recorded with 3072 x 2304 pixels with a 0.985 nm pixel size.

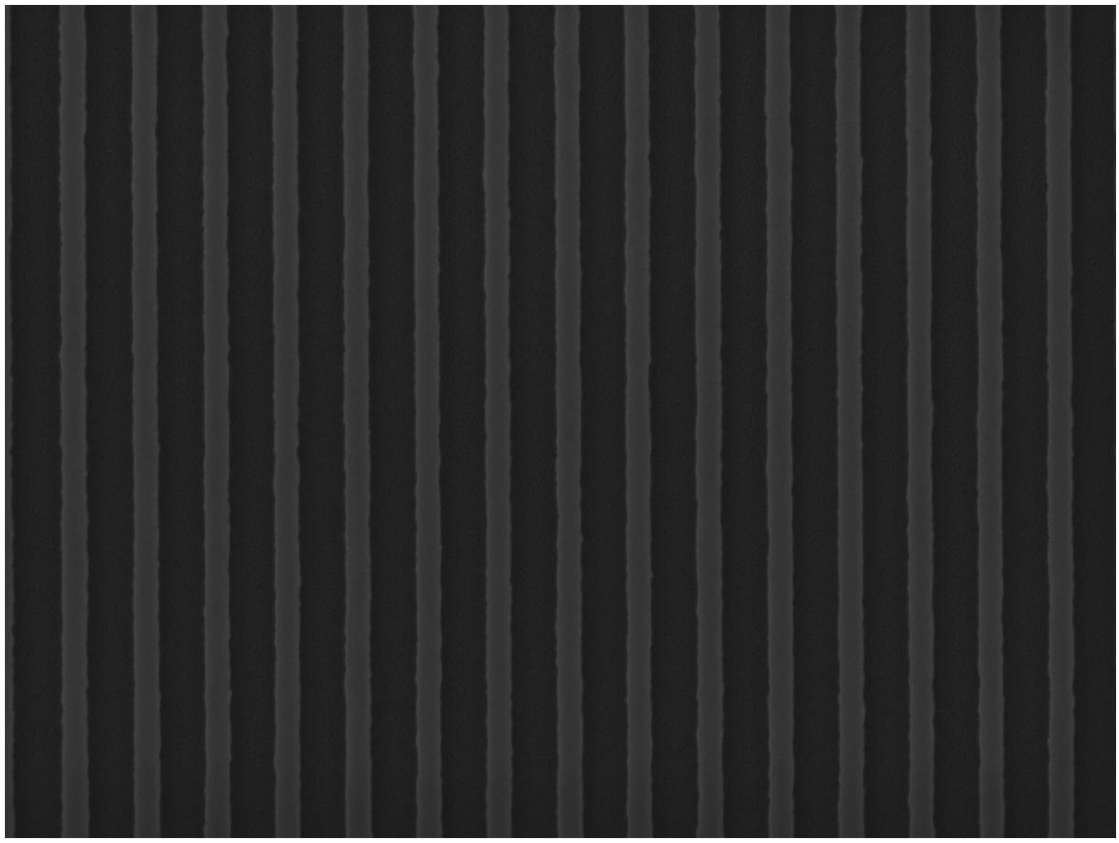

Figure 5-21. SEM of l/s test patterns of the linear resist control with 27.6 nm of pattern blur. Original images recorded with 3072 x 2304 pixels with a 0.985 nm pixel size.

conformation simulations may yield intermolecular interaction data that could further explain this phenomenon.

5.5 Acknowledgement

Financial support from the Semiconductor Research Corporation (GRC-1677.001 and GRC-1675.002) is greatly appreciated. Research was performed in part at the Cornell NanoScale Facility, a member of the Nation Nanotechnology Infrastructure Network and the Cornell Center for Materials Research, which are supported by the National Science Foundation (ECS-0335765 and DMR-0520404). Macromolecular Chemistry I and Macromolecular Chemistry II at the University of Bayreuth are thanked for the generous use of their polymer synthesis and characterization facilities. D.C.F. was supported by a GRC and Applied Materials fellowship.

REFERENCES

1. Constantoudis, V., et al., *Line edge roughness and critical dimension variation: Fractal characterization and comparison using model functions.* Journal of Vacuum Science & Technology B, 2004. **22**(4): p. 1974-1981.

2. Gogolides, E., et al., *A review of line edge roughness and surface nanotexture resulting from patterning processes.* Microelectronic Engineering, 2006. **83**(4-9): p. 1067-1072.

3. Constantoudis, V., et al., *Modeling of line edge roughness transfer during plasma etching.* Microelectronic Engineering, 2009. **86**(4-6): p. 968-970.

4. Akira, M., et al., *International Technology Roadmap for Semiconductors - Lithography*. 2009.

5. Patsis, G.P. and E. Gogolides, *Effects of model polymer chain architectures of photoresists on line-edge-roughness. Monte Carlo simulations.* Journal of Physics: Conference Series, 2005. **10**: p. 389-392.

6. Chochos, C.L., et al., *Hyberbranched Polymers for Photolithographic Applications - Towards Understanding the Relationship between Chemical Structure of Polymer Resin and Lithographic Performance.* Advanced Materials, 2009. **21**: p. 1121-1125.

7. Patsis, G.P., E. Gogolides, and K. Van Werden, *Effects of photoresist polymer molecular weight and acid-diffusion on line-edge roughness.* Japanese Journal of Applied Physics, Part 1: Regular Papers, Brief Communications & Review Papers, 2005. **44**(8): p. 6341-6348.

8. He, D. and F. Cerrina, *Process dependence of roughness in a positive-tone chemically amplified resist.* Journal of Vacuum Science & Technology, B: Microelectronics and Nanometer Structures, 1998. **16**(6): p. 3748-3751.

9. Likos, C.N. and H.M. Harreis, *Star polymers: from conformations to interactions to phase diagrams.* Condensed Matter Physics, 2002. **29**: p. 173-200.

10. Likos, C.N., *Soft matter with soft particles.* Soft Matter, 2006. **2**: p. 478-498.

11. Likos, C.N., et al., *Star Polymers Viewed as Ultrasoft Colloidal Particles.* Physical Review Letters, 1998. **80**(20): p. 4450-4453.

12. Sutherland, R.J. and R.B. Rhodes, *Dispersant viscosity index improvers*, U.S. Patent, Editor. 1994, Shell Oil Company: United States. p. 1-7.

13. Spinelli, H.J., *Silicone containing acrylic star polymers*. 1991, E. I. du Pont de Nemours and Company. p. 1-9.

14. Hunter, R.J., *Foundations of Colloid Science, Vol. 1*. 1986, New York: Oxford University Press.

15. Grest, G., L.J. Fetters, and J.S. Huang, *Star polymers: experiment, theory, and simulation.* Advances in Chemical Physics, 1996. **94**((Polymeric Systems)): p. 67-163.

16. Hsu, H.-P., W. Nadler, and P. Grassberger, *Scaling of Star Polymers with 1-80 Arms.* Macromolecules, 2004. **37**(12): p. 4658-4663.

17. von Ferber, C. and Y. Holovatch, *Field-theoretical renormalization group analysis for the scaling exponents of star polymers.* Condensed Matter Physics, 2002. **29**: p. 117-136.

18. Dzubiella, J. and A. Jusufi, *Star-polymer-colloid mixtures.* Condensed Matter Physics, 2002. **30**: p. 285-305.

19. Bohrisch, J., et al., *New Polyelectrolyte Architectures.* Advances in Polymer Science, 2004. **165**: p. 1-41.

20. Ganazzoli, F., *Conformations and dynamics of stars and dendrimers: the Gaussian Self-Consistent approach.* Condensed Matter Physics, 2002. **5**(1): p. 37-71.

21. Plamper, F.A., et al., *Synthesis, Characterization and Behavior in Aqueous Solution of Star-Shaped Poly(acrylic acid).* Macromolecular Chemistry and Physics, 2005. **206**: p. 1813-1825.

22. Forman, D.C., et al., *Synthesis, Characterization and Properties of Star-Shaped Poly(tert-Butyl Methacrylate) Oligomers.* Manuscript in preparation, 2010.

23. Wieberger, F., et al., *Solution behavior of poly(tert-butylmethacrylate) star oligomers.* Manuscript in preparation, 2010.

24. Forman, D.C., et al., *Precision Synthesis of Star-Shaped Oligomer Terpolymers with Saccharose Cores.* Manuscript in preparation, 2010.

25. Liechty, W.B., et al., *Polymers for drug delivery systems.* Annual Review of Chemical and Biomolecular Engineering, 2010. **1**: p. 149-173.

26. Adair, J.H., et al., *Recent developments in the preparation and properties of nanometer-size spherical and platelet-shaped particles and composite particles.* Materials Science & Engineering: R: Reports, 1998. **23**(4-5): p. 139-242.

27. Matz, G.F., et al., *Low molecular weight water soluble polymer composition and method of use*, in *PCT Int. Appl.*, W.I.P. Organization, Editor. 2001, Calgon Corporation, USA.

28. De Leon-Rodriguez, L.M., et al., *MRI Detection of VEGFR2 in Vivo Using a Low Molecular Weight Peptoid-$(Gd)_8$-Dendron for Targeting.* Journal of the American Chemical Society, 2010. **132**(37): p. 12829-12831.

29. Ito, H., *Chemical Amplification Resists for Microlithography.* Advances in Polymer Science, 2005. **172**: p. 37-245.

30. De Silva, A., et al., *A fundamental study on dissolution behavior of high-resolution molecular glass photoresists.* Chemistry of Materials, 2008. **20**(23): p. 7292-7300.

31. Forman, D.C., et al., *Chemically Amplified Star-Shaped Oligomers as 'Star Resists' for Next Generation Lithography.* Manuscript in preparation, 2010.

32. Forman, D.C., et al., *Comparison of star and linear ArF resists.* Proceedings of SPIE, 2010. **7639**(Pt. 1, Advances in Resist Materials and Processing Technology XXVII): p. 76390P/1-76390P/8.

33. Schmidt, H.-W., *Combinatorial techniques for lithography.* Manuscript in preparation, 2010.

34. Patsis, G.P., et al., *Roughness analysis of lithographically produced nanostructures: off-line measurement and scaling analysis.* Microelectronic Engineering, 2003. **67-68**: p. 319-325.

35. Constantoudis, V., et al., *Quantification of line-edge roughness of photoresists. II. Scaling and fractal analysis and the best roughness descriptors.* Journal of Vacuum Science & Technology, B: Microelectronics and Nanometer Structures--Processing, Measurement, and Phenomena, 2003. **21**(3): p. 1019-1026.

36. Barabasi, A.-L. and H.E. Stanley, *Fractal Concepts in Surface Growth*. 1st ed. ed. 1995, Cambridge, England: Cambridge University Press.

37. Naulleau, P.P. and J.P. Cain, *Experimental and model-based study of the robustness of line-edge roughness metric extraction in the presence of noise.* Journal of Vacuum Science & Technology, B: Microelectronics and Nanometer Structures--Processing, Measurement, and Phenomena, 2007. **25**(5): p. 1647-1657.

38. Yamaguchi, A., et al., *Characterization of line-edge roughness in resist patterns and estimation of its effect on device performance.* Proceedings of SPIE, 2003. **5038**: p. 689-698.

39. Bunday, B.D., et al., *CD-SEM measurement line-edge roughness test patterns for 193-nm lithography.* Proceedings of SPIE, 2003. **5038**: p. 674-688.

40. Tang, W. and K. Matyjaszewski, *Kinetic Modeling of Normal ATRP, Normal ATRP with $[Cu^{II}]_0$, Reverse ATRP and SR&NI ATRP.* Macromolecular Theory and Simulations, 2008. **17**: p. 359-375.

41. Goto, A. and T. Fukuda, *Kinetics of living radical polymerization.* Progress in Polymer Science, 2004. **29**: p. 329-385.

42. Matyjaszewski, K. and J. Xia, *Atom Transfer Radical Polymerization.* Chemical Reviews, 2001. **101**(9): p. 2921-2990.

43. Cowie, J.M.G., *Glass transition temperature-molecular weight relations for oligomers and amorphous polymers.* European Polymer Journal, 1975. **11**(4): p. 297-300.

44. Mack, C., *Fundamental Principles of Optical Lithography: The Science of Microfabrication*. 2007: John Wiley & Sons, Ltd.

45. Kang, S., et al., *Characterization of the Photoacid Diffusion Length and Reaction Kinetics in EUV Photoresists with IR Spectroscopy.* Macromolecules, 2010. **43**(9): p. 4275-4286.

46. Jusufi, A. and C.N. Likos, *Colloquium: Star-branched polyelectrolytes: The physics of their conformations and interactions.* Reviews of Modern Physics, 2009. **81**(4): p. 1753-1772.